Department of Medicine I
Medical University of Vienna

Institute of Cancer Research

YB-1 drives aggressive behavior of mesothelioma cells and YB-1 inhibition sensitizes mesothelioma cells to chemotherapy

Master's thesis submitted for the fulfillment of requirements
for the degree of

Master of Science M.Sc.

submitted by

Dominik Emminger, B.Sc.

Vienna, August 2020

Supervision

External supervisor (Medical University of Vienna)

Assoc. Prof. Dr. Michael Grusch

Internal supervisor (University of Veterinary Medicine Vienna)

Univ.-Prof. Dr. rer.nat. Florian Grebien

Danksagung

An dieser Stelle möchte ich mich bei all den Menschen in meinem Leben bedanken, die einen großen Beitrag zu dieser Arbeit geleistet und mich auf ihre Art und Weise unterstützt haben. Danke!

Assoz. Prof. Dr. Michael Grusch. Du hast meine Arbeit schneller korrigiert, als ich sie schreiben konnte. Deine Tür stand mir immer offen für alle möglichen drive-by Fragen. Mit Deiner Art, Dinge zu sehen und zu interpretieren, hast Du meine wissenschaftliche Denkweise und meinen Horizont erweitert. Ich kann mich wirklich glücklich schätzen einen so engagierten PI gefunden zu haben.

Dr. Karin Schelch. Du hast mir einen großen Teil Deines spannenden Projekts anvertraut. Ich durfte bei Dir alle möglichen und vielfältigen Methoden ausprobieren und habe irrsinnig viel gelernt. Du hast meine Arbeit ebenso schnell korrigiert und hattest jederzeit ein offenes Ohr für meine Fragen. Auch abseits des Labor-Alltags hatten wir viel Spaß beim Philosophieren und dem einen oder anderen Bier (meistens waren es mehr).

Arbeitsgruppe Grusch. Danke für das tolle Arbeitsklima – es war eine Freude bei euch zu arbeiten. **Barbara,** Du warst jederzeit hilfsbereit und ich habe unseren morgendlichen Kaffee sehr genossen. Unser Büro war ein wirklich angenehmer Arbeitsort. **Jelena,** Du hast uns alle motiviert, das Labor sauber zu halten und uns mütterlich umsorgt, bespielsweise als Du mir zu Zeiten von Corona sicherheitshalber die Kamera desinfiziert hast, bevor ich sie benutzt habe.

Brigita, Du hast mir geholfen, viele Dinge aus einem anderen Blickwinkel zu sehen und mich am (vorläufigen) Höhepunkt der Corona Pandemie bei Dir einziehen lassen. Zu zweit war es bedeutend einfacher diese angespannte Phase durchzustehen.

Der allergrößte Dank gilt meiner **Mutter.** Ohne Deine Unterstützung und Dein unerschütterliches Vertrauen in mich wäre ich heute nicht hier.

Abstract

Background: Malignant pleural mesothelioma (MPM) is a rare but aggressive, asbestos-related tumor which has one of the worst prognoses of all cancers with a 5-year overall survival of 5-10%. Standard of care treatment – a combination of cisplatin and pemetrexed – has remained unchanged for over a decade and new therapeutic options are urgently needed. Strong evidence supports the notion that YB-1 drives resistance to platinum-based chemotherapeutics. Despite this knowledge, there are no studies exploring the effects of inhibition of YB-1 on cisplatin resistance in MPM.

Hypothesis and aims: The hypothesis was that YB-1 plays a crucial role in aggressiveness and resistance to chemotherapy in MPM cells. This thesis aimed to assess the impact of overexpression of YB-1 on proliferation, invasion and chemoresistance in MPM cell lines. Furthermore, the effects of siRNA-mediated knockdown of YB-1 and modulation of post translational modifications alone and in combination with cisplatin were explored.

Methods: YB-1 overexpression was achieved using a doxycycline-inducible Tet-On system. Effects of overexpression on clonogenicity, invasiveness, proliferation, chemoresistance and tumorigenicity were evaluated via clonogenic survival assays, 3D spheroid sprouting assays, SYBR green-based proliferation assays and a mouse model. Combination effects of cisplatin with YB-1 knockdown via siRNA, inhibition of phosphorylation at serine 102 by BI-D1870 and stabilization of acetylation at lysine 81 by entinostat were investigated via cell viability assays. Combination indices were calculated using compusyn software based on the Chou-Talalay method.

Results: We found that YB-1 overexpression stimulated cell scattering and epithelial-mesenchymal transition-like morphology changes in all four MPM cell lines. Invasive sprouting through a collagen matrix was significantly increased in the VMC40 cell line. Proliferation and sensitivity to cisplatin did not change when YB-1 was overexpressed. Overexpression of YB-1 also did not induce tumorigenicity in the non-tumorigenic SPC212 cell line. Conversely, silencing YB-1 dramatically reduced cell viability and combination with cisplatin treatment led to synergistic effects. Additionally, both BI-D1870 and entinostat reduced proliferation of MPM cells. Strikingly, we also observed partly synergistic growth-inhibiting effects of BI-D1870 and entinostat in combination with cisplatin.

Conclusion: Our data show that YB-1 plays an important role in the aggressive behavior of MPM cells. Targeting YB-1 via siRNA or pharmacologically reduced MPM cell growth. Furthermore, combination with cisplatin showed promising effects. Consequently, we propose YB-1 to be considered as a therapeutic target in MPM.

Zusammenfassung

Hintergrund: Das maligne Pleuramesotheliom (MPM) ist ein seltener, aggressiver und Asbest-assoziierter Tumor mit einer der schlechtesten Prognosen aller Krebsarten – die 5-Jahres-Überlebensrate liegt bei 5-10%. Die Standardmedikation besteht aus einer Kombination von Cisplatin und Pemetrexed und hat sich seit über einem Jahrzehnt nicht geändert. Neue Therapieoptionen werden dringend benötigt. Es gibt starke Hinweise darauf, dass YB-1 die Resistenz gegen platinbasierte Chemotherapeutika antreibt. Trotzdem gibt es noch keine Studien über die Auswirkungen der Hemmung von YB-1 auf die Resistenz gegen Cisplatin bei MPM.

Hypothese und Ziele: Die Ausgangshypothese dieser Arbeit ist, dass YB-1 maßgeblich zum aggressiven Verhalten und zur Chemoresistenz im MPM beiträgt. Daher war das Ziel dieser Studie, die Auswirkung von YB-1 Überexpression auf Proliferation, Invasion und Chemoresistenz zu untersuchen. Des Weiteren sollte evaluiert werden, wie sich YB-1 Knock-down und pharmakologische Hemmung auf die Resistenz von MPM Zellen gegen Cisplatin auswirkt.

Methoden: Überexpression von YB-1 wurde mit einem Doxycyclin-induzierbaren System erreicht und die Auswirkungen auf Klonogenität, Invasion, Proliferation, Chemoresistenz und Tumorigenität wurden anhand von Überlebensassays, 3D Sphäroidwachstumsassays, Proliferationsassays und einem Mausversuch untersucht. Sowohl YB-1 Knock-down durch siRNA, als auch pharmakologische Hemmung der Phosphorylierung von YB-1 an Serin 102 durch BI-D1870 und Hemmung der Deacetylierung an Lysin 81 durch Entinostat wurden mit Cisplatin kombiniert und mittels Zellwachstumstests untersucht. Die Kombinationsindizes (KIs) wurden mit dem Compusyn Programm basierend auf der Chou-Talaly Methode berechnet.

Resultate: YB-1 Überexpression stimulierte die Streuung der Zellen und diese nahmen Morphologien an, die epithelial-mesenchymal Übergängen ähneln. Invasion durch eine Kollagenmatrix war in der Zelllinie VMC40 signifikant erhöht. Andererseits hatte die Überexpression keine Auswirkungen auf Chemoresistenz und Proliferation der untersuchten MPM Zellen und konnte in der nicht-tumorigenen Linie SPC212 kein Tumorwachstum in Mäusen induzieren. YB-1 Knock-down durch siRNA reduzierte das Zellwachstum drastisch und führte zu einer verstärkten Wirkung in Kombination mit Cisplatin. Des Weiteren reduzierten sowohl BI-D1870, als auch Entinostat das Wachstum unserer MPM Zellen als Monotherapie. Bemerkenswerterweise führten beide Inhibitoren in Kombination mit Cisplatin zu einer verstärkten Wirkung.

Fazit: Unsere Daten zeigen, dass YB-1 eine wichtige Rolle in der Aggressivität von MPM Zellen spielt. In Anbetracht der Tatsache, dass sowohl das Silencing von YB-1, als auch die Hemmung posttranlationaler Modifikatoren von YB-1 das Zellwachstum verringerten und in Kombination mit Cisplatin sogar zu einer verstärkten Wirkung führten, erscheint es sinnvoll, YB-1 als potenzielles neues Therapietarget im MPM in Erwägung zu ziehen.

Table of Contents

1. INTRODUCTION

1.1. Cancer

1.1.1. Cancer in numbers

Non-communicable diseases (NCD) are the leading cause of death worldwide and were responsible for 71% of all deaths in 2016 (Sirohi et al., 2018). There were an estimated 18.1 million new cancer cases and 9.6 million cancer deaths in 2018 (Bray et al., 2018). According to the World Health Organization (WHO), cancer is the first or second leading cause of premature death (before the age of 70) in 91 of 172 countries (Figure 1). Incidence and mortality rates of cancer continue to rise, in part due to aging populations (van Hoeve et al., 2015). Another reason is that improvements in other NCDs have been made faster than in cancer (Shah et al., 2019). One in five people will develop cancer before the age of 75 (WHO, 2020).

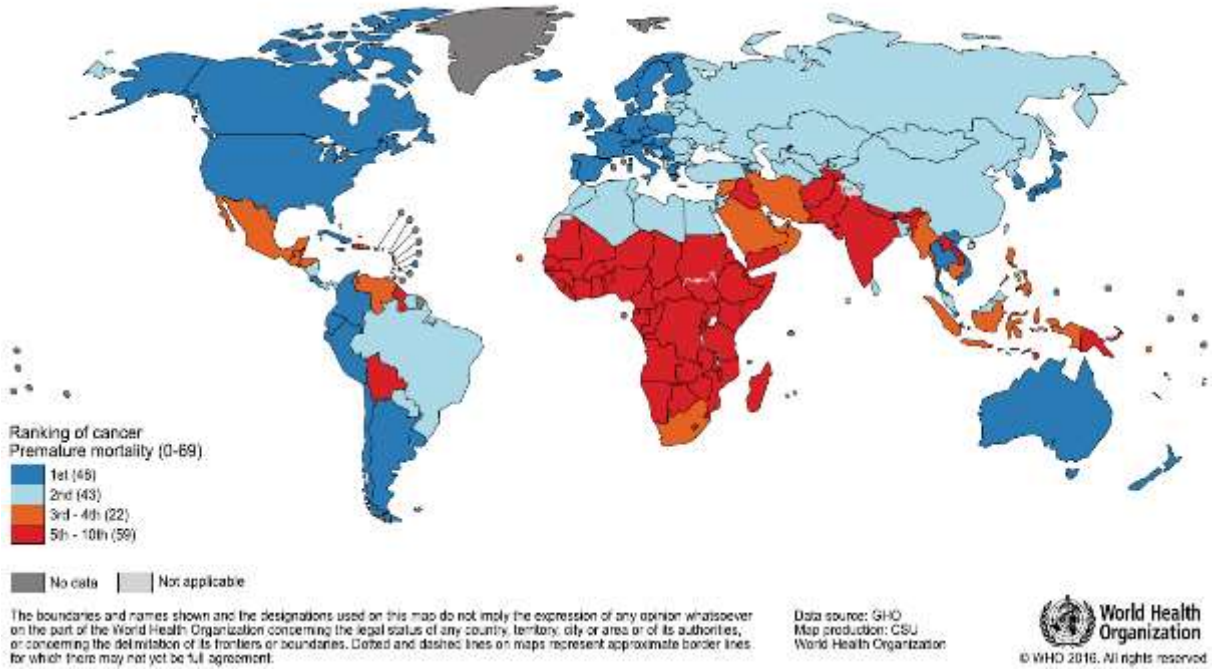

Figure 1: Ranking of cancer as cause of premature death (before the age of 70) per nation in 2015. Source: World Health Organization (Bray et al., 2018).

1.1.2. Hallmarks of cancer

In 2000, Hanahan and Weinberg published their famous review article “The Hallmarks of Cancer” (Hanahan and Weinberg, 2000). In focusing on the phenotypes of cancer, they side-stepped the fragmentary understanding of signal-processing circuits at the time (Weinberg, 2014) and defined six hurdles every cancer cell has to overcome in order to transform from a normal cell to a cancer cell. These hallmarks are well-established and comprise sustaining proliferative signaling, evading growth suppressors, resisting cell death, inducing angiogenesis, enabling replicative immortality and activating invasion and metastasis. In 2011, Hanahan and Weinberg published an updated review (Hanahan and Weinberg, 2011). They added two enabling characteristics – genome instability and mutation and tumor-promoting inflammation – and two emerging hallmarks – deregulating cellular energetics and avoiding immune destruction. Each hallmark is briefly discussed below. A schematic overview is depicted in Figure 2.

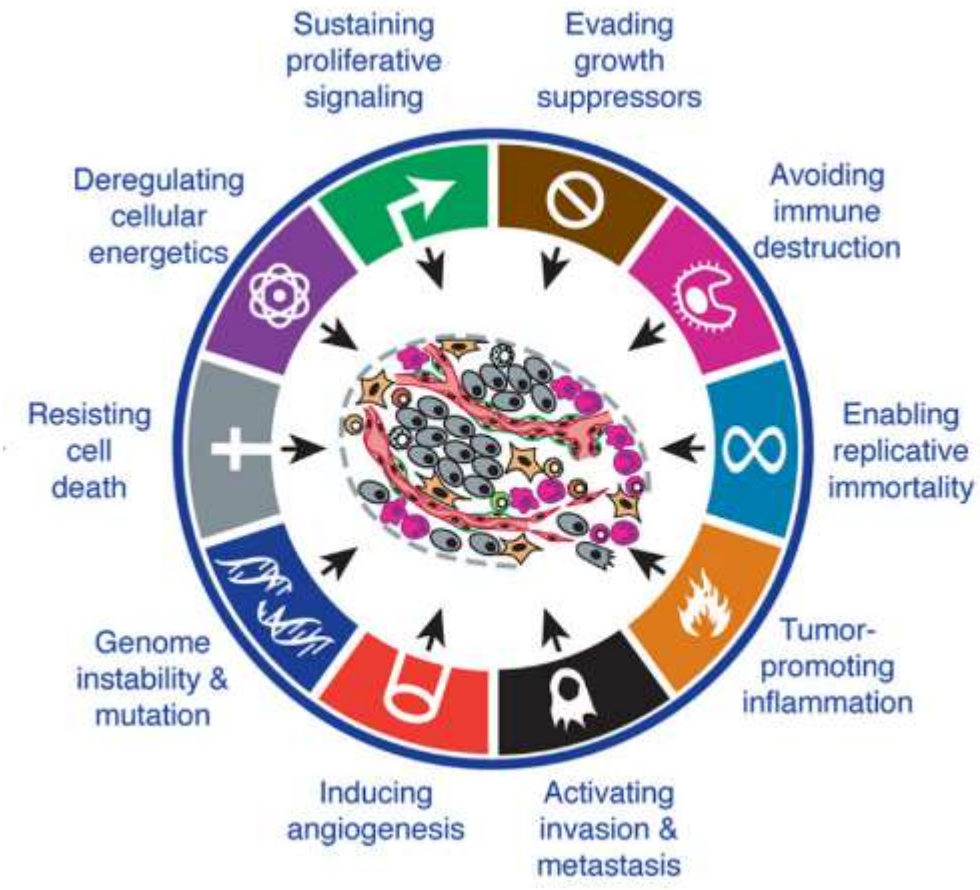

Figure 2: The hallmarks of cancer (Hanahan and Weinberg, 2011).

One of the most fundamental capabilities of cancer cells is **sustaining proliferative signaling**. Normal cells and tissues carefully maintain cell number homeostasis. Cancer cells are able to produce their own growth signals or stimulate normal cells to provide these signals. Another way is to upregulate receptors and become more responsive to the limited growth signals. Cancer cells were also shown to constitutively activate downstream components, rendering them independent of growth signals. A prominent example for this are activating *BRAF* mutations which occur in 40-60% of melanomas and lead to oncogenic mitogen-activated protein kinase (MAPK) pathway activation (Cheng et al., 2018).

Evading growth suppressors is another important step in becoming a cancer cell. Tumor suppressors normally control cell growth and proliferation. The two best known examples are tumor protein p53 (TP53) and retinoblastoma protein (RB). RB inhibits cell cycle progression from G1 to S phase until the cell is ready to divide, largely based on extracellular signals. TP53 acts as an intracellular sensor of stresses such as DNA damage. Upon recognition of DNA damage, TP53 can halt cell cycle progression until the damage is repaired. In case of irreparable damage, TP53 induces apoptosis. It is also crucial for instigating senescence if the telomeres are too short. The many functions of TP53 award it its name “the guardian of the genome” (Lane, 1992). An analysis of The Cancer Genome Atlas (TCGA) datasets of 10,225 patients across 32 cancers revealed that ~37% had mutations in the *TP53* gene (Donehower et al., 2019), highlighting its importance for tumor suppression.

Resisting cell death is also a major capability of cancer cells. Programmed cell death by apoptosis is a cell intrinsic strategy to avoid propagation of irreparably damaged cell populations. By overcoming apoptosis, cancer cells are able to proliferate even if their DNA is highly altered. Loss of *TP53*, downregulation of apoptotic signals or upregulation of survival signals are methods to avoid apoptosis. B-cell lymphoma 2 (BCL-2) is a prominent example for the latter. BCL-2 prevents the permeabilization of the mitochondrial membrane by BCL-2-like protein 4 (BAX) and BCL-2 homologous antagonist/killer (BAK) and is upregulated in many cancers (Adams and Cory, 2018).

In the adult, angiogenesis is only briefly activated for physiological processes such as wound healing and the menstrual cycle. In order to grow beyond 1-2 mm^3 in size, solid tumors need to grow new blood vessels (Hillen and Griffioen, 2007). By **inducing angiogenesis,** they ensure their nutrient and oxygen supply. Growing cancers activate endothelial cells by

secretion of pro-angiogenic factors with vascular endothelial growth factor (VEGF) and fibroblast growth factor 2 (FGF2) being two of the most important examples (Rajabi and Mousa, 2017).

Telomeres protect chromosomes from end-to-end fusions and deterioration during replication. In each division, the telomeres become shorter and shorter until they reach a point where the cell must enter senescence to avoid crisis. Thus, telomere length naturally limits cell divisions. However, 85-95% of all cancer cells express telomerase, an enzyme capable of elongating telomere sequences that under physiological conditions is only expressed in germ cells and stem cells. Moreover, 5-15% activate the alternative lengthening of telomeres (ALT) pathway (Okamoto and Seimiya, 2019), thereby **enabling replicative immortality.**

Epithelial cells are able to lose their cell-cell adhesion, increase their migratory and invasive capabilities and gain a mesenchymal phenotype. This development is called epithelial-mesenchymal transition (EMT) and occurs during physiological processes, for instance embryogenesis, organogenesis and wound healing. Cancer cells hijack the EMT program, thereby **activating invasion and metastasis**. Upregulation of EMT transcription factors (TF) such as the SNAIL, TWIST and ZEB families is important at all steps of cancer progression (Brabletz et al., 2018).

The first of the two more recently described enabling characteristics is **genome instability and mutation**. Cells utilize many different repair programs for maintenance of their DNA. It is estimated that a single cell is subjected to 70,000 DNA lesions each day (Tubbs and Nussenzweig, 2017). About 75% are single strand breaks and repaired by base excision repair (BER), nucleotide excision repair (NER) or mismatch repair (MMR). Double strand breaks are repaired via homologous recombination (HR) or non-homologous end joining (NHEJ) with the latter introducing insertions and deletions. In order to accumulate the mutations required for tumorigenesis, cancer cells inactivate these pathways. Triple-negative breast cancers were shown to have defects in DNA repair in 60-69% of cases (Gilmore et al., 2019). The term “BRCAness” originates from the fact that mutations in the tumor suppressor genes *breast cancer 1* (*BRCA1*) and *BRCA2* lead to impaired HR.

The other enabling characteristic is **tumor-promoting inflammation**. Tumors are also termed "wounds that do not heal". Cancer cells hijack innate immune cells such as macrophages which then become tumor-associated macrophages (TAM). Chronic inflammation prompted by TAMs provides tumors with growth signals, promotes metastasis and invasion by secretion of matrix metalloproteinases (MMP) for the editing of the extracellular matrix (ECM) and induces angiogenesis (Ma et al., 2020). In addition, the inflammatory environment also results in increased levels of reactive oxygen species (ROS) leading to oxidative DNA damage and plays an important role in tumor progression (Aggarwal et al., 2019).

Deregulating cellular energetics is described as one of the two emerging hallmarks. Cancer cells are known to perform aerobic glycolysis. Otto Warburg was the first to describe this metabolic switch whereby cancer cells utilize glycolysis instead of mitochondrial oxidative phosphorylation despite the presence of oxygen (Warburg, 1930). This so-called Warburg Effect generates ~18 fold less adenosine triphosphate (ATP) per glucose molecule than oxidative phosphorylation. The reason why this would confer a growth advantage to cancer cells is subject to ongoing research. A possible explanation is that uncontrolled proliferation requires more molecules for biosynthesis and through aerobic glycolysis, glucose can be utilized in many different ways for anabolic processes (Liberti and Locasale, 2016).

The last of the second generation of the hallmarks of cancer is **avoiding immune destruction**. The immune system constantly seeks out and destroys transformed cells which could become cancer – a process called immunosurveillance. Natural Killer (NK) cells and cytotoxic T cells (CTL) are the effector cells which circulate the body and eliminate thousands of premalignant cells each day. There are three established outcomes of natural immunosurveillance: elimination, equilibrium and escape (Figure 3). Elimination occurs if the immune system eradicates the premalignant cells and restores tissue homeostasis. Equilibrium is a state in which there is a balance between immune effector cells and the suppressive environment of the tumors and the premalignant lesion does not progress further. However, if the scale tips towards a more suppressive environment, the immune cells cannot control the premalignant lesion any longer and a primary tumor develops (Finn, 2018).

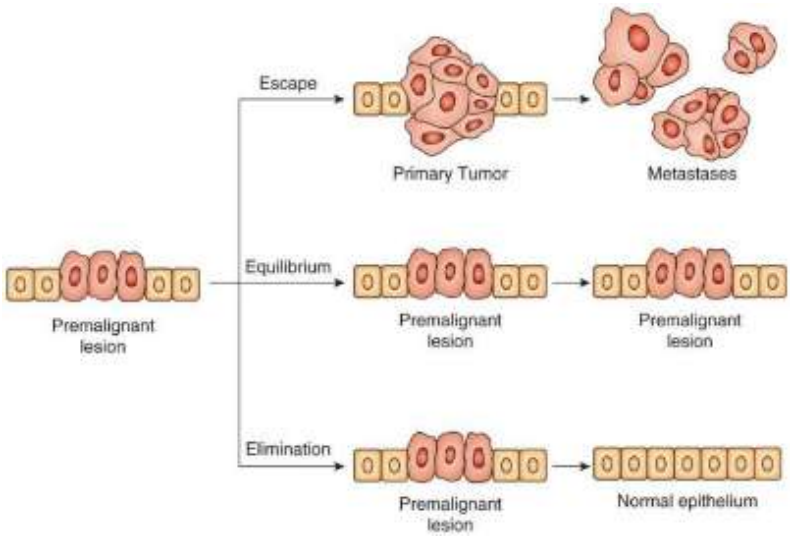

Figure 3: The three established outcomes of natural immunosurveillance against cancer (Finn, 2018).

1.2. Malignant pleural mesothelioma

1.2.1. Characterization

Malignant pleural mesothelioma (MPM) is a rare but highly aggressive cancer stemming from the mesothelial cells of the pleural linings of the chest cavity and lungs (Figure 4). MPM is the most common form of mesotheliomas, accounting for more than 80% of cases (Neumann et al., 2013).

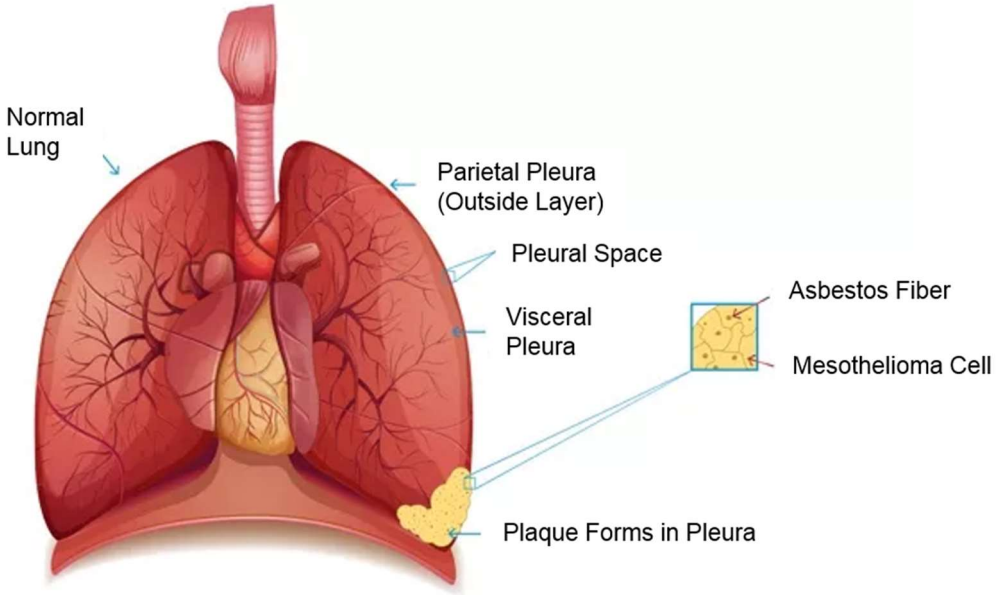

Figure 4: Schematic depiction of MPM modified from asbestos.com (accessed July 21st 2020).

MPM can be divided into three main histological subtypes based on their morphology: epithelioid, biphasic and sarcomatoid (Figure 5). Epithelioid MPM is characterized by polygonal, oval or cuboidal cells (Geltner et al., 2016). It shows the highest median overall survival (OS) with 14.4 months and is the most commonly diagnosed form with 68% of cases (Verma et al., 2018). Sarcomatoid MPM displays spindle cell morphology and resembles sarcoma. It has the worst median OS with 5.3 months and is found in 18% of cases. Biphasic MPM is a mixed type which shows epithelioid and sarcomatoid features and accounts for 13% of cases with a median OS of 9.5 months. Recently, new subdivisions were proposed based on architectural patterns, cytologic and stromal features and whether tumors are localized, adenomatoid or well-differentiated (Nicholson et al., 2020).

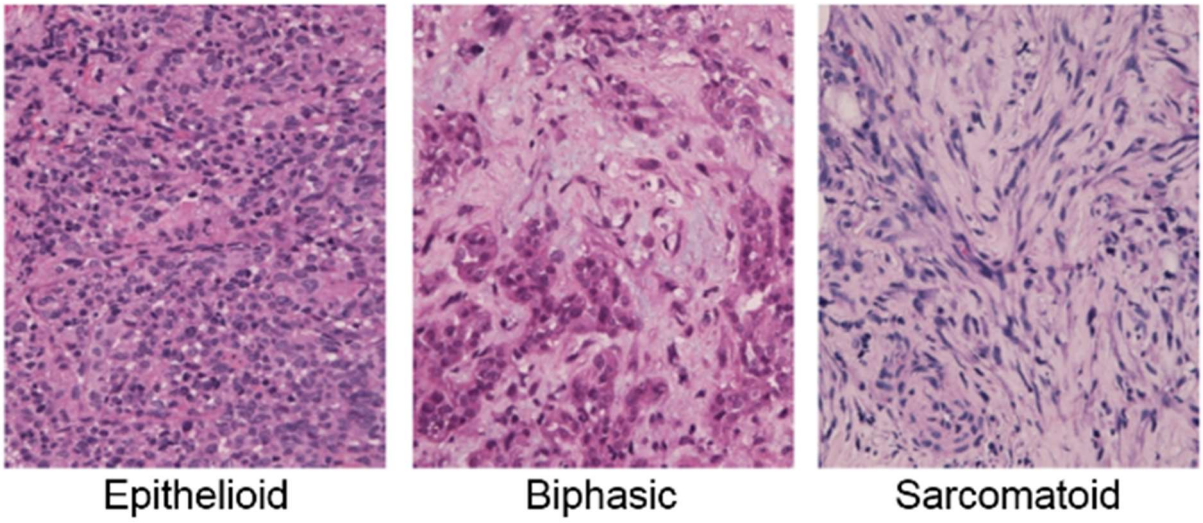

Figure 5: Tumor specimens representing the three main histological subtypes of MPM. Pictures kindly provided by Dr. Karin Schelch.

1.2.2. Link to asbestos exposure

Unlike many other malignancies, there is a clear connection between a single causative agent and development of MPM, with asbestos being responsible for 70-90% of cases (Attanoos et al., 2018). The latency period after exposure ranges between 20-50 years and most patients die 9-12 months after diagnosis (Nuyts et al., 2018).

Asbestos describes a group of naturally occurring minerals which form thin and long fibers. Due to its physical characteristics such as non-flammability, high tensile strength, chemical, electrical and thermal resistance, asbestos was – and still is – used in the construction industry leading to occupational exposure of workers. Asbestos was also used in a wide variety of

products, for instance in cigarette filters, cosmetics, laboratory equipment or as fake snow in the movie “The Wizard of Oz”. The earliest link between asbestos exposure and development of cancer of the pleura was described by H. W. Wedler in 1943 (Wedler, 1943). He reported that approximately 20% of German asbestos workers developed lung cancer and mesothelioma. In 1978, a mesothelioma epidemic was described where 50% of all deaths were caused by the disease in three villages in Cappadocia (Baris et al., 1978). Initially, asbestos was thought to be the cause, but instead researchers found erionite to be the culprit. Erionite is a fibrous mineral contained in the zeolite stones which are used as building material in the area. Interestingly, germline BRCA1-associated protein *(BAP1)* mutations were identified to predispose families to develop MPM (Attanoos et al., 2018). Further causes of MPM include radiation treatment for other malignancies (Chang et al., 2017) or infection with simian virus 40 (SV40), though this is still subject to debate (Mazzoni et al., 2012).

Despite the clear link between asbestos exposure and MPM development, nine of the ten most populated countries still have not completely banned asbestos usage (Takahashi and Landrigan, 2016) and the incidence of MPM is expected to rise in the next years (Linton et al., 2012). Incidence rates differ greatly and some countries are still projected to reach their peaks (Table 1).

Table 1: Predicted peak incidences and years of MPM in various countries (Neumann et al., 2013).

Country	Incidence at peak (new cases per million per year)	Peak year(s)	Predicted deaths per year at peak	Study
Australia	40	2010	1000	Leigh 2002 (e8)
United Kingdom	38	2016	2040	Tan 2010 (e9)
Germany	20	2015–2020	1600	Pesch 2010 (e10) Peto 1999 (e11)
France	20	2020–2040	1300	Banaei 2000 (e12)
USA	15	2010	2800	Larson 2007 (e13)
Japan	15	2025–2033	1200	Azuma 2009 (e14)
Spain	11	2016	520	Pitarque 2008 (e15)
Netherlands	10	2028	900	Segura 2003 (e16)

1.2.3. Carcinogenesis

Bound asbestos poses no threat, but when it gets released and becomes airborne, it can be inhaled into the lungs. Fibers then travel to the pleura and get in contact with normal mesothelial cells. Asbestos fibers are able to directly interact with chromosomes and the

spindle apparatus, leading to aneuploidy and chromosomal aberrations (Hesterberg and Barrett, 1985). Fibers shorter than 5 µm can be phagocytosed by macrophages, but longer fibers persist and lead to chronic inflammation (Rudd, 2010). The inflammatory environment combined with ROS production promotes transformation of mesothelial cells and gives rise to MPM (Thompson et al., 2014). A schematic overview of this process is shown in Figure 6.

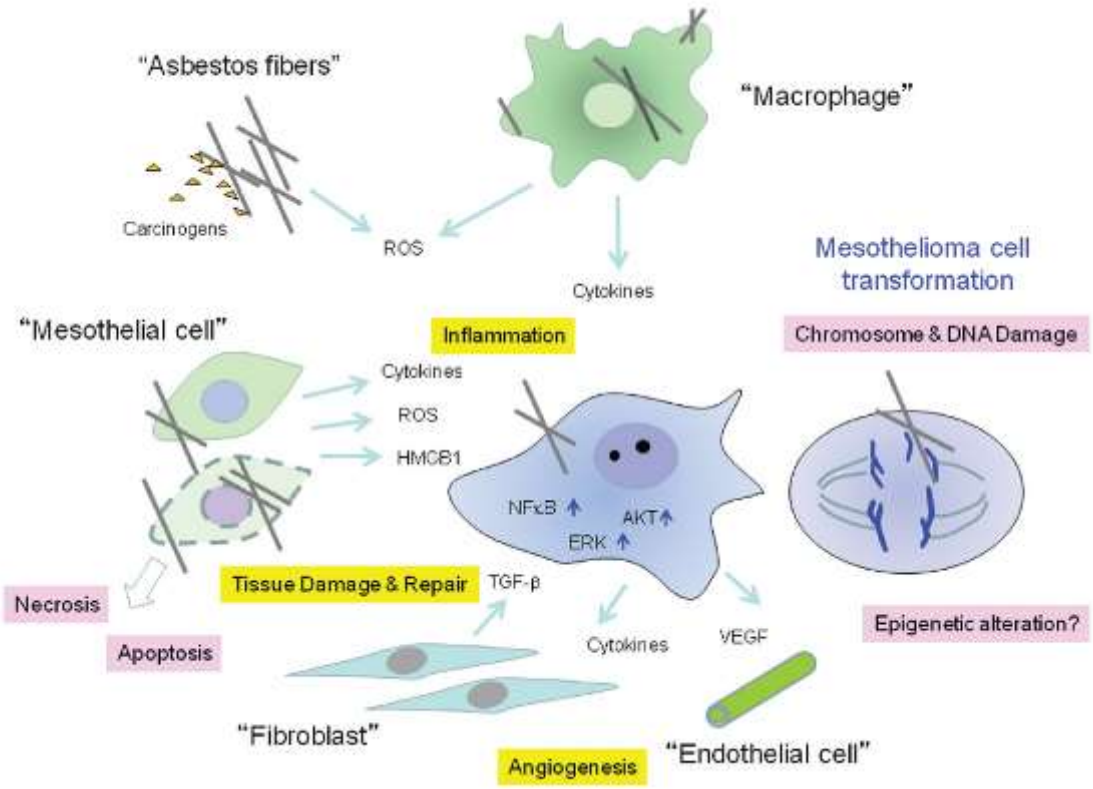

Figure 6: Schematic depiction of MPM carcinogenesis by inhalation of asbestos fibers (Sekido, 2013).

Tumor suppressor genes are frequently altered in MPM. The *cyclin-dependent kinase inhibitor 2A (CDKN2A)/alternative reading frame (ARF)* gene shows homozygous deletions in over 70% of cases in MPM (Sekido, 2013). *CDKN2A/ARF* encodes $p14^{ARF}$ and cyclin-dependent kinase 4 and 6 (CDK4/6) inhibitor $p16^{INK4a}$. Through inhibition of CDK4/6, $p16^{INK4a}$ facilitates RB-dependent cell cycle arrest (Witkiewicz et al., 2011). By degradation of mouse double minute 2 homolog (MDM2), $p14^{ARF}$ stabilizes p53 (Pomerantz et al., 1998). Alternatively, $p14^{ARF}$ induces G_2 cell cycle arrest by inactivation of Cyclin-dependent kinase 1 (CDK1) in a p53-independent manner (Normand et al., 2005). Germline mutations in the *BAP1* gene were reported to lead to an extraordinarily high incidence of cancers (69.74%), including MPM

(Carbone et al., 2013). *BAP1* is involved in DNA double strand break repair, cell cycle regulation and chromatin remodeling (Yu et al., 2014). Somatic *BAP1* mutations are reported in 25-60% of MPM cases (Xu et al., 2014). Moesin-Ezrin-Radixin-Like Protein (Merlin) is encoded by the Neurofibromin 2 *(NF2)* gene and presents another tumor suppressor which is altered in 38% of MPM cases (Andujar et al., 2013). Merlin is located at the plasma membrane and binds to receptor tyrosine kinases (RTK) and integrins, facilitating contact inhibition (Beltrami et al., 2013). Loss of merlin results in anchorage-independency and aids in invasion and migration of transformed cells (McClatchey and Giovannini, 2005).

The oncogene Notch-1 was reported to be overexpressed in MPM cells compared to normal controls (Graziani et al., 2008). Notch-1 inhibits the tumor suppressor Phosphatase and tensin homolog (PTEN) and activates the pro-survival phosphatidylinositol 3-kinase (PI3K)/Akt/ mammalian target of rapamycin (mTOR) signaling pathway (Graziani et al., 2008). It was also shown that SV40 infection activates Notch-1 (Bocchetta et al., 2003) and leads to transformation and immortalization of normal human pleural mesothelial cells (Bocchetta et al., 2000).

1.2.4. Therapy

MPM is usually diagnosed at advanced stages due to delayed and unspecific symptom onset and is often resistant to chemotherapy (Scherpereel et al., 2018). Standard of care treatment for MPM is combination chemotherapy with cisplatin and pemetrexed with palliative intent (Baas et al., 2015). Thus far it is also the only Food and Drug Administarion (FDA) and European Medicines Agency (EMA) approved frontline therapy for MPM (Nicolini et al., 2020). Cisplatin crosslinks to the purine bases of the DNA, causing DNA damage, interfering with DNA repair and finally leading to apoptosis (Dasari and Tchounwou, 2014). Pemetrexed was the first approved agent for MPM therapy (Rollins and Lindley, 2005) and is an antifolate. Tumor cells rely on *de novo* nucleotide synthesis which is inhibited by pemetrexed (Goudar, 2008). Nevertheless, only 41% of patients respond to combination therapy (Cinausero et al., 2018).

Individual patients are eligible for surgical procedures such as extrapleural pneumonectomy (EPP) or pleurectomy/decortication (P/D) with curative intent (Scherpereel et al., 2018). EPP

involves resection of the lung, pericardium, diaphragm, and pleural linings. D/P is lung-sparing, removing only the pleurae (Sugarbaker et al., 2014).
Radiotherapy is mainly used as palliative treatment (van Zandwijk et al., 2013), although some patients may benefit from multimodality treatment combining chemotherapy, radiotherapy and surgery.

Angiogenesis inhibitors have been tested in the clinics with limited success due to suboptimal patient selection resulting from lack of good biomarkers (Nicolini et al., 2020). Nevertheless, some improvement could be achieved. In the phase III MAPS clinical trial, bevacizumab, a monoclonal antibody targeting VEGF, was reported to improve OS (18.8 vs. 16.1 months) and progression-free survival (PFS, 9.2 vs. 7.3 months) when administered alongside cisplatin and pemetrexed combination therapy (Zalcman et al., 2016).

Loss of arginine argininosuccinate synthase 1 (ASS1) expression has been reported in up to 50% of MPM (Szlosarek et al., 2006) and arginine depletion has been shown to lead to synthetic lethality (Locke et al., 2016). In a phase I clinical trial, pegylated arginine deiminase (ADI-PEG 20) was combined with cisplatin and pemetrexed. The combination achieved 78% overall response rate in 4 patients with non-small cell lung cancer (NSCLC) and 5 patients with MPM. One patient with sarcomatoid MPM, which is considered chemotherapy resistant, responded to this treatment (Beddowes et al., 2017).

Recently, immunotherapies are evaluated for all kinds of cancers including MPM. Immune checkpoint inhibitors aim to reactivate immune cells curbed by tumors. Programmed cell death protein 1 (PD1) is expressed on activated T and B cells. Binding of its ligand, programmed death-ligand 1 (PD-L1), results in apoptosis or exhaustion (Gibbons Johnson and Dong, 2017). PD-L1 was shown to be expressed in 40% of MPM tumors and these patients had a much worse median survival (5 vs. 14.5 months) (Mansfield et al., 2014). Clinical trials with pembrolizumab, an anti-PD1 ICI, as second or third line treatment reported mixed results as reviewed by Nicolini and colleagues (Nicolini et al., 2020).

MicroRNA (miRNA) replacement therapy presents a novel approach. In MPM, miRNA-16 is often downregulated and re-expression and delivery of miRNA-16 mimics inhibited tumor growth significantly *in vitro* and *in vivo* (Reid et al., 2013). In the MesomiR phase I clinical trial, this approach was applied to patients with relapsed MPM. Bacterial shells targeting epidermal

growth factor receptor (EGFR) were loaded with miRNA-16 mimics, resulting in partial response in 5% and stable disease in 68% of patients (van Zandwijk et al., 2017).

Figure 7 shows a summary of current and novel approaches for the treatment of MPM. Despite the many different strategies, only small improvements can be reported so far and new therapies are urgently needed.

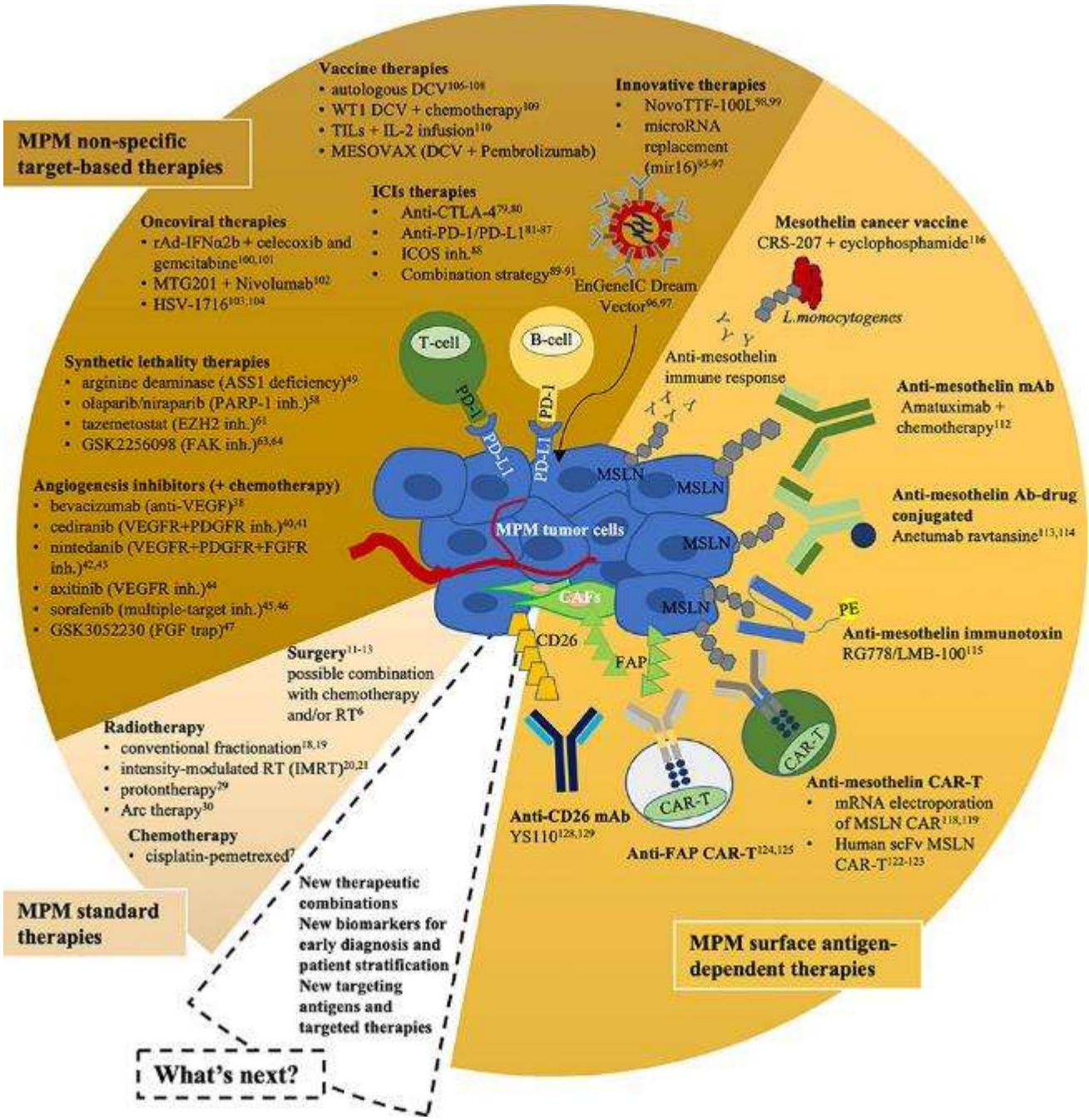

Figure 7: Summary of current and novel approaches for the treatment of MPM (Nicolini et al., 2020).

1.3. Y-box-binding protein 1

Y-box-binding protein 1 (YB-1) was first discovered as a repressor of *major histocompatibility complex class II (MHC class II)* gene transcription. YB-1 binds the Y-box – an inverted CCAAT box – of the promotor of MHC class II (Didier et al., 1988). It is encoded by the *YBX1* gene and belongs to the cold-shock domain protein family which contains a conserved nucleic-acid-binding domain that is able to bind RNA and DNA (Wolffe et al., 1992). YB-1 is a transcription and translation factor and plays a critical role in many cellular processes such as proliferation, DNA damage repair, chemotherapy resistance and invasion and metastasis (Johnson et al., 2019).

1.3.1. YB-1 in cancer

YB-1 is overexpressed in many cancers and associated with poor prognosis (Lasham et al., 2013). *In silico* analysis of transcriptomics data suggests that YB-1 is a highly prognostic marker in NSCLC and MPM and that higher YB-1 expression correlates with poor OS (Johnson et al., 2019) (Figure 8).

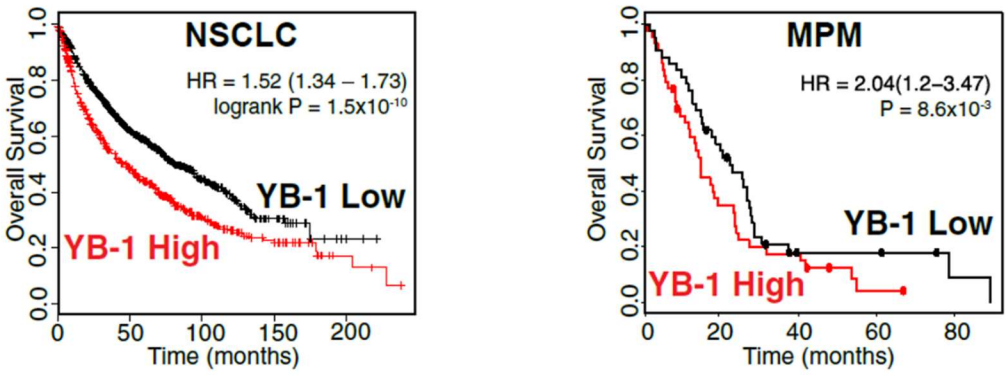

Figure 8: High YB-1 expression correlates with poor overall survival in patients with NSCLC and MPM (Johnson et al., 2019)

YB-1 is involved in the dysregulation of the cell cycle by upregulation of expression of activating E2 promotor binding factors (E2F) transcription factors such as E2F1 (Lasham et al., 2012) and simultaneous downregulation of inhibiting E2F transcription factors such as E2F7 (Finkbeiner et al., 2009). YB-1 also plays a role in the PI3K/Akt/mTOR pathway through induction of PI3K catalytic subunit alpha (PI3KCA) (Astanehe et al., 2009). Additionally, YB-1 activates various members of the MAPK pathways (Figure 9) (Lasham et al., 2013).

Knockdown of YB-1 via small interfering RNA (siRNA) and miRNA-137 mimic were reported to significantly reduce growth of MPM cells (Johnson et al., 2018).

Cells undergo apoptosis when they have accumulated sufficient DNA damage. YB-1 protects cancer cells from programmed cell death in several ways. Normally, activation of the cell surface receptor Fas leads to apoptosis via the executioner caspases 3 and 7 (Kaufmann et al., 2012). YB-1 transcriptionally inhibits *FAS* in acute T cell leukemia cells (Lasham et al., 2000) and also *BAX* gene expression in normal mammary epithelial cells (Homer et al., 2005). Furthermore, YB-1 prevents induction of pro-apoptotic genes by interfering with TP53 in squamous cell carcinoma cells (Okamoto et al., 2000).

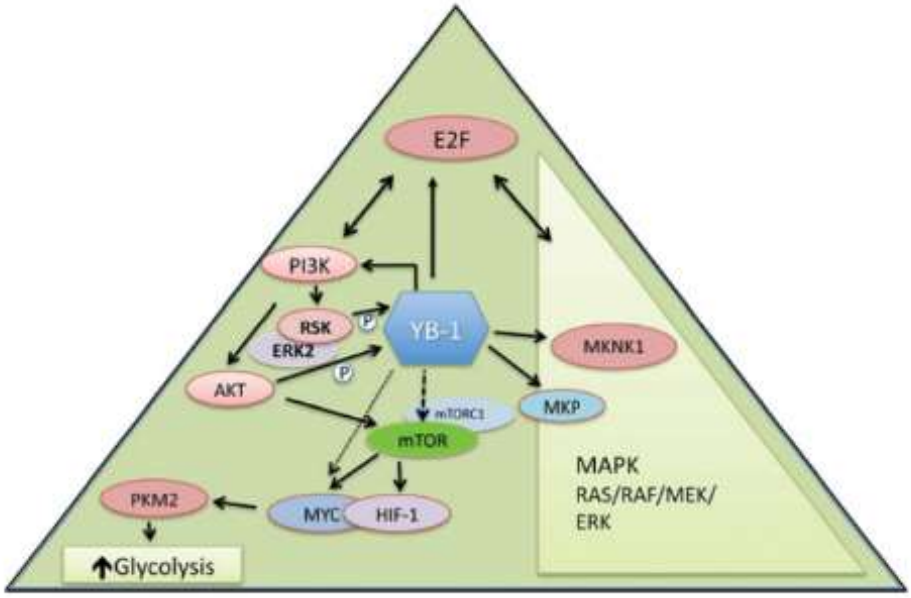

Figure 9: Involvement of YB-1 in multiple proliferation signaling pathways (Lasham et al., 2013)

Moreover, YB-1 is involved in resistance to chemotherapy in many cancers such as melanoma (Schittek et al., 2007), prostate cancer (Shiota et al., 2014), breast cancer (To et al., 2010) and ovarian cancer (Kang et al., 2013). Treatment with cisplatin induces overexpression of YB-1 in bladder cancer (Shiota et al., 2010) and knockdown of YB-1 sensitizes various cancers to cisplatin (Johnson et al., 2019). Furthermore, overexpression of YB-1 is reported to increase multi-drug resistance protein 1 (MDR1) expression and subsequent resistance to doxorubicin in breast cancer cells (Bargou et al., 1997).

As tumors grow, the need for nutrients and oxygen also increases. Hypoxia in solid tumors leads to expression of hypoxia-inducible factors (HIF) – the master regulators of oxygen homeostasis (Semenza, 2014). Neovascularization with underdeveloped and leaky blood vessels follows, to support tumor growth. YB-1 activates translation of HIF-1α in hypoxic conditions while its knockdown dramatically reduces invasion and metastasis of sarcoma cells *in vivo* (El-Naggar et al., 2015). This effect is rescued by re-expression of HIF-1α (El-Naggar et al., 2015).

YB-1 also plays a critical role in immune evasion. Cancer cells often express PD-L1 to deactivate effector T cells and dampen the immune response. Tao and colleagues showed that YB-1 directly binds to the promoter of PD-L1 and YB-1 knockdown reverses chemoresistance by activation of T cells due to inhibited PD-L1 expression in the microenvironment of hepatocellular carcinoma (Figure 10) (Tao et al., 2019).

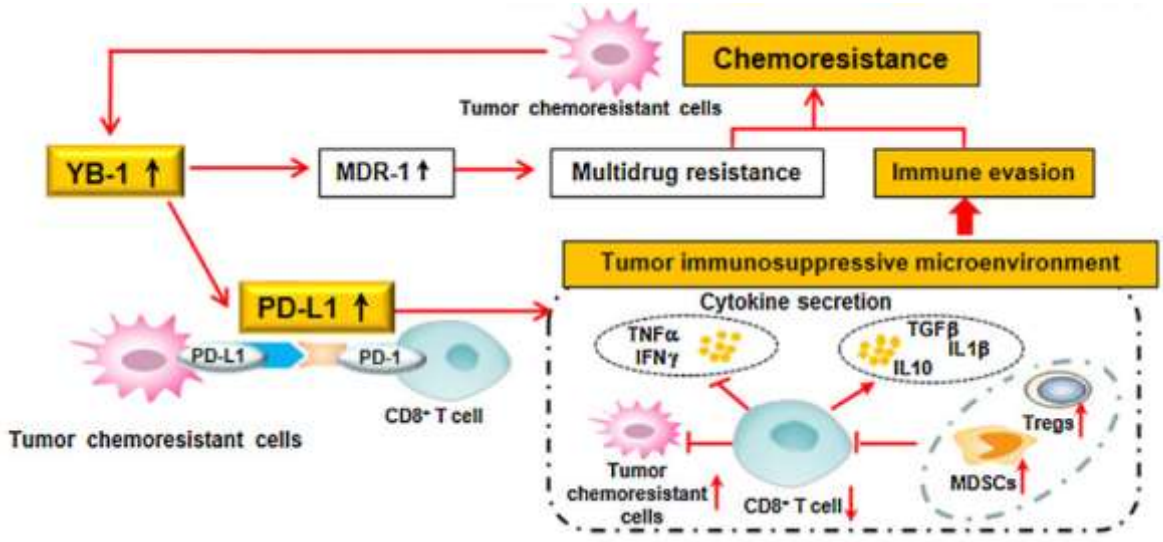

Figure 10: Schematic overview of the involvement of YB-1 in chemotherapy resistance and immune evasion (Tao et al., 2019)

EMT is often hijacked by cancer cells to form metastases and YB-1 is critically involved in this process. Cadherins are transmembrane cell adhesion molecules (CAM) that maintain cell-to-cell contacts. By enhancing translation of SNAIL, YB-1 downregulates expression of epithelial cadherin (E-cadherin), one of the steps necessary for EMT (Evdokimova et al., 2009). Furthermore, YB-1 regulates matrix-metalloproteinase-1 (MMP1) expression which is crucial for remodeling of the ECM during invasion (Lim et al., 2019). Knockdown of YB-1 was reported

to significantly reduce invasive capacity in MPM (Johnson et al., 2018), melanoma (Kosnopfel et al., 2018) and triple-negative breast cancer (TNBC) (Lim et al., 2019).

YB-1 is secreted into the extracellular space upon certain stresses such as lipopolysaccharide (LPS) treatment (Frye et al., 2009). During oxidative stress, YB-1 upregulates expression of Ras GTPase-activating protein-binding protein 1 (G3BP1) which is essential for stress granule formation and increases metastatic capacity and invasion in sarcoma cells (Somasekharan et al., 2015). It was also shown that secreted YB-1 increases motility and proliferation rates in kidney cells (Frye et al., 2009).

As a result of the multifunctionality of YB-1, it is involved in virtually all of Hanahan and Weinberg's hallmarks of cancer (Figure 11). Lasham and colleagues argue that YB-1 is a master regulator of malignancy deserving of the same status as other multi-potent oncogenes such as Ras and Myc (Lasham et al., 2013).

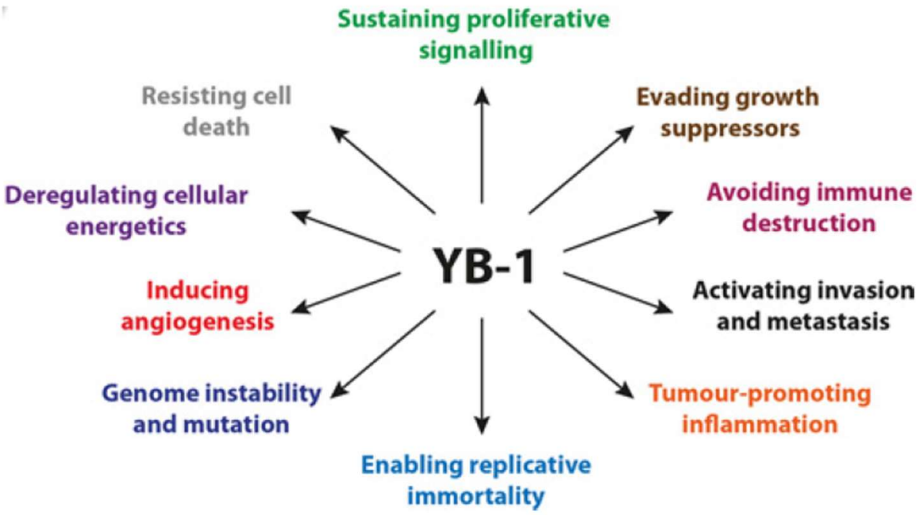

Figure 11: Involvement of YB-1 in the hallmarks of cancer (Lasham et al., 2013)

1.3.2. Localization and post-translational modifications of YB-1

Localization and activity of YB-1 is governed by various post-translational modifications (Figure 12). YB-1 is phosphorylated at Serine 102 (Ser102) by Akt (Sutherland et al., 2005) and p90 ribosomal S6 kinase (RSK) (Mendoza et al., 2011). Phosphorylation at this site leads to nuclear localization of YB-1 in melanoma cells (Kosnopfel et al., 2018). When YB-1 is mutated and phosphorylation at Ser102 is blocked, YB-1 predominantly stays in the cytoplasm and increases tumorigenicity and metastatic capacity of melanoma cells *in vitro* and *in vivo* (Kosnopfel et al., 2018). Localization of YB-1 also seems to be linked to cell cycle progression. During G_1 and S phase, YB-1 is mainly found to be perinuclear and relocates to the nucleus during transition from G_2 to M phase (Mehta et al., 2020b). Dephosphorylation at Ser102, 165 and 176 is reported to be required for this process as it increases accessibility of the nuclear localization signal (NLS) (Mehta et al., 2020b). YB-1 is also reported to be critically involved in microtubule organization during cytokinesis and knockdown of YB-1 results in cytokinesis failure in zebrafish (Mehta et al., 2020a).

Nuclear factor erythroid 2-related factor 2 (NRF2) is a TF which regulates expression of several antioxidant proteins to protect cells from ROS. Deacetylation of YB-1 at Lysine 81 (Lys81) is reported to be required for translation of NRF2 (El-Naggar et al., 2019). Hyperacetylation of YB-1 at this residue mediated by histone deacetylase (HDAC) class I inhibitor entinostat blocks translation of NRF2 and other stress factors, dramatically reducing metastasis formation of Ewing sarcoma cells *in vivo* (El-Naggar et al., 2019).

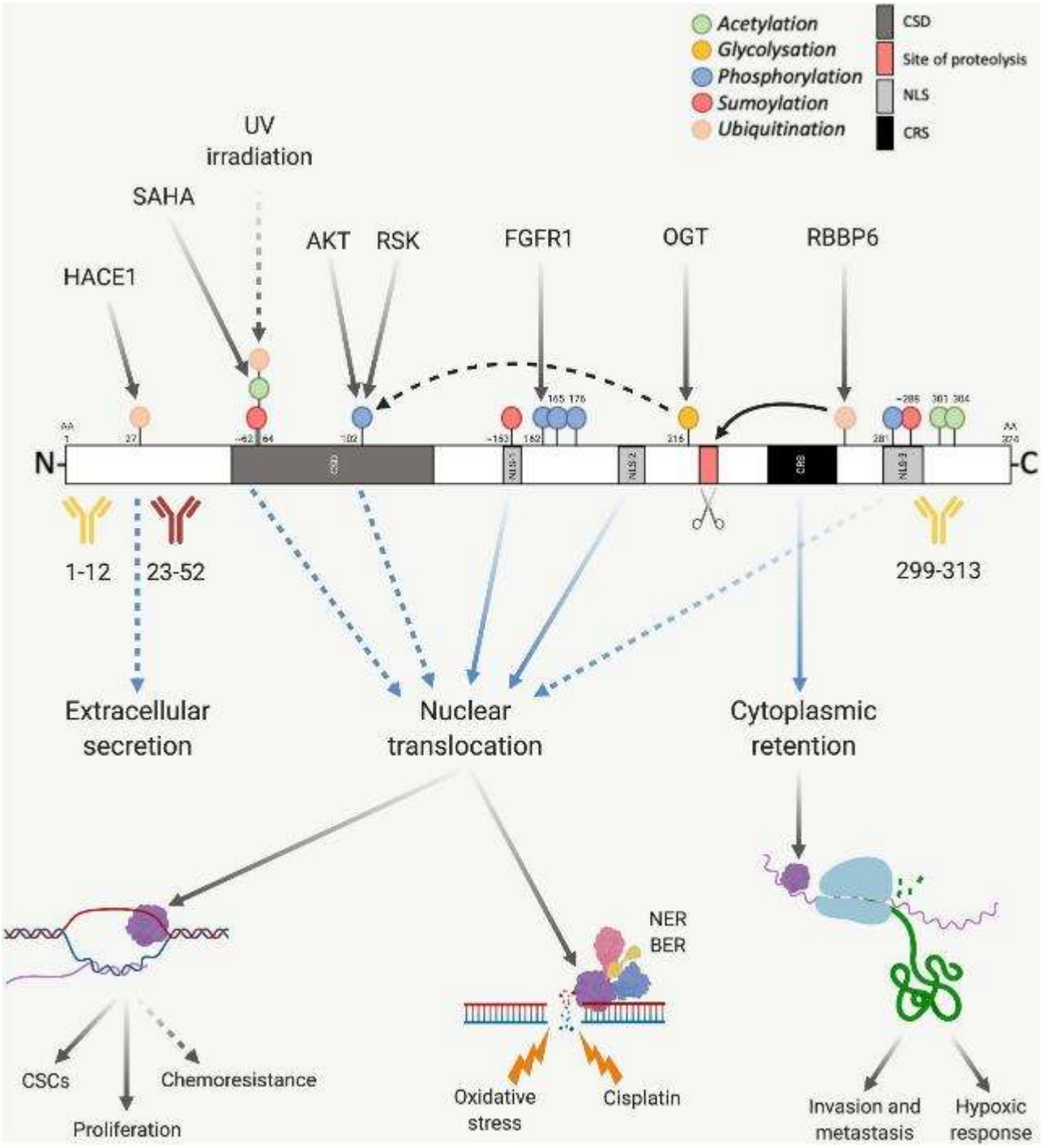

Figure 12: Reported post-translational modifications of YB-1 (Johnson et al., 2019)

1.4. Hypothesis and aims

MPM is a rare but aggressive cancer with poor prognosis. Standard of care treatment has not changed in the past decade and new therapeutic options are desperately needed. YB-1 is critically involved in invasion, metastasis and resistance to chemotherapy in several cancers, including MPM. Strong evidence supports the notion that YB-1 drives resistance to platinum-based chemotherapeutics such as cisplatin – which is part of the standard of care treatment for patients with MPM. Despite this knowledge, there are no studies exploring the effects of inhibition of YB-1 on cisplatin resistance in MPM.

We hypothesize that YB-1 plays a crucial role in aggressive behavior and resistance to chemotherapy in MPM cells. This thesis aimed to assess the impact of YB-1 overexpression on proliferation, migration, invasion and chemoresistance in MPM cell lines. Furthermore, the effects of siRNA-mediated knockdown of YB-1, inhibition of phosphorylation and stabilization of acetylation are explored.

2. MATERIALS AND METHODS

2.1. Cell culture

Adherent MPM cells were cultured in cell culture-treated polystyrene 25 cm^2 flasks (CytoOne) in an incubator at 37 °C and 5% CO_2. Cells were passaged twice a week and diluted 1:5 or 1:20 (dependent on their proliferation rate) and supplied with 5 ml of Roswell Park Memorial Institute (RPMI) medium supplemented with 10% fetal calf serum (FCS, Biowest). For passaging, used up medium was discarded and cells were washed with phosphate-buffered saline (PBS). Subsequently, PBS was discarded. For adherent cell detachment, 400 µl of trypsin/ethylenediaminetetraacetic acid (EDTA, Sigma-Aldrich) were added and cells were incubated for 5 min at 37 °C and 5% CO_2 in an incubator. Following detachment, trypsin was inactivated by addition of 5 ml RPMI medium supplemented with 10% FCS (R10). Cells were split according to their respective doubling times. No antibiotics were used for cell lines without transgenes.

For freezing culture backups, cells were trypsinized, trypsin was inactivated with 5 ml R10 and cell suspensions were centrifuged at 300 x g for 5 min. Media were discarded and cell pellets were resuspended in R10 and 5% (v/v) DMSO (Amresco). Cells were frozen slowly at a rate of 1 °C per minute in a cryo-freezing container.

MPM cell lines used for experiments can be seen in Table 2.

Table 2: List of MPM cell lines used for experiments.

Cell line	Type	Transgene	Source
MM05	Biphasic	-	The Prince Charles Hospital, Brisbane
MSTO	Biphasic	-	ATCC, Rockville
SPC212	Biphasic	-	University of Zurich
VMC40	Biphasic	-	Medical University of Vienna
MM05 Y	Biphasic	Dox-inducible YB-1	Grusch lab, Medical University of Vienna
MSTO Y	Biphasic	Dox-inducible YB-1	Grusch lab, Medical University of Vienna
SPC212 Y	Biphasic	Dox-inducible YB-1	Grusch lab, Medical University of Vienna
VMC40 Y	Biphasic	Dox-inducible YB-1	Grusch lab, Medical University of Vienna
SPC212 pYB-1	Biphasic	Stable overexpression of YB-1	Asbestos Disease Research Institute, Sydney

10 x PBS:

80 g/l NaCl (Merck)
2 g/l KCl (Merck)
17.8 g/l NaH_2PO_4 (Merck)
2.4 g/l KH_2PO_4 (Merck)

2.2. Cell treatment and drugs

2.2.1. Doxycycline-inducible overexpression

Previously laboratory-established doxycycline-inducible YB-1 overexpression cell models were used to assess effects of YB-1 overexpression. In these models, exogenous *YBX1* gene controlled by 3rd generation tetracycline (Tet) responsive promoter was introduced via retroviral transduction. Overexpression was induced by supplementation of 100 ng/ml doxycycline (Sigma Aldrich).

Figure 13 displays a schematic representation of the Tet-On system. The expression plasmid was designed to harbor a puromycin resistance gene. Cells were selected once a week by adding 0.8 µg/ml puromycin (Thermo Scientific). The plasmid map can be seen in Figure 14.

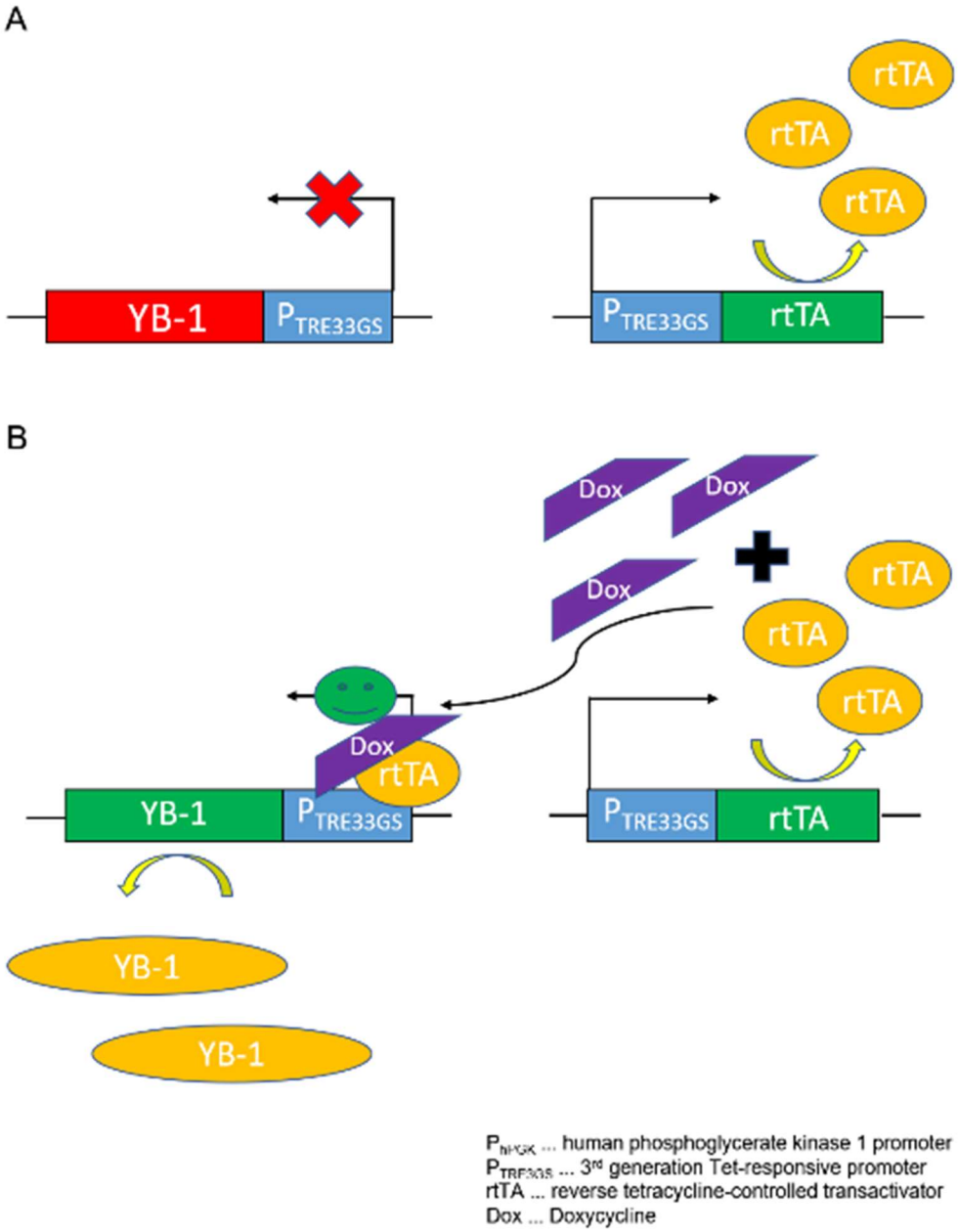

Figure 13: Schematic overview of the Tet-On system used for induced overexpression of YB-1. ***A****: Reverse tetracycline-controlled transactivator (rtTA) is constantly expressed under human phosphoglycerate kinase 1 promoter (P_{hPGK}). Without doxycycline (Dox) supplementation, rtTA is unable to bind and activate the 3rd generation Tet-responsive promoter (P_{TRE3GS}).* ***B****: When Dox is supplemented with the culture media, rtTA undergoes a conformational change and can now bind P_{TRE3GS}, thereby activating transcription of YB-1.*

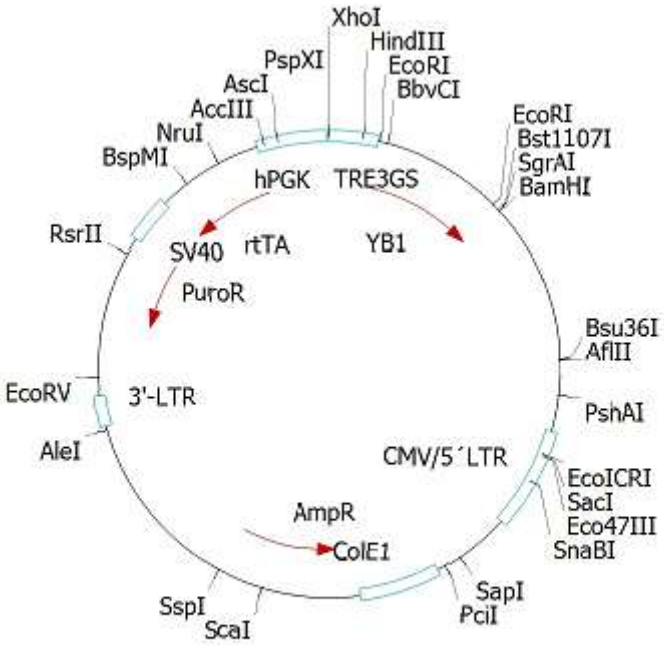

Figure 14: Plasmid map of doxycycline-inducible Tet-On system used for YB-1 overexpression. The reverse tetracycline-controlled transactivator (rtTA) is constantly expressed under the human phosphoglycerate kinase 1 promoter (hPGK). YB-1 is controlled by the 3rd generation Tet-responsive promoter (TRE3GS). Puromycin resistance (PuroR) gene expression for cell culture selection is controlled by the simian virus 40 (SV40) promoter.

2.2.2. Reverse transfection of small interfering RNA (siRNA)

Small interfering RNA (siRNA) was used to temporarily knockdown YB-1 expression via reverse transfection. Lipofectamine RNAiMAX (Thermo Scientific) was diluted in serum-free RPMI (R0) medium to obtain a 1% solution and incubated for 5 min at room temperature (RT). Final concentrations of siRNA ranging from 0.1 nM to 10 nM were prepared in R0 medium. This was done by preparing siRNA at 12 x the desired final concentration, since the siRNA would be further diluted 12 x in the final volume (e.g. 10 µl siRNA in a final volume of 120 µl). The 1% lipofectamine solution was added to the siRNA and the mixture was incubated for at least 20 min at RT. Subsequently, the lipofectamine and siRNA mixture was added to the middle of the well of 6-well plates (CytoOne), flat bottom 96-well plates (CytoOne) or 8-well chamber slides (Thermo Scientific). Then the desired cell number suspended in R10 was added. Cells were incubated at 37 °C and 5% CO_2 in an incubator. Used ratios of cell

suspension volumes to lipofectamine and siRNA volumes can be seen in Table 3. Sequences used for siRNA-mediated knockdown of YB-1 are listed in Table 4.

Table 3: Lipofectamine, siRNA and cell suspension ratios used for reverse transfection.

	96-well plate	**6-well plate**	**8-well chamber slide**
Lipofectamine 1%	10 µl	200 µl	30 µl
siRNA	10 µl	200 µl	30 µl
Cell suspension	2 x 10^3 cells in 100 µl	2 x 10^5 cells in 2 ml	1.5 x 10^4 cells in 300 µl

Table 4: siRNA sequences used for knockdown of YB-1 (GenePharma).

	Sequence (5' – 3')
siRNA (*YBX1*)	UUUGCUGGUAAUUGCGUGGAGGACC
Non-silencing siRNA	ACGUGACACGUUCGGAGAATT

2.2.3. Cisplatin

Cisplatin was dissolved in 1.5 ml dimethyl formamide (DMF) and 6.7 ml R0 to make a 10 mM stock solution and stored in 50 µl aliquots at -20 °C. As some precipitation was observed, 50 µl PBS was added to fully dissolve cisplatin to make a 5 mM solution before use. Cisplatin was used in final concentrations ranging from 0.5 µM to 15 µM. Each aliquot was only thawed once and leftovers were discarded after the experiment.

Cisplatin (10 mM):

25 mg Cisplatin (Sigma-Aldrich)
1.5 ml DMF (Sigma-Aldrich)
6.7 ml R0

2.2.4. BI-D1870

BI-D1870 was dissolved in DMSO as a 10 mM stock solution. Aliquots were stored at -20 °C. BI-D1870 was used in final concentrations ranging from 1 µM to 15 µM. DMSO was used as vehicle control.

BI-D1870 (10 mM):

5 mg BI-D1870 (Santa Cruz)
1.2774 ml DMSO

2.2.5. Entinostat

Entinostat was dissolved in DMSO as a 50 mM stock solution. Stock solution was further diluted with DMSO and 5 mM aliquots were stored at -20 °C. Entinostat was used in final concentrations ranging from 0.5 µM to 15 µM. DMSO was used as vehicle control.

Entinostat (50 mM):

10 mg Entinostat (Selleckchem)
0.5313 ml DMSO

2.3. Assays and experiments

2.3.1. Combination treatment / proliferation assay

For evaluation of MPM cell proliferation, 2 x 10^3 MPM cells per well were seeded into tissue culture-treated flat bottom 96-well plates in 100 µl R10. Next day, R10 medium containing various combinations and concentrations of cisplatin, entinostat and BI-D1870 was added and cells were incubated at 37 °C and 5% CO_2 for 24 to 72 hours.

A detailed list of used treatments and final concentrations can be seen in Table 5. Treatment combinations, respective concentrations and volumes can be seen in Table 6. For YB-1

knockdown, siRNA targeting YB-1 was reverse transfected as described in chapter 2.2.2. Twenty-four hours after reverse transfection, treatments were added.

After incubation, media containing dead cells were discarded and plates were frozen at – 80°C overnight. Next day, plates were thawed at RT for 45 min and 200 µl lysis buffer containing 0.025 µl SYBR green I (10,000 x, Invitrogen) DNA dye were added to the wells. Cells were incubated at RT for 2 hours protected from light. Fluorescence intensity was measured on a Tecan Infinite M200 Pro plate reader (excitation 485 nm, emission 535 nm).

MPM cell proliferation was evaluated under different treatment combinations. From these results, combination indices (CI) were calculated using compusyn software based on the Chou-Talalay method (Chou and Talalay, 1983). This method allows to calculate if the effect of a specific treatment combination is additive (CI = 1), antagonistic (CI > 1) or synergistic (CI < 1). If the combination of two treatments leads to a bigger effect than their added individual effects, the drugs are synergistic. If the combination leads to smaller effects, the drugs are antagonistic. The potency of a synergistic or antagonistic interaction is determined by the deviation of the CI from 1 (Chou, 2006).

Table 5: Different treatments and their respective final concentrations used for SYBR green-based proliferation assays.

Treatment	Doxycycline	Cisplatin	siRNA	BI-D1870	Entinostat
Final conc.	100 ng/ml	0.5 – 15 µM	0.1 – 10 nM	1 – 15 µM	0.5 – 15 µM

20 x Lysis buffer:

200 mM Tris HCl pH = 8.0
50 mM EDTA
2% (v/v) Triton X-100 (Serva)

Table 6: Treatment combinations, their respective prepared concentrations and volumes used for SYBR green-based proliferation assays. Apart from siRNA, all treatments were prepared in R10 medium.

	Treatment	Cell suspension	Prepared conc. in Vol.	Final volume
Combinations	Cisplatin	100 µl	4 x final conc. in 50 µl	200 µl
	Doxycycline		4 x final conc. in 50 µl	
	Cisplatin	120 µl	2 x final conc. in 120 µl	240 µl
	siRNA		12 x final conc. in 10 µl	
	Cisplatin	100 µl	4 x final conc. in 50 µl	200 µl
	BI-D1870		4 x final conc. in 50 µl	
	Cisplatin	100 µl	4 x final conc. in 50 µl	200 µl
	Entinostat		4 x final conc. in 50 µl	
	siRNA	120 µl	12 x final conc. in 10 µl	240 µl
	BI-D1870		2 x final conc. in 120 µl	
	siRNA	120 µl	12 x final conc. in 10 µl	240 µl
	Entinostat		2 x final conc. in 120 µl	

2.3.2. Clonogenic survival assay

For assessment of the clonogenic survival potential of MPM cell lines, they were seeded at a density of 1.5 x 10^3 cells per well in a 6-well plate in triplicates and supplied with 2 ml R10 medium. Doxycycline was added at a final concentration of 100 ng/ml to the treatment groups. MPM cells were inspected regularly and left to grow for up to 2 weeks in an incubator at 37 °C and 5% CO_2. Media and doxycycline were refreshed every 72 hours.

When clonogenic survival assays were stopped, media were removed and cells were washed with PBS. Colonies were fixed with 1 ml of 3:1 methanol/acetic acid for 30 min at RT. Fixation

solution was discarded and colonies were stained with 1 ml 1 x crystal violet staining solution for 20 min at RT. Staining solution was removed and cells were washed with distilled H_2O (dH_2O). Colonies were air-dried overnight and micrographs were taken.

For photometric quantification, colonies were destained with 2% (w/v) sodium dodecyl sulfate (SDS, Sigma-Aldrich) in PBS for 10 – 30 min on a shaker at RT. Absorbance was measured on a Tecan Infinite M200 Pro plate reader (560 nm).

Fixation solution (50 ml):

12.5 ml Acetic acid (Merck)
37.5 ml Methanol (PanReac AppliChem)

1,000 x Crystal violet staining stock solution (10 ml):

1 g Crystal violet (Roth)
10 ml Absolute ethanol (Scharlau)

2.3.3. Spheroid sprouting assay

Three g methyl cellulose (Sigma-Aldrich) were autoclaved. Next, 125 ml R0 mediu pre-warmed to 60 °C were added and stirred on a magnetic stirrer at RT for 20 min. Another 125 ml R0 medium pre-warmed to RT were added and stirred for 2 hours at 4 °C. Methyl cellulose was centrifuged at 4,000 x g at RT for 2 hours. Clear supernatant was aliquoted and stored at -20 °C. Before use, methyl cellulose was thawed, centrifuged at 4,000 x g for 30 min at RT and stored at 4 C.

For spheroid generation, 5 x 10^3 cells were suspended in 100 µl R10 medium and 20% (v/v) methyl cellulose and pipetted into 96-well U-bottom suspension plates (Greiner Bio-One). Plates were centrifuged at 5,000 x g at RT for 5 min. Before embedding, spheroids were incubated for 48 hours in an incubator at 37 °C and 5% CO_2.

The next day, 96-well flat bottom plates were coated with 50 µl 1% (w/v) low melting point ultrapure agarose (LMP, Life Technologies) and stored at 4 °C overnight. Therefore, 2% LMP agarose aliquots were prepared by adding 0.2 g of LMP agarose to 10 ml dH_2O and the mixture was briefly boiled to dissolve the agarose. Aliquots were stored at RT. For coating, 2% LMP agarose aliquots were melted at 100 °C for 10 min and diluted 1:1 with pre-warmed R0 medium.

The following day, spheroids were embedded in a collagen matrix. Collagen was prepared on ice according to the manufacturer's instructions. Next, 50 µl of medium were removed from 96-well U-bottom plates containing the spheroids and 50 µl of collagen were added. Subsequently, the spheroid/collagen mixture was transferred to the agar-coated 96-well flat bottom plates. Plates were incubated in an incubator at 37 °C and 5% CO_2 for 1 hour to facilitate hardening of the collagen matrix. Following incubation, 100 µl of R10 medium were added. Doxycycline was added to the treatment groups at a concentration of 250 ng/ml (2.5 x final concentration as the overall volume of agar coating, collagen, spheroids and medium was 250 µl). Plates were incubated for 72 hours in an incubator at 37 °C and 5% CO_2.

Micrographs were taken 1 hour after embedding and then every 24 hours. For each group, three to five spheroids were evaluated in three independent experiments. Lengths of ten sprouts per spheroid were analyzed using ImageJ software.

1 ml collagen (2 mg/ml):

100 µl 10 x PBS
13.8 µl 1 N NaOH (Merck)
286.2 µl dH2O
600 µl Collagen type I from rat tail (3.3 mg/ml, Corning)

2.3.4. Immunofluorescence staining

MPM cells were seeded onto 8-well chamber slides at a density of 1.5 x 10^4 cells in 300 µl of R10 medium and incubated at 37 °C and 5% CO_2. After 24 hours, 100 µl R10 medium containing 400 ng/ml doxycycline were added to the treatment groups (4 x final concentration,

as the overall volume of cell suspension and treatment was 400 µl). For siRNA-mediated knockdown of YB-1, used lipofectamine, siRNA and cell suspension ratios can be seen in Table 3. After an additional incubation of 24 hours at 37 °C and 5% CO_2, cells were fixed with 200 µl 4% (w/v) paraformaldehyde (PFA, Sigma-Aldrich) for 15 min at RT. PFA was removed and cells were washed with PBS three times for 5 min. Next, cells were blocked with 5% (w/v) bovine serum albumin (BSA, Sigma-Aldrich) in PBS and 0.3% (v/v) Triton X-100 for 1 hour at RT. Following blocking, cells were incubated in primary antibody in 1% BSA in PBS and 0.3% Triton X-100 in a humid chamber at 4 °C overnight. Cells were washed with PBS three times for 5 min and incubated in 200 µl secondary antibody in 1% BSA in PBS and 0.3% Triton X-100 for 1 hour at RT in a humid chamber and protected from light. Phalloidin-fluorescein isothiocyanate (FITC) and 4′,6-diamidin-2-phenylindol (DAPI) were also added in this step. Cells were washed with PBS three times for 5 min. Chamber slides were sealed with vectashield mounting medium (Vector). Additionally, nail polish was applied to the edges of the cover slips. Slides were stored at 4 °C protected from light.

Micrographs of immunofluorescence staining were taken on a ZEISS LSM700 confocal microscope.

Primary and secondary antibodies, their manufacturers, dilutions and blocking solution used can be seen in Table 7.

Table 7: Blocking solution, stainings, primary and secondary antibodies used for immunofluorescence.

Primary antibody	Manufacturer	Catalogue number	Dilution / conc.	Diluent in PBS
Sheep anti-YB-1*			1:1,000	1% (w/v) BSA and 0.3% (v/v) Triton-X
Secondary antibody				
Donkey anti-goat-Alexa Fluor 647	Invitrogen	A21447	1:1,000	1% (w/v) BSA and 0.3% (v/v) Triton-X
Stainings				
Phalloidin-FITC	Sigma-Aldrich	P5282	1:1,000	added to secondary antibody solution
DAPI	Sigma-Aldrich	D9542	1.5 µg/ml	added to secondary antibody solution
Blocking solution				5% (w/v) BSA and 0.3% (v/v) Triton-X

*Kindly provided by Prof. Antony Braithwaite, University of Otago, New Zealand

2.3.5. Xenograft experiment

2.3.5.1. Animals

Fourteen (n = 7) to nineteen (n = 2) week old female virgin severe combined immunodeficient (SCID) mice were used for a xenograft model. Animals were kept in a specific pathogen-free environment with a controlled 12 hour light–dark cycle. All procedures were performed in sterile condition in a laminar flow hood.

Experiments were done according to the regulations of the Ethics Committee for the Care and Use of Laboratory Animals at the Medical University Vienna (proposal number BMWF-66.009/0157-V/3b/2019), The U.S. Public Health Service Policy on Human Care and Use of Laboratory Animals as well as the United Kingdom Coordinating Committee on Cancer Prevention Research's Guidelines for the Welfare of Animals in Experimental Neoplasia.

2.3.5.2. Xenograft experiment

SPC212 cells stably overexpressing YB-1 (SPC212 pYB-1) were cultured in cell culture-treated polystyrene 75 cm^2 flasks (CytoOne) with R10 medium and left to grow in an incubator at 37 °C and 5% CO_2. For injection, SPC212 pYB-1 cells were prepared at a concentration of 1 x 10^7 cells/ml in either just R0 medium or R0 medium containing 25% (v/v) matrigel (Corning). Pipette tips, media and Eppendorf tubes were pre-cooled at 4 °C overnight before preparation. Matrigel was thawed and prepared on ice to avoid hardening.

SCID mice were injected subcutaneously into the right flank with 1 x 10^6 SPC212 pYB-1 cells in 100 µl R0 medium (four mice) or R0 medium with 25% matrigel (five mice) using pre-cooled needles.

Once a week tumor growth and weight were evaluated. After 14 weeks, mice were sacrificed by cervical dislocation.

2.4. RNA expression analysis

2.4.1. RNA isolation

For RNA isolation, 3 x 10^5 cells were seeded in 6-well plates in 2 ml R10 medium and incubated at 37 °C and 5% CO_2 for 24 hours. For induced overexpression of YB-1, doxycycline was added at a final concentration of 100 ng/ml to the treatment groups. For siRNA-mediated knockdown of YB-1, 5 nm siRNA were reverse transfected as described in chapter 2.2.2. After 24 hours, cells were washed with PBS and RNA was isolated using innuPREP RNA Mini Kit (Analytikjena) according to the manufacturer's protocol. All steps were performed at RT. In brief, 400 µl of lysis solution RL were added and cells were incubated for 2 min at RT. Cells were scraped off and incubated for another 3 min at RT. The lysed cell solutions were transferred to Spin Filter D columns and centrifuged for 2 min at 11,000 x g. Filtrates were transferred to Spin Filter R columns. Four hundred µl of 70% (v/v) ethanol were also added and whole volumes were mixed. The solutions were centrifuged for 2 min at 11,000 x g and the filtrates were discarded. Five hundred µl of Washing Solution HS were added to the columns and centrifuged at 11,000 x g for 1 minute. The filtrates were discarded, 700 µl Washing Solution LS were added to the columns and centrifuged at 11,000 x g for 1 minute. The filtrates were discarded and the columns were dried by centrifugation at 11,000 x g for 3 min. The columns were put into marked RNase-free elution tubes. Thirty µl RNase-free H_2O were added directly onto the filters of the columns and incubated for 1 minute. Lastly, the

columns were centrifuged at 11,000 x g for 1 minute and the isolated RNAs were stored at -20 °C for short term storage or -80 °C for long term storage.

RNAs were quantified using NanoDrop Spectrophotometer ND-1000 (Peqlab). Optical density was measured at 260 nm. Agarose gel electrophoresis was performed to check for RNA integrity.

2.4.2. Agarose gel electrophoresis

To check the quality of the isolated RNA, agarose gel electrophoreses were performed. Two µg of sample RNA were mixed with RNase-free H_2O to make up 10 µl and 4 µl Vistra Green loading dye were added. Samples were loaded onto gels containing 1.2% - 1.5% (w/v) low electroendosmosis agarose (Biozym) and 1 x Tris-borate EDTA buffer (TBE). Gels were run at 60 V for the first 20 min. Subsequently voltage was increased to 120 V for 60 min. RNA was inspected on a Gel Doc XR (Bio-Rad). If the isolated RNA was not degraded, cDNA was synthesized.

1 x TBE:

10.8 g/l Tris base (Sigma-Aldrich)
5.5 g/l Boric acid (Sigma-Aldrich)
4 ml/l 0.5 M EDTA, pH = 8.0

Vistra Green loading dye:

666 µl Loading dye (Fermentas)
700 µl dH_2O
500 µl 80% Glycerol (Merck)
133 µl 0.5 M EDTA
Vistra Green 10,000 x (Amersham)

2.4.3. Synthesis of cDNA

For reverse transcription from RNA to cDNA, 2 µg high quality RNA were diluted with RNAse-free H_2O for a total volume of 13 µl. For denaturation, samples were incubated at 70 °C for 10 min and subsequently put on ice. After cooling down, 7 µl cDNA Master-Mix were added and samples were incubated at 42 °C for 1 hour. Reverse transcription was stopped by denaturation of reverse transcriptase at 70 °C for 10 min. Lastly, cDNA was diluted 1:1 by adding 20 µl RNAse-free H_2O. Samples were stored at -20 °C.

1 x cDNA Master-Mix (7 µl total volume):

4 µl Reaction Buffer for RT (5 x, Thermo Scientific)
1 µl dNTPs (10 mM, Thermo Scientific)
0.5 µl RiboLock RNase Inhibitor (40 U/µl, Thermo Scientific)
0.5 µl Random Hexamer Primer (0.2 µg/µl, Thermo Scientific)
1 µl RevertAid Reverse Transcriptase (200 U/µl, Thermo Scientific)

2.4.4. Quantitative real time reverse transcription polymerase chain reaction (qRT-PCR)

For quantitative RNA expression level comparison, qRT-PCRs were performed. One µl of sample cDNA was pipetted into a Hard-Shell 96-well PCR Plate (Bio-Rad) and 11 µl iTaq Universal SYBR Supermix containing primers for the genes of interest were added. Samples were prepared in duplicates. Plates were sealed airtight with Microseal 'B' PCR Plate Sealing Film (Bio-Rad). PCRs were run on a C1000 Touch Thermal Cycler (Bio-Rad) using the conditions seen in Table 8. Every cycle, fluorescence intensity was measured. For normalization, the housekeeping genes *GAPDH* and *ACTB* were used. Primer sequences can be seen in Table 9.

2 x iTaq Universal SYBR Green Supermix (11 µl per sample):

12.5 µl iTaq Universal SYBR Green Supermix (Bio-Rad)
1 µl Forward primer 1 µl (20 µM)
1 µl Reverse primer 1 µl (20 µM)
8.5 µl dH_2O

Table 8: Standard conditions for iTaq Universal SYBR Green qRT-PCR.

	Temperature (°C)	Time (min)	Repetitions
Stage 1	50	00:10	1 x
Stage 2	95	10:00	1 x
Stage 3	95	00:15	40 x
	60	01:00	

Table 9: Primers used for mRNA expression analysis via qRT-PCR.

Direction	Target	Sequence
Forward	*YBX1*	GGAGTTTGATGTTGTTGAAGGA
Reverse		TTCTTCTCTGGAGGGGACTG
Forward	*GAPDH*	AGCTCACTGGCATGGCCTTC
Reverse		ACGCCTGCTTCACCACCTTC
Forward	*ACTB*	ACTCTTCCAGCCTTCCTTC
Reverse		GATGTCCACGTCACACTTC

2.5. Protein analysis

2.5.1. Protein isolation

For protein isolation, 3×10^5 cells were seeded in 6-well plates in 2 ml R10 media and incubated at 37 °C and 5% CO_2 for 24 hours. Next day, treatments listed in Table 10 were added. For siRNA-mediated knockdown of YB-1, 1 nm and 5 nm final concentrations of siRNA were reverse transfected as described in chapter 2.2.2. Forty-eight hours after treatment or reverse transfection, proteins were isolated. Plates were put on ice and media were discarded. Cells were washed with PBS, PBS was discarded and 50 µl Lysis Buffer II (LB II) were added and cells were scraped off. Plates were incubated on ice for 10 min. Whole cell lysates were

transferred to 1.5 ml Eppendorf tubes and centrifuged at 13,000 x g and 4 °C for 10 min. Supernatants were transferred into marked Eppendorf tubes and stored at -20 °C.

Protein concentrations were evaluated by Bradford Protein Assay (Bio-Rad) according to the manufacturer's protocol. Absorbance was measured at 595 nm on a Tecan Infinite M200 Pro plate reader.

Table 10: Different treatments and their respective final concentrations used for protein isolation.

Treatment	Doxycycline	BI-D1870
Final conc.	100 ng/ml	1 µM &10 µM

Lysis Buffer II:

1 mM EDTA
150 mM NaCl
0.5 mM Na_3VO_4 (Sigma-Aldrich)
1.5 mM $MgCl_2$ (Merck)
10% Glycerol (Merck)
50 mM HEPES (PAA Laboratories)
10 mM NaF (Sigma-Aldrich)
1% (v/v) Triton X-100

2.5.2. SDS-Page

Samples were loaded on polyacrylamide gels and separated according to their molecular weight (kDa). For each sample, 15 – 25 µg were diluted with LB II and mixed with 5 x reducing Laemmli buffer. Samples were denatured at 100 °C for 5 min, put on ice and spun down. Next, samples were loaded on polyacrylamide (PAA) gels consisting of a 10% separating gel and a 3.75% stacking gel. PageRuler Prestained Protein Ladder (Thermo Scientific) was used as a marker. Gel electrophoresis was run on a Mini-PROTEAN Tetra Cell system (Bio-Rad) using a PowerPac HC system (Bio-Rad) at 60 V for 20 min and at 110 V after samples had reached the separating gel. The run was ended when the protein front reached the bottom of the gel.

3.75% PAA stacking gel (5 ml):

3.6 ml dH_2O
0.625 ml Tris 0.5 M pH = 8.8
0.1 ml 10% (w/v) SDS
0.625 ml 30% Acrylamide/Bis 29:1 (Bio-Rad)
50 µl APS (Merck)
7.5 µl Temed (Amresco)

10% PAA separating gel (15 ml):

5.88 ml dH_2O
3.75 ml Tris 1.6 M pH = 8.8
0.3 ml 10% (w/v) SDS
5.025 ml 30% Acrylamide/Bis 29:1 (Bio-Rad)
37.5 µl APS (Merck)
14 µl Temed (Amresco)

5 x Reducing Laemmli buffer:

300 mM Tris base pH = 6.8
60% (w/v) Glycerol
10% (w/v) SDS
0.025 % Bromophenolblue (Serva)
7% β-Mercaptoethanol (Sigma-Aldrich)

SDS-running buffer:

25 mM Tris base
192 mM Glycine (Bio-Rad)
0.1% (w/v) SDS

2.5.3. Western blot

Separated proteins were transferred onto Hypond-P polyvinylidene difluoride (PVDF) membranes (GE Healthcare) using a Mini-PROTEAN Tetra Cell system (Bio-Rad) according to the manufacturer's instructions. Before transfer, PVDF membranes were activated in methanol for a few seconds. Proteins were transferred at constant 300 mA for 1 hour at RT with an added pre-cooled ice pack in the buffer.

The quality of the transfer was examined via Ponceau S (Sigma-Aldrich) staining for 10 min. Membranes were blocked in 5% milk (Sigma-Aldrich) or 5% BSA in tris-buffered saline with 0.1% tween (TBS/T). Subsequently, membranes were incubated in primary antibody at 4 °C overnight. The next day, membranes were washed three times for 10 min in TBS/T and incubated in horse radish peroxidase (HRP)-linked secondary antibody for 1 hour at RT. Thereafter, membranes were washed three times for 10 min in TBS/T and finally once in TBS for 10 min. Bound antibodies were detected using a Clarity Western ECL Substrate kit (Bio-Rad). All washing steps were performed at RT.

Primary and secondary antibodies and dilutions used are seen in Table 11.

Table 11: Primary and secondary antibodies used for western blot development.

Primary antibody	**Manufacturer**	**Reference**	**Dilution**	**Diluent in TBS/T**
Rabbit anti-YB-1	Abcam	ab12148	1:1,000	3% BSA (w/v)
Rabbit anti-Phospho-YB-1 (Ser102)	Cell signaling	C34A2	1:1,000	5% BSA (w/v)
Mouse anti-β-actin	Sigma-Aldrich	A5441	1:2,000	5% BSA (w/v)
Secondary antibody				
Rabbit anti-mouse-HRP	Dako	P0260	1:10,000	2.5% milk (w/v)
Goat anti-rabbit-HRP	Dako	P0448	1:10,000	2.5% milk (w/v)

10 x Ponceau S stock solution (25 ml):

2% (w/v) Ponceau S (Sigma-Aldrich)
10% (v/v) Acetic acid
2.5 ml PBS (10 x)
20 ml dH_2O

10 x TBS (1 l):

80 g/l NaCl
2 g/l KCl
30 g/l Tris base

TBS/T:

1 x TBS
0.1% (v/v) Tween 20 (Sigma-Aldrich)

20 x Transfer buffer (1 l):

58.6 g/l glycine (Bio-Rad)
116.2 g/l Tris base
37.5 ml 20% (w/v) SDS

2.6. Statistical analysis

Data were analyzed using GraphPad Prism 8. Statistical differences were evaluated using two-tailed, unpaired Student's t-tests with 95% confidence intervals. Differences were considered statistically significant (*), very significant (**) and highly statistically significant (***) at $p < 0.05$, $p < 0.01$ and $p < 0.001$, respectively.

The half maximal inhibitory concentrations (IC_{50}s) were calculated by analyzing full dose-response curves using GraphPad Prism 8. Combination indices (CI) were calculated based on the Chou-Talalay method (Chou and Talalay, 1983) using CompuSyn software.

All data are shown as means ± standard deviation (SD).

3. RESULTS

3.1. Part 1: Impact of YB-1 overexpression in MPM cell lines

3.1.1. Doxycycline treatment induces overexpression of YB-1 in MPM cell lines transduced with the Tet-On system

To confirm the doxycycline-induced YB-1 overexpression, we looked at RNA and protein expression of our MPM cell line panel after doxycycline treatment.

As shown in Figure 15A, 24 hours after doxycycline treatment *YBX1* mRNA levels increased compared to untreated controls. Significant increases were found for MM05 Y ($p = 0.0102$) and SPC212 Y ($p = 0.0157$) with log2 fold changes of 1.9 and 1.7 respectively. *YBX1* mRNA overexpression did not reach statistical significance in MSTO Y ($p = 0.4233$) and VMC40 Y ($p = 0.3545$). The housekeeping genes *ACTB* and *GAPDH* were used for normalization.

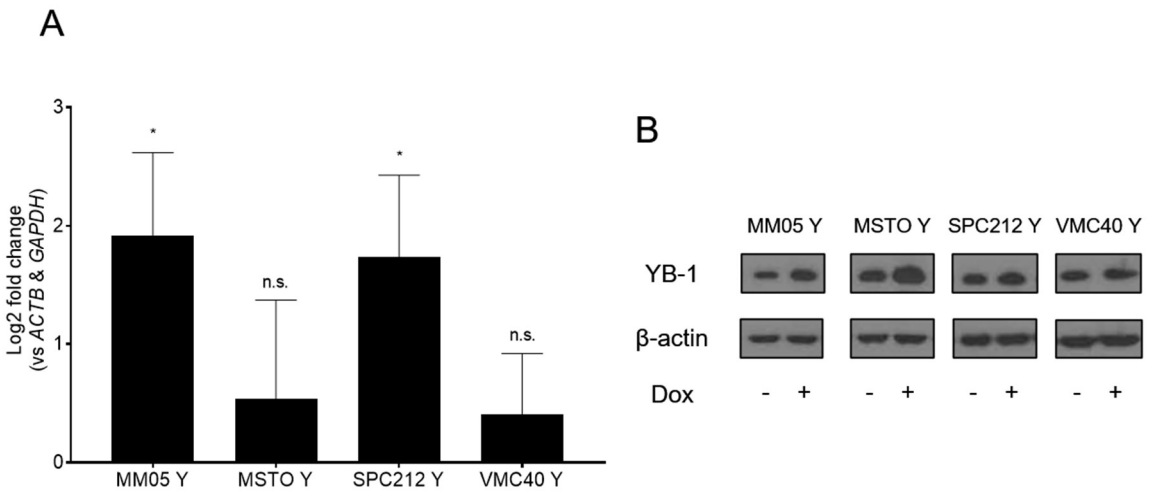

Figure 15: Tet-On system transduced MPM cells overexpressed YB-1 after doxycycline treatment at 100 ng/ml. ***A****: qRT-PCR analysis of our MPM cell panel. MM05 Y ($p = 0.0102$) and SPC212 Y ($p = 0.0157$) showed significant increases of YBX1 mRNA levels 24 hours after doxycycline treatment with log2 fold changes of 1.9 and 1.7 respectively. Overexpression did not reach statistical significance in MSTO Y and VMC40 Y compared to controls. Housekeeping genes ACTB and GAPDH were used for normalization.* ***B****: Western blot analysis of whole cell lysates of our MPM cell panel. MM05 Y, MSTO Y and SPC212 Y cells showed increased YB-1 protein levels 48 hours after doxycycline (Dox) treatment compared to controls (Co). The housekeeping protein β-actin was used as loading control.*

When looking at the protein level, doxycycline treatment induced a clear increase of YB-1 expression in MM05 Y, MSTO Y and SPC212 Y compared to controls after 48 hours (Figure 15B). The housekeeping protein β-actin was used as loading control. In SPC212 Y, overexpression was also investigated by immunofluorescence staining and a slight increase of YB-1 expression was found (Figure 16).

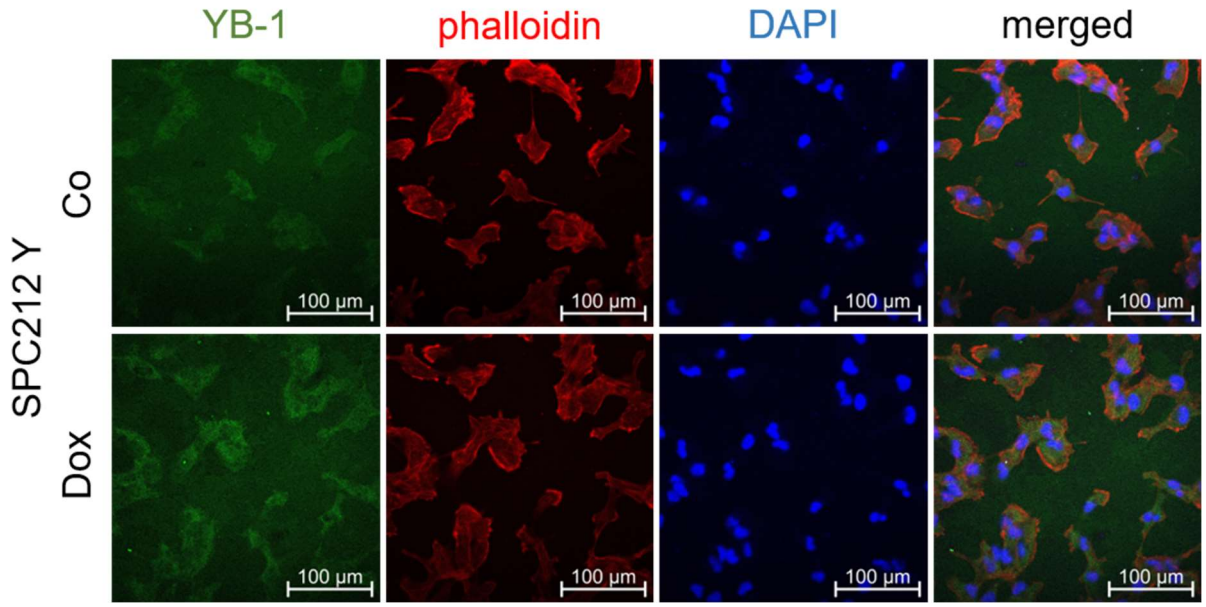

Figure 16: Immunofluorescence staining of SPC212 Y. YB-1 protein levels were slightly increased 48 hours after doxycycline treatment at 100 ng/ml compared to control. Phalloidin was used for visualization of the actin filaments and DAPI was used as nuclear counterstain.

3.1.2. YB-1 overexpression does not increase proliferation or cisplatin resistance in MPM cell lines

Overall, doxycycline increased YB-1 expression in at least 3 of the 4 cell models and thus we next investigated the impact of increased YB-1 on MPM cell proliferation. YB-1 overexpression did not alter proliferation of our MPM cell panel over the course of 72 hours in a SYBR green-based proliferation assay (Figure 17). MSTO Y was the fastest growing cell line, followed by SPC212 Y and MM05 Y while VMC40 Y cells displayed the lowest growth rate.

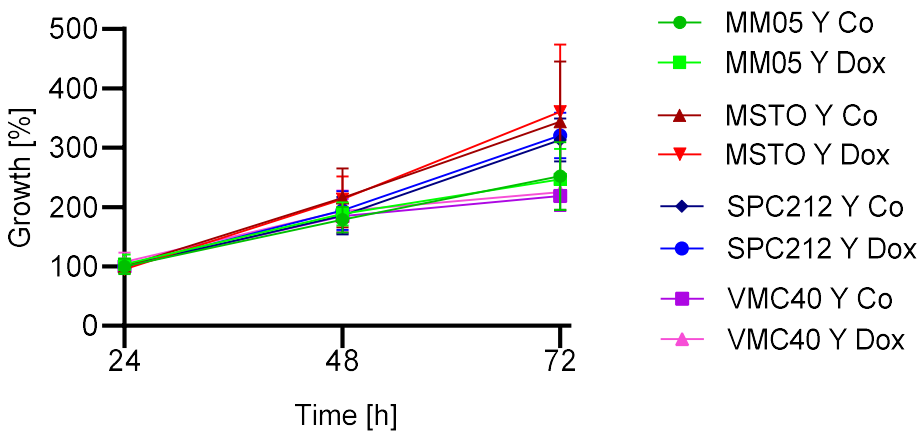

Figure 17: SYBR green-based proliferation assay of our MPM cell line panel depicted as percentual growth. Doxycycline (Dox)-induced YB-1 overexpression did not alter cell growth in a 72-hour time span compared to control (Co). MSTO Y cells showed the fastest growth, followed by SPC212 Y and MM05 Y. VMC40 Y was the slowest growing cell line in this panel.

Furthermore, YB-1 overexpression did not significantly increase clonogenicity in a clonogenic survival assay over a timespan of up to two weeks and even decreased clone formation in MM05 Y cells (p = 0.047) as quantified by photometric analysis of destained colonies (Figure 18).

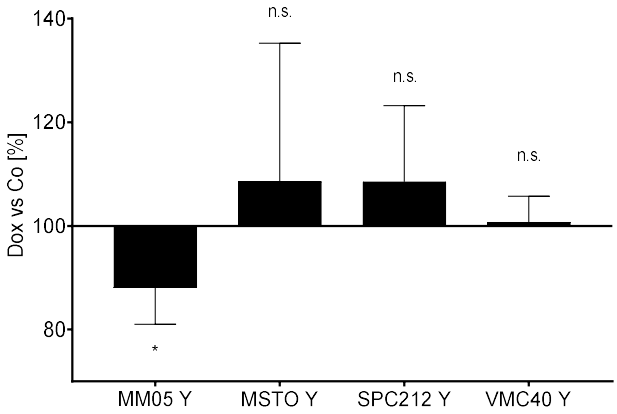

Figure 18: Clonogenic survival assay of our MPM cell line panel. Doxycycline (Dox) was added when cells were seeded. Dox and media were refreshed every 72 hours. The experiments were stopped before the clones grew confluent. Growth of Dox treated cells was compared to controls (Co).

YB-1 is associated with chemoresistance in multiple cancers (Johnson et al., 2019) and higher nuclear expression of YB-1 was observed in ovarian cancer cells with acquired cisplatin

resistance (Yahata et al., 2002). Therefore, we wanted to investigate whether induced YB-1 overexpression conferred resistance of our MPM cell line panel to the standard of care MPM therapeutic cisplatin. Doxycycline-induced overexpression of YB-1 did not increase resistance to cisplatin chemotherapy at concentrations of 1 µM to 15 µM for 48 hours (Figure 19A) and 72 hours (Figure 19B) in a SYBR green-based proliferation assay. The IC_{50} of cisplatin remained largely unchanged with doxycycline-induced overexpression of YB-1 at 48 hours and 72 hours. As expected, IC_{50} values were lower at 72 hours compared to 48 hours (Table 12).

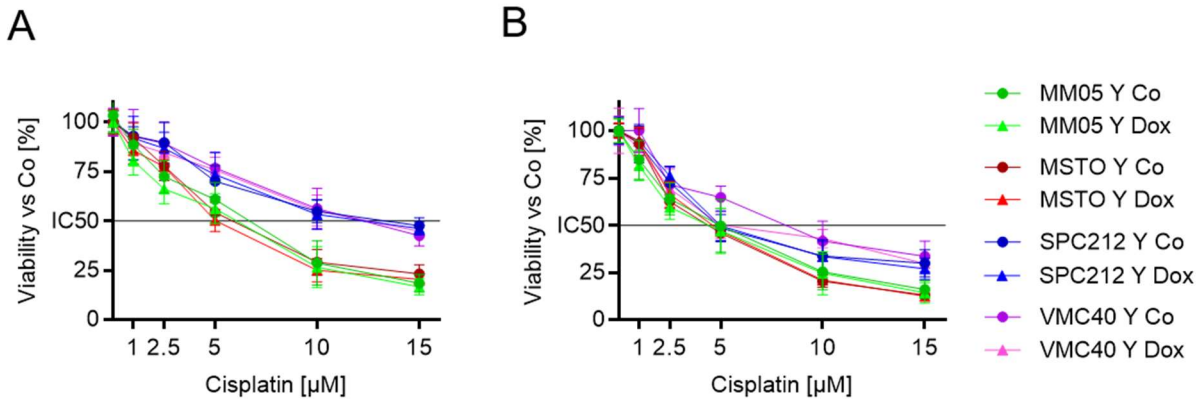

Figure 19: SYBR green-based proliferation assay of our MPM cell line panel. Doxycycline-induced overexpression of YB-1 (Dox) had no effect on resistance to cisplatin treatment as measured after 48 (A) and 72 (B) hours compared to controls (Co). Cell growth was nearly exactly the same at all cisplatin concentrations ranging from 1 µM to 15 µM.

Table 12: Cisplatin IC_{50} values of our MPM cell line panel after 48 and 72 hours with or without doxycycline-induced overexpression of YB-1.

	IC_{50} [µM]			
	48 hours		**72 hours**	
	Co	**Dox**	**Co**	**Dox**
MM05 Y	5.66	4.69	4.31	3.81
MSTO Y	5.68	4.98	4.10	4.35
SPC212 Y	12.40	12.14	5.74	5.83
VMC40 Y	12.16	12.80	7.78	6.24

3.1.3. YB-1 overexpression induces scattering and EMT-like changes in MPM cells and increases invasiveness of VMC40 Y

Although doxycycline-induced overexpression of YB-1 had limited effects on proliferation, we noticed EMT-like changes in the clonogenic survival assays. MPM cells switched from polygonal to more elongated shapes, had reduced cell cell contacts and showed enhanced scattering (Figure 20).

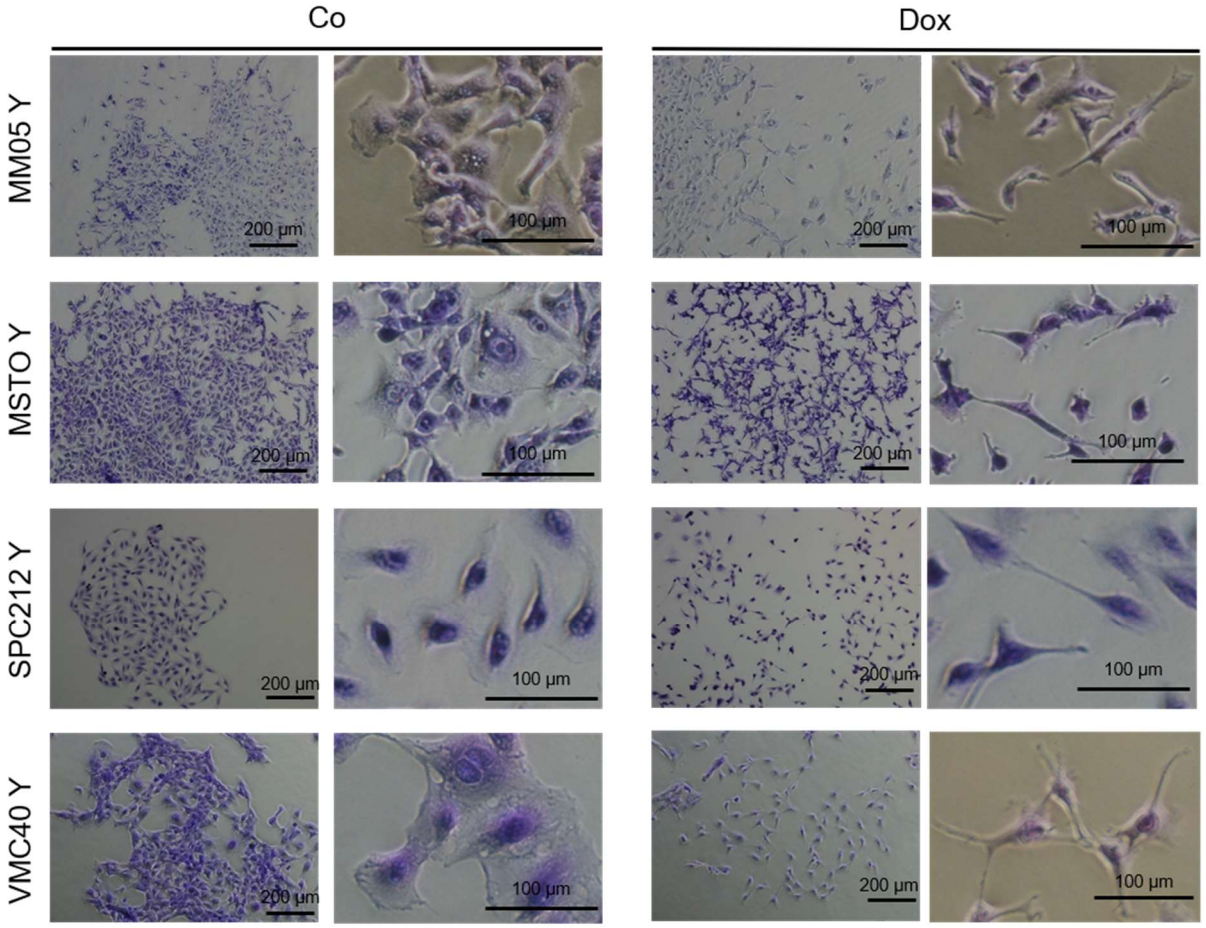

Figure 20: Micrographs of clonogenic survival assays of our MPM cell line panel. Doxycycline-induced overexpression of YB-1 (Dox) enhanced scattering compared to controls (Co). YB-1 overexpression also led to EMT-like morphology changes, as displayed by MPM cells switching from polygonal to more elongated shapes.

YB-1 overexpression was also reported to promote EMT and migration in lung adenocarcinoma cells (Ha et al., 2015). Additionally, considering the behavioral changes prompted by overexpression of YB-1, we wanted to examine its effects on invasiveness of

MPM cells. Indeed, we found that VMC40 Y cells produced longer sprouts in a collagen matrix when overexpression was induced (Figure 21). Generally, in the untreated controls, MSTO Y produced the longest sprouts with an average length of 1.79 mm at 72 hours, followed by SPC212 Y (0.68 mm) and VMC40 Y (0.65 mm) while MM05 Y produced the shortest sprouts with an average length of 0.63 mm (Figure 22A-D). At endpoint, average sprouting length was significantly higher for doxycycline treated VMC40 Y compared to controls ($p = 0.0023$, Figure 22D). MM05 Y, SPC212 Y and MSTO Y showed no significant differences although average sprout length was markedly shorter for doxycycline treated MSTO Y (Figure 22B, 1.36 mm vs 1.79 mm). Representative micrographs of tumor spheroids 24 hours, 48 hours and 72 hours after seeding can be seen in Figure 23.

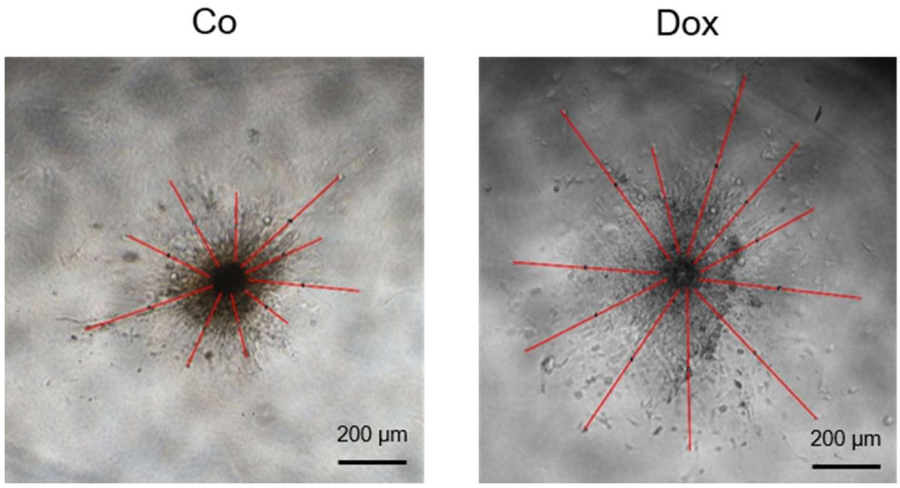

Figure 21: Spheroid sprouting assay of VMC40 Y 72 hours after embedding in a collagen matrix. Doxycycline induced overexpression of YB-1 (Dox) led to increased invasion and longer sprouts compared to controls (Co). Red lines indicate measured sprouting lengths.

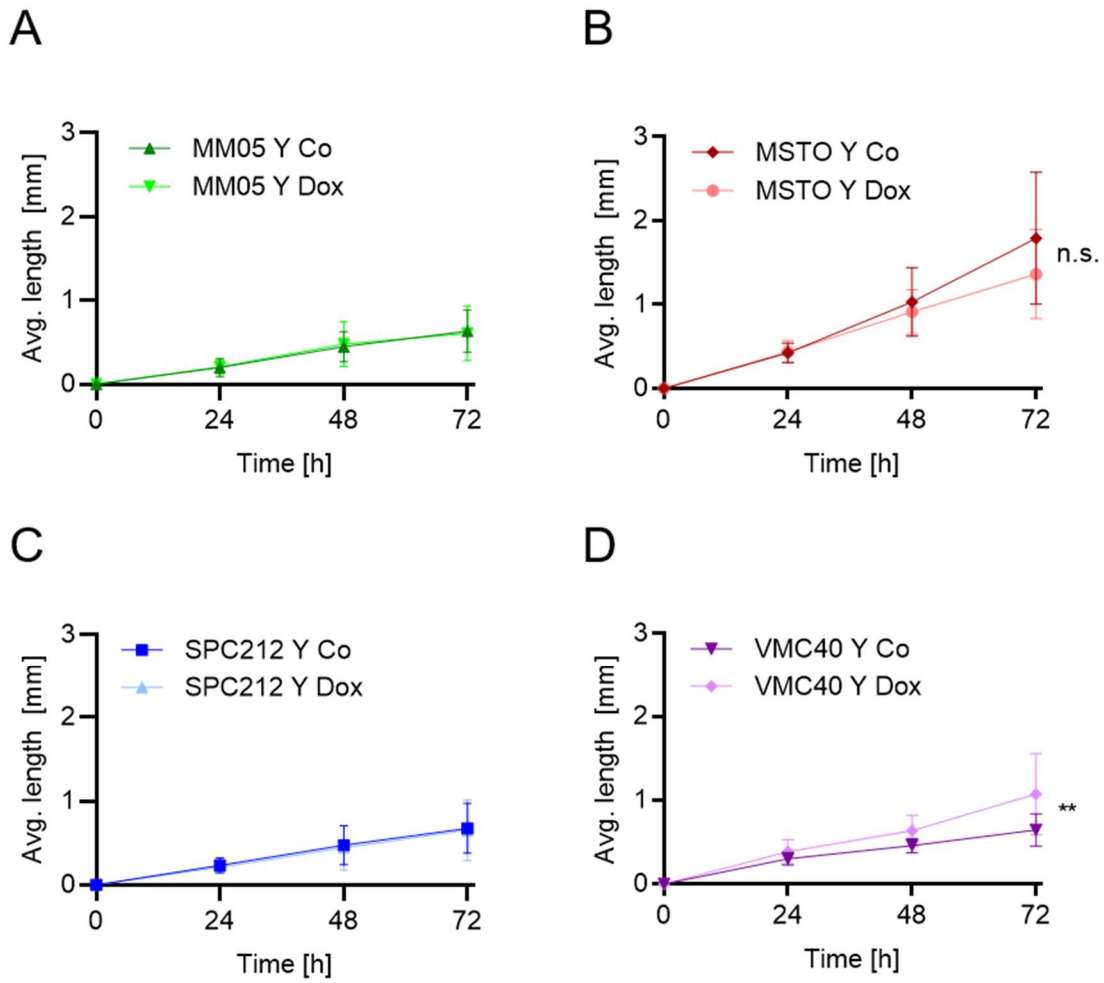

Figure 22: Spheroid sprouting assay of our MPM cell line panel in a collagen matrix with Doxycycline-induced overexpression of YB-1 (Dox) compared to controls (Co) over the course of 72 hours. ***A,C:*** *Sprouting length was not altered in MM05 Y and SPC212 Y when YB-1 was overexpressed.* ***B:*** *YB-1 overexpression in MSTO Y led to shorter sprouts, although the difference was not statistically significant.* ***D:*** *VMC40 Y produced significantly longer sprouts when YB-1 was overexpressed after doxycycline treatment compared to controls.*

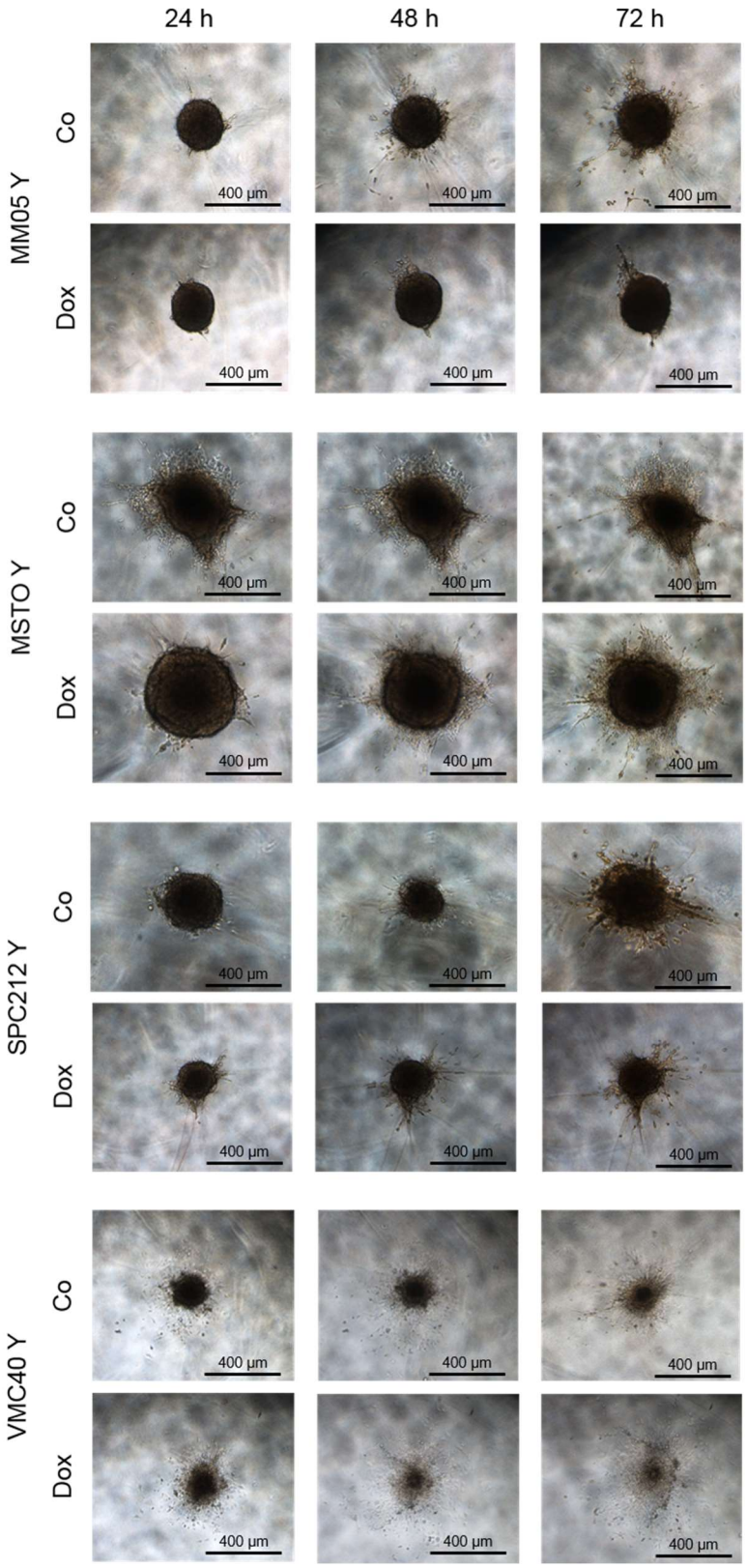

Figure 23: Representative micrographs of spheroid sprouting assay of doxycycline-induced overexpression of YB-1 (Dox) compared to controls (Co) in our MPM cell line panel. Micrographs were taken every 24 hours.

3.1.4. Stable overexpression of YB-1 does not induce tumorigenicity of non-tumorigenic MPM cells *in vivo*

From a previous experiment in our laboratory it was known that SPC212 MPM cells are not tumorigenic in SCID mice. We showed that overexpression of YB-1 in MPM cells can lead to increased invasion and scattering and induce EMT-like morphology changes. Therefore, we also investigated whether overexpression of YB-1 could induce tumor growth *in vivo* in a non-tumorigenic MPM cell line. To avoid having to feed our mice daily with doxycycline, we chose previously generated SPC212 pYB-1 cells, as they stably overexpress YB-1. Female virgin SCID mice were injected with 1 x 10^6 SPC212 pYB-1 cells (n = 4), however, no tumors formed over the course of 14 weeks. This picture did not change when matrigel was added to the injection (25%, n = 5). At endpoint, mice were asymptomatic and lymph nodes adjacent to the injection sites were healthy.

3.2. Part 2: Targeting YB-1 in MPM cells

Since YB-1 is highly expressed in many MPM cells and supports malignant behavior, we evaluated the therapeutic potential of inhibiting YB-1 using different targeting strategies.

3.2.1. Drug-induced growth inhibition of MPM cells

3.2.1.1. Knockdown of YB-1 via siRNA inhibits growth of MPM cells effectively

As knockdown of YB-1 was reported to reduce viability of non-small cell lung cancer cells (NSCLC) (Zhao et al., 2016) and MPM cells (Johnson et al., 2018) and high expression of YB-1 correlates with poor patient outcomes in MPM (Johnson et al., 2019), we wanted to investigate the effects of siRNA-mediated knockdown of YB-1 in our MPM cell line panel.

First, we tested the efficacy of siRNA-mediated knockdown of YB-1. As shown in Figure 24A, mRNA levels of YB-1 were markedly reduced 24 hours after reverse transfection with 5 nM siRNA. SPC212 showed the biggest decrease in YB-1 mRNA transcripts with a log2 fold change of -5.5, followed by MSTO (-4.429), VMC40 (-3.42) and MM05 (-2.854). We also observed the siRNA-mediated knockdown on protein level. YB-1 protein expression was markedly reduced 48 hours after reverse transfection with 1 nM and 5 nM YB-1 siRNA in MM05 and SPC212 MPM cells as shown by western blot (Figure 24B) and by 1 nM YB-1 siRNA in SPC212 as shown by immunofluorescence staining (Figure 25).

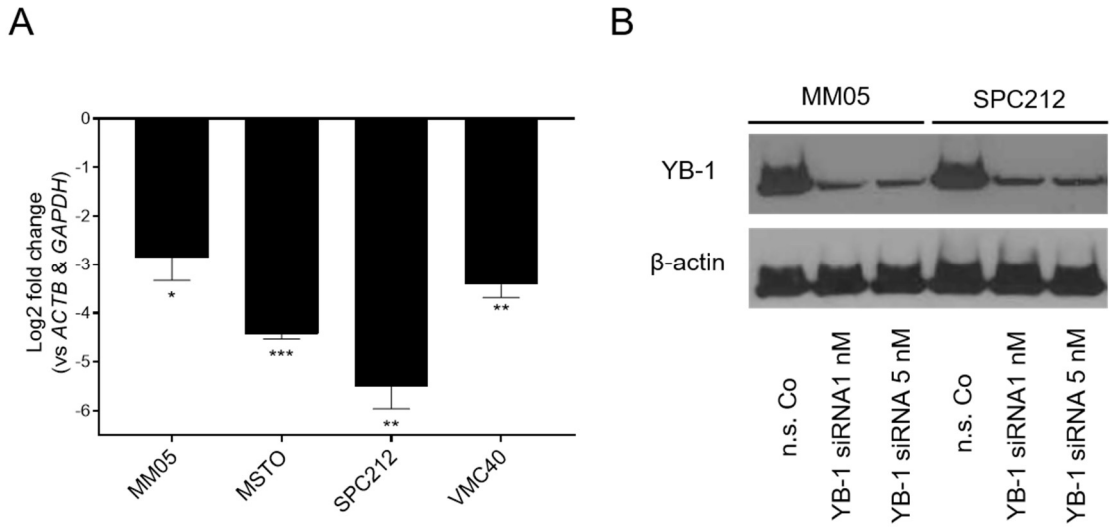

*Figure 24: YB-1 knockdown mediated by reverse transfection with siRNA. **A**: RT-qPCR of our MPM cell line panel 24 hours after reverse transfection with 5 nM YB-1 siRNA. All cell lines showed a marked decrease in YB-1 mRNA expression compared to 5 nM non-silencing control (n.s. Co). **B**: Western blot of MM05 and SPC212 48 hours after reverse transfection with 1 nM and 5 nM YB-1 siRNA. Both cell lines displayed a strong decrease in YB-1 protein even at 1 nM concentration, compared to 5 nM n.s. Co. Housekeeping protein β-actin was used as loading control.*

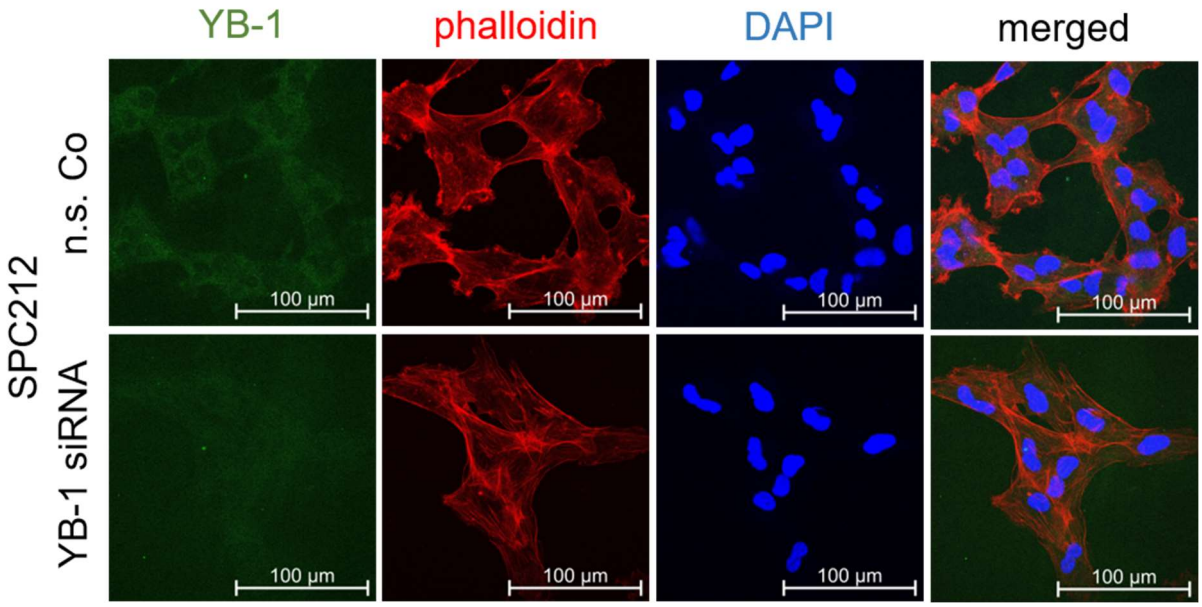

Figure 25: Immunofluorescence staining of YB-1 48 hours after reverse transfection with 1 nM YB-1 siRNA in SPC212. YB-1 protein expression was decreased compared to 1 nM non-silencing control (n.s. Co). Actin filaments were stained with phalloidin and DAPI was used to stain the nuclei.

Next, we wanted to examine the effects of siRNA-mediated knockdown of YB-1 on proliferation in our MPM cell line panel (Figure 26). SPC212 and MSTO were most sensitive to YB-1 knockdown with IC_{50}s of 0.48 nM and 0.67 nM respectively at 96 hours. VMC40 was more resistant with an IC_{50} of 2.9 nM. We did not reach IC_{50} experimentally for MM05 as the biggest reduction of cell viability was 28.1% at 5 nM siRNA.

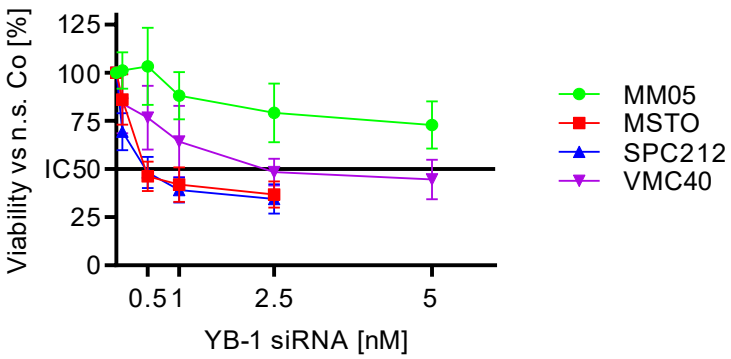

Figure 26: SYBR green-based proliferation assay of our MPM cell line panel 96 hours after reverse transfection of YB-1 siRNA compared to non-silencing control (n.s. Co). In MSTO and SPC212 2.5 nM n.s. Co siRNA were transfected whereas 5 nM n.s. Co siRNA were transfected in MM05 and VMC40.

3.2.1.2. BI-D1870 inhibits phosphorylation of YB-1 at Ser102 in SPC212 and inhibits growth of MPM cells partially in a YB-1 dependent manner

Phosphorylation of YB-1 was reported to be required for its function in cytokinesis (Mehta et al., 2020a). We tested the inhibitor BI-D1870 to assess whether blocking phosphorylation would mimic the knockdown. BI-D1870 is a specific inhibitor of p90 ribosomal S6 kinase (RSK) 1-4 (Sapkota et al., 2007) thereby inhibiting phosphorylation of downstream YB-1 at Ser102. Western blot analysis showed that BI-D1870 inhibited phosphorylation of YB-1 at Ser102 at a concentration of 10 µM in SPC212 (Figure 27). In MM05, Ser102 phosphorylation was not affected at the used concentrations.

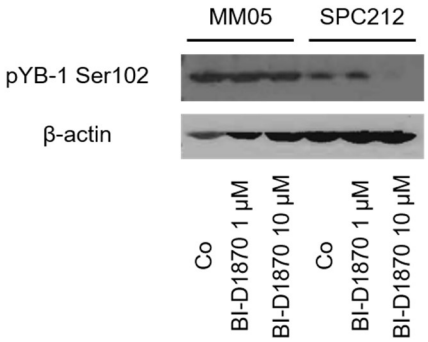

Figure 27: Western blot of MM05 and SPC212 after treatment with BI-D1870 at concentrations of 1 µM and 10 µM for 24 hours. MM05 showed a slight reduction in YB-1 phosphorylation at Ser102 at 10 µM, while it was not detectable anymore in SPC212 at the same concentration.

Additionally, BI-D1870 inhibited growth of our MPM cell line panel in a concentration dependent manner. SPC212 was the most sensitive cell line in our panel with an IC_{50} of 8.65 µM, followed by MSTO with 14.06 µM (Figure 28). VMC40 and MM05 were more resistant with IC_{50}s of 16.63 µM and 19.08 µM. As we did not reach these values experimentally, they were extrapolated by GraphPad Prism 8.

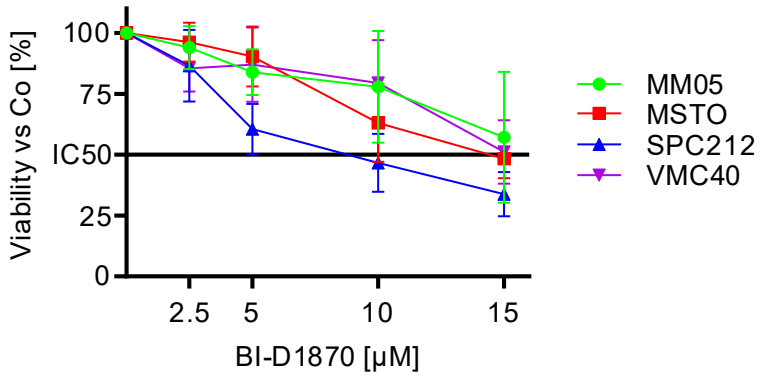

Figure 28: SYBR green-based proliferation assay of our MPM cell line panel 72 hours after BI-D1870 treatment compared to DMSO vehicle control (Co).

Assuming that two compounds hitting the same target should produce antagonistic effects, we tested the combined treatment with siRNA-mediated knockdown of YB-1 to validate that BI-D1870 exerts its effects via YB-1. When BI-D1870 was added after reverse transfection of siRNA targeting YB-1, we indeed found antagonistic effects in MSTO. The respective cell growth inhibition by BI-D1870 was higher in the control group transfected with non-silencing siRNA than in the treatment group with siRNA targeting YB-1 (Figure 29). BI-D1870 alone reduced MSTO cell viability by 56.05 % at a concentration of 15 µM. YB-1 knock down with 2.5 nM resulted in 60.86% reduction of cell viability in MSTO. Further addition of 15 µM of BI-D1870 only reduced cell viability by 5.28%. Knockdown of YB-1 blunted the effects of BI-D1870 in MSTO, therefore BI-D1870 seems to exert its growth inhibition at least partially via YB-1 in this cell line.

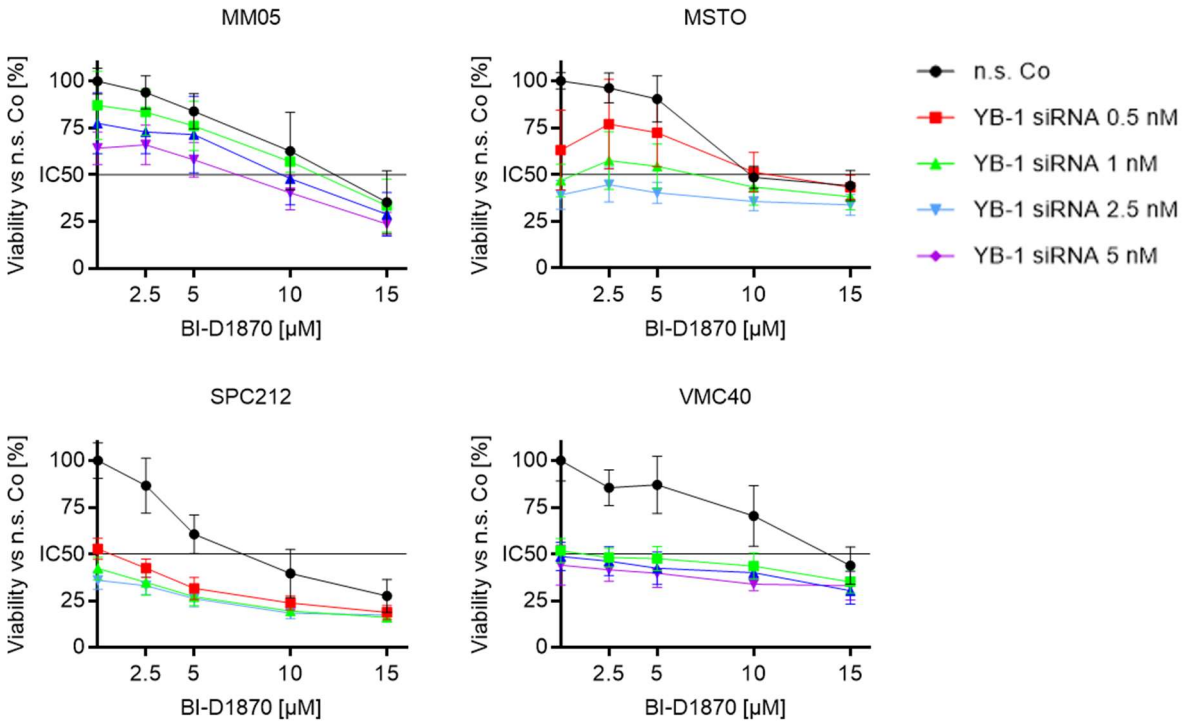

Figure 29: SYBR green-based proliferation assay of our MPM cell line panel. BI-D1870 was added 24 hours after siRNA-mediated knockdown of YB-1 via reverse transfection. Cell growth was measured after additional 72 hours of incubation and compared to non-silencing control (n.s. Co) siRNA. DMSO was used as vehicle control.

From these results, we calculated the CI values using compusyn software based on the Chou-Talalay method as described in chapter 2.3.1. Briefly, a treatment combination has an

antagonistic effect if the calculated CI values are >1, a synergistic effect if CI values are <1 and an additive effect if CI values are =1. As can be seen in Figure 30, we observed antagonistic effects at various concentrations of siRNA and BI-D1870 in MSTO. In contrast, the combination treatment led to highly synergistic effects in SPC212 and VMC40 with CI values of around 0.5. As YB-1 was knocked down prior to treatment, BI-D1870 could exert its effects via different mechanisms in these cell lines. In MM05 we found mostly antagonistic and additive effects.

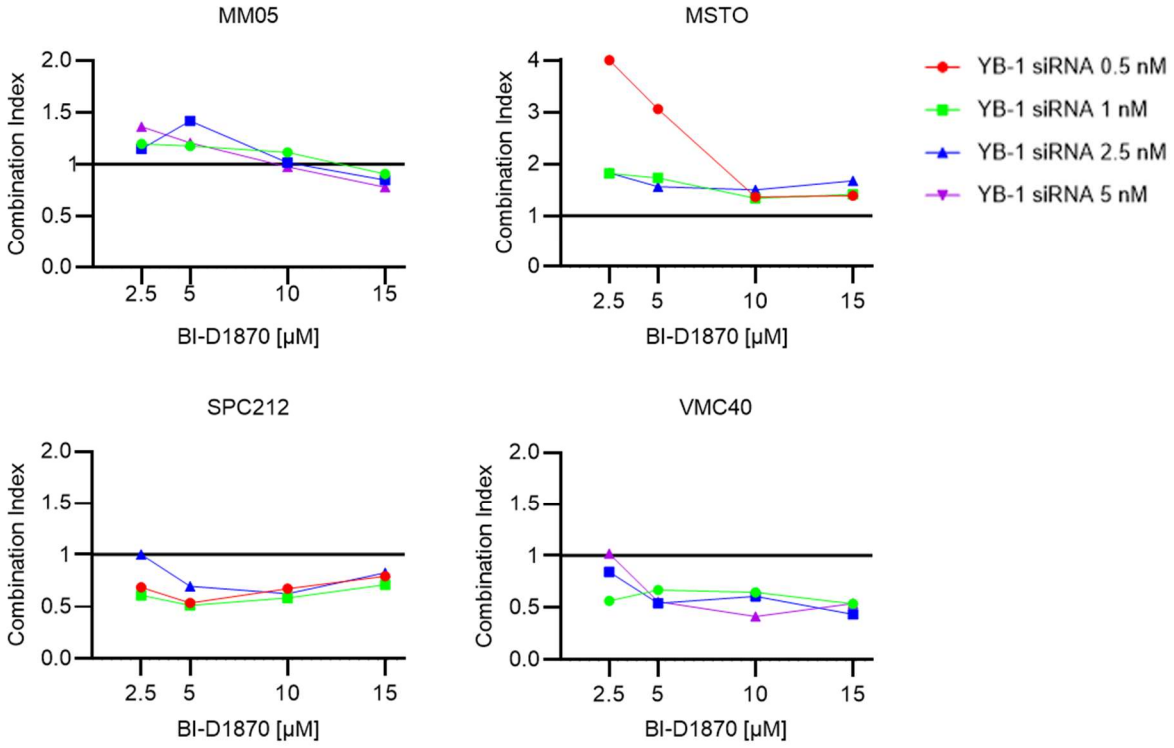

Figure 30: Combination indices (CI) for the combined treatment of our MPM cell line panel with siRNA-mediated knockdown of YB-1 and BI-D1870 as calculated via compusyn software. A treatment combination has an antagonistic effect if the calculated CI values are >1, a synergistic effect if CI values are <1 and an additive effect if CI values are =1.

3.2.1.3. Entinostat effectively inhibits growth of MPM cells partially in a YB-1 dependent manner

Recently, it was reported that the histone deacetylase (HDAC) class I inhibitor entinostat (MS-275) hinders deacetylation of YB-1, thereby leading to hyperacetylation and blocking its activity (El-Naggar et al., 2019). We wanted to assess the effects of this inhibitor in our MPM cell panel. Entinostat reduced viability in a dose dependent manner (Figure 31). VMC40 was the most sensitive cell line in our panel with an IC_{50} of 0.99 µM at 72 hours, followed by MSTO (1.263 µM) and SPC212 (2.05 µM). MM05 was the most resistant cell line with an IC_{50} of 4.12 µM.

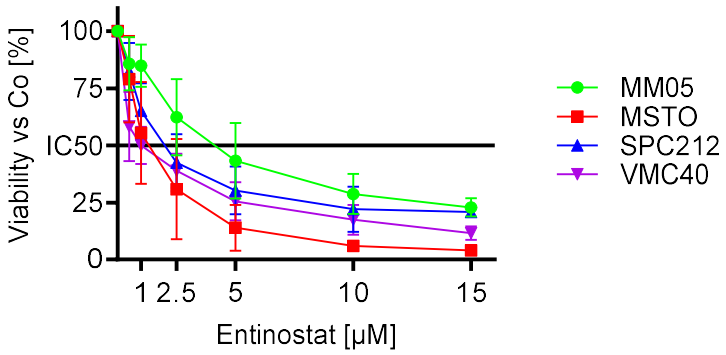

Figure 31: SYBR green-based proliferation assay of our MPM cell line panel 72 hours after treatment with entinostat compared to DMSO vehicle control (Co).

As validation that entinostat exerts its effects via YB-1, we, again, tested the combined treatment with siRNA (Figure 32). When entinostat was added after reverse transfection of siRNA targeting YB-1, we found antagonistic effects. The respective cell growth inhibition by entinostat was higher in the control group with non-silencing siRNA than in the treatment group with siRNA targeting YB-1. Entinostat alone reduced MPM cell viability in a range from 75.14% in MM05 to 94.37% in MSTO at concentrations of 5 µM. If YB-1 was silenced prior to entinostat treatment, the added reduction in cell viability was between 0% and 25% in MM05, SPC212 and VMC40. At some concentrations of YB-1 siRNA, we could observe slightly higher cell viability in SPC212, MSTO and MM05 at 2.5 µM and 5 µM concentrations of entinostat. In general, knockdown of YB-1 blunted the effects of entinostat, suggesting that entinostat exerted its growth inhibition at least partially via YB-1.

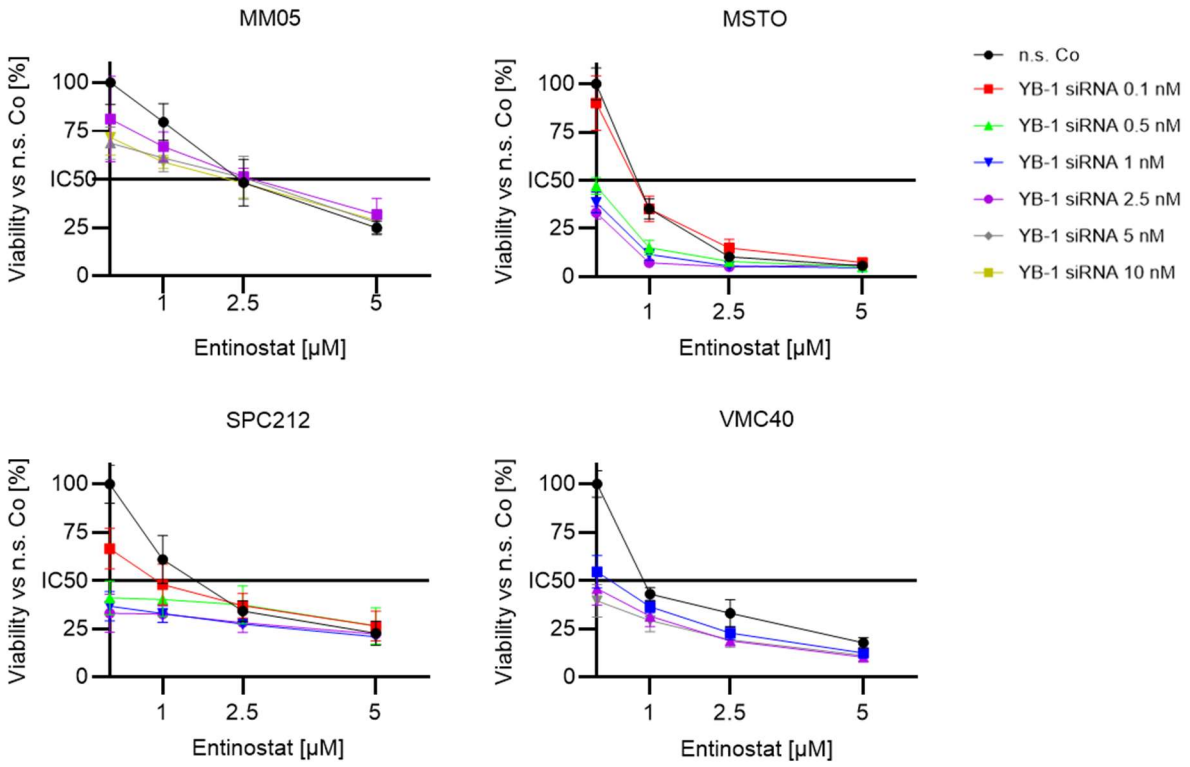

Figure 32: SYBR green-based proliferation assay of our MPM cell line panel. Entinostat was added 24 hours after siRNA-mediated knockdown of YB-1 via reverse transfection. Cell growth was measured after additional 72 hours of incubation and compared to non-silencing control (n.s. Co) siRNA. DMSO was used as vehicle control.

When we calculated the CI values, we found that most combinations of siRNA and entinostat showed antagonistic effects in MM05 and SPC212 (Figure 33). Combination treatment led to synergistic effects for low concentrations in MSTO and all concentrations in VMC40, suggesting that entinostat exerted its effects via YB-1 independent mechanisms in these cell lines.

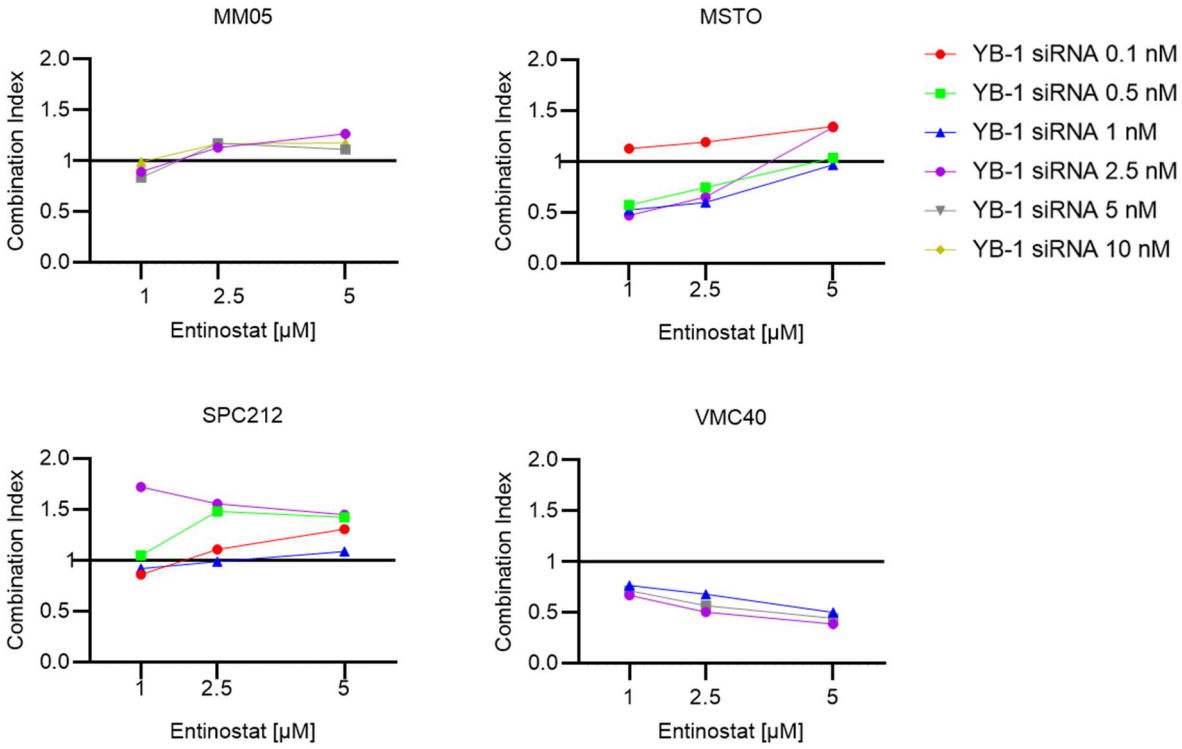

Figure 33: Combination indices (CI) for the combined treatment of our MPM cell line panel with siRNA-mediated knockdown of YB-1 and entinostat as calculated via compusyn software. Most combinations in MM05 and SPC212 showed CI values >1, representing antagonistic effects. In contrast, MSTO and VMC40 showed highly synergistic effects, suggesting that entinostat exerted its effect in an YB-1 independent manner in these cell lines.

3.2.2. Combination treatments with cisplatin

3.2.2.1. Knockdown of YB-1 via siRNA sensitizes MPM cells to cisplatin

YB-1 is associated with platinum-based chemotherapy resistance in multiple cancers (Johnson et al., 2019) and silencing YB-1 was shown to induce cisplatin sensitization in several cancers such as neuroblastoma (Wang et al., 2017), bladder cancer (Shiota et al., 2011) and melanoma (Schittek et al., 2007). Therefore, we investigated the effects of siRNA-mediated knockdown of YB-1 on cisplatin resistance in MPM cells. Cisplatin was added 24 hours after reverse transfection of siRNA targeting YB-1 and cell viability was measured after an additional 72 hours (Figure 34). As shown previously, YB-1 siRNA by itself was especially potent in reducing cell viability of MPM cell lines MSTO and SCP212. Cell viability of MSTO was reduced by 62.24% at 1 nM YB-1 siRNA alone. VMC40 and MM05 were more resistant to the combined treatment.

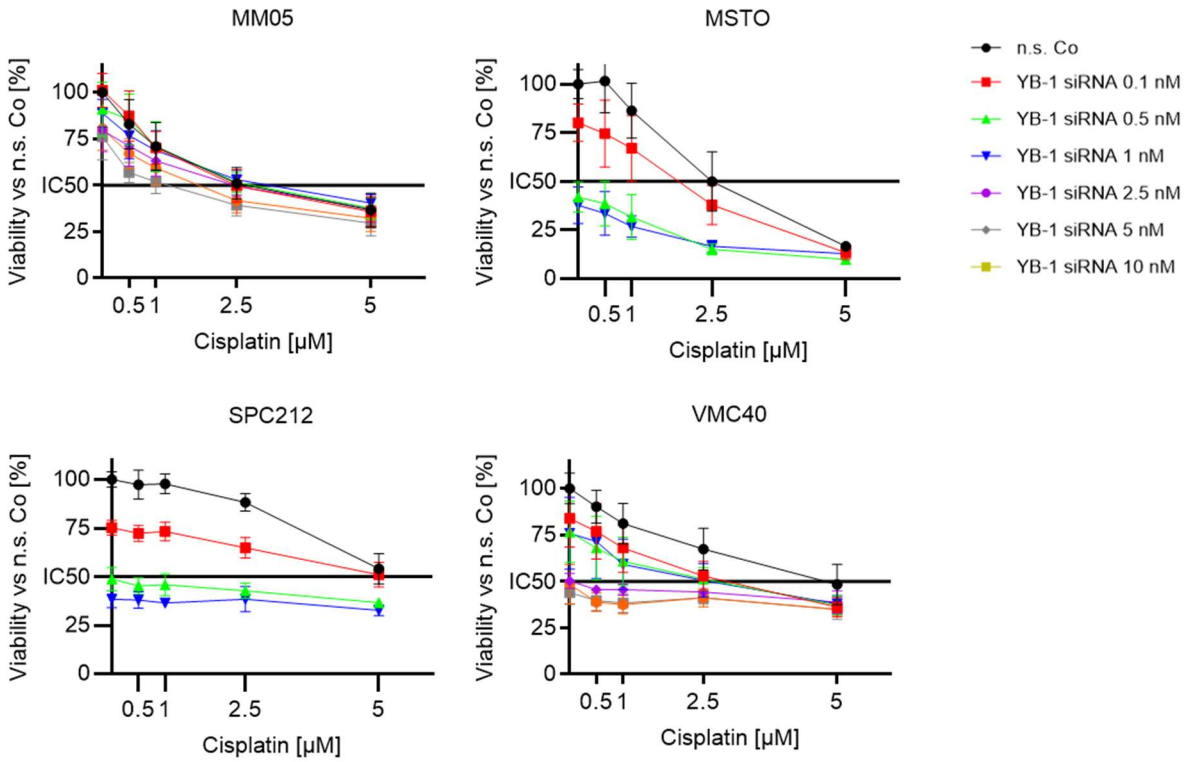

Figure 34: SYBR green-based proliferation assay of our MPM cell line panel. Cisplatin was added 24 hours after siRNA-mediated knockdown of YB-1 via reverse transfection. Cell growth was measured after 72 hours of cisplatin treatment and compared to non-silencing control (n.s. Co) siRNA.

From these results, we calculated the CI values using compusyn software. As can be seen in Figure 35, we found additive to synergistic effects (CI < 1) at various concentrations of siRNA targeting YB-1 and cisplatin in MM05, MSTO and VMC40. SPC212 showed additive to antagonistic effects with CI values > 1.

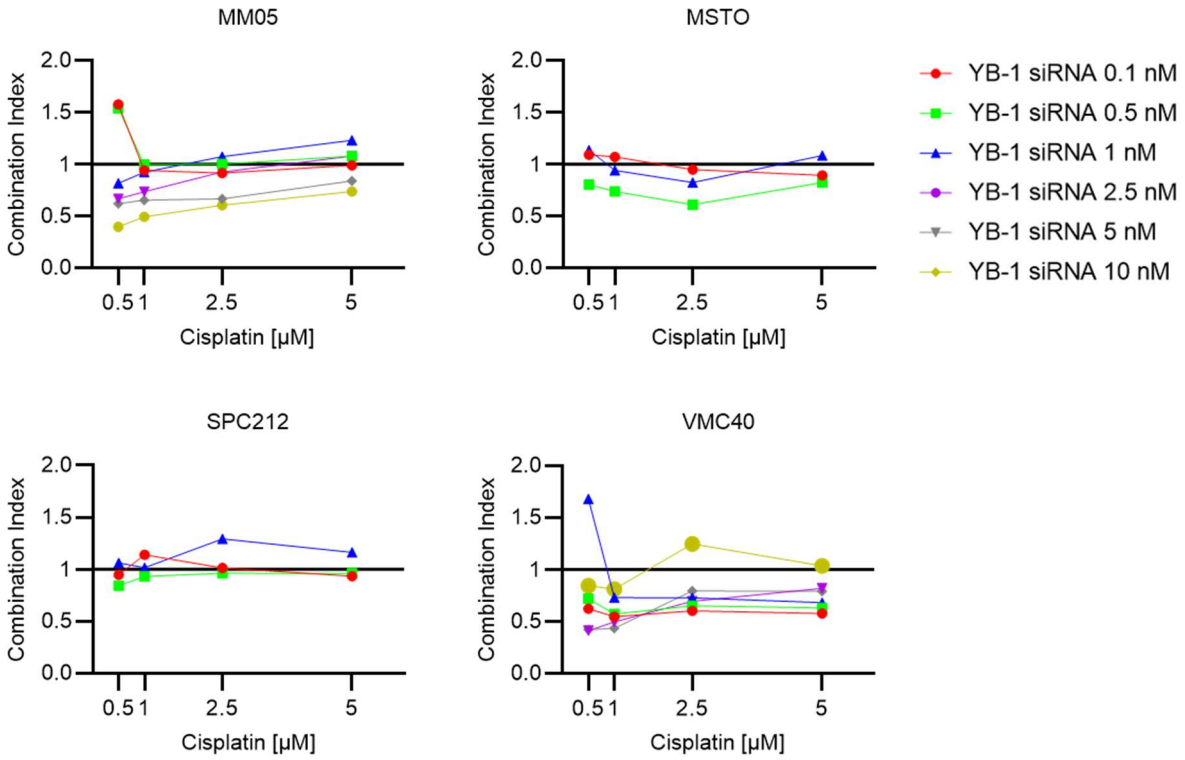

Figure 35: Combination indices (CI) for the treatment of our MPM cell line panel with siRNA-mediated knockdown of YB-1 in combination with cisplatin as calculated via compusyn software. MM05, MSTO and VMC40 showed strong synergistic effects with CI values around 0.5 for low cisplatin concentrations. For SPC212, the majority of the used siRNA and cisplatin concentrations led to antagonistic effects (CI > 1).

3.2.2.2. Inhibition of phosphorylation of YB-1 at Ser102 shows partly antagonistic effects with cisplatin

Since knockdown of YB-1 sensitized MPM cells to cisplatin, we wanted to evaluate whether inhibition of YB-1 phosphorylation could mimic this effect. Cisplatin and BI-D1870 were combined at several concentrations and cell viability was measured after 72 hours of incubation (Figure 36). SPC212 was the most susceptible cell line to the combined treatment.

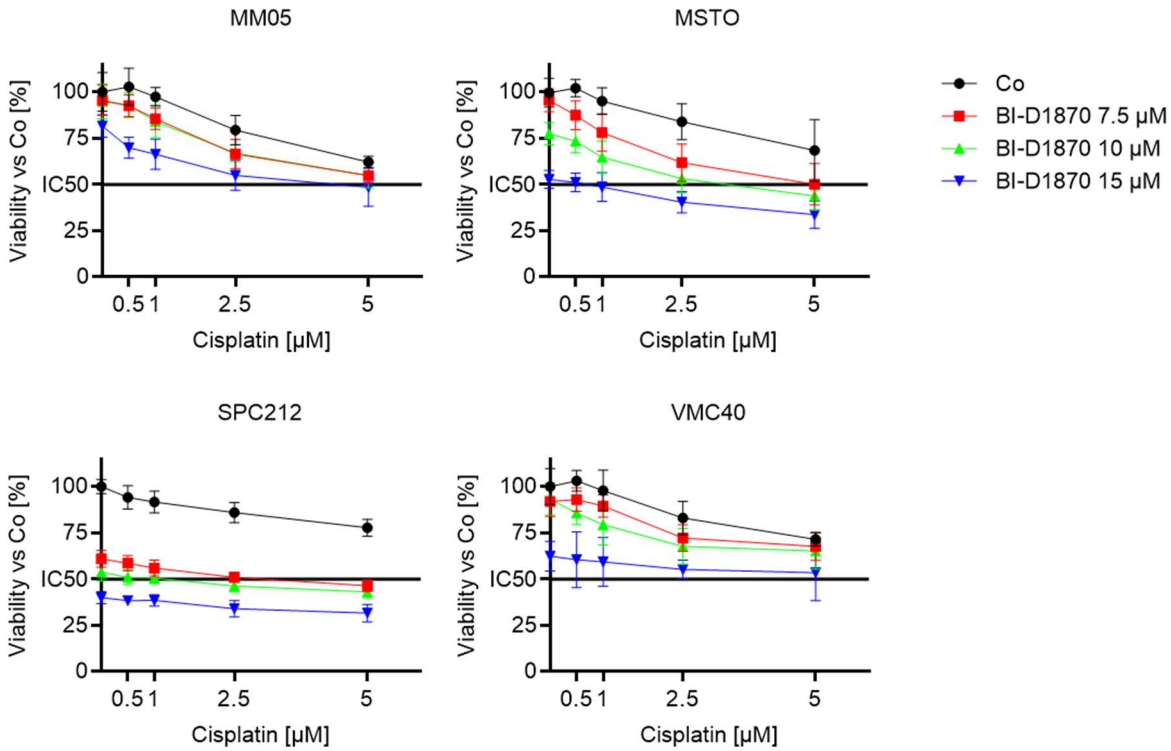

Figure 36: SYBR green-based proliferation assay of our MPM cell line panel 72 hours after combined treatment with cisplatin and BI-D1870. Cisplatin was added at concentrations ranging from 0.5 µM to 5 µM and BI-D1870 was added at concentrations ranging from 7.5 µM to 15 µM. Combination treatment was compared to cisplatin treatment alone (Co). DMSO was used as vehicle control.

When calculating the CI values, most combinations of BI-D1870 and cisplatin led to antagonistic effects (CI > 1) in MSTO and VMC40 cells (Figure 37). Interestingly, MM05 displayed strong synergistic effects for this combination with CIs of around 0.5 and SPC212 showed additive to synergistic effects for all combinations tested.

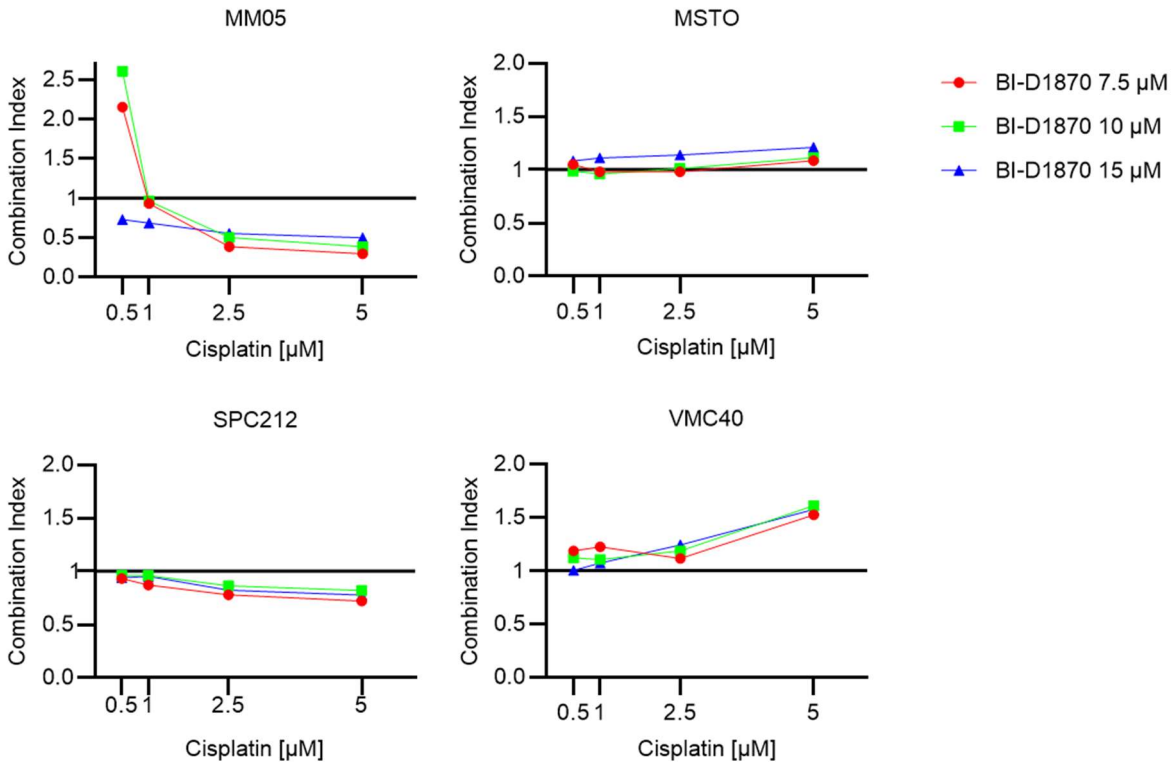

Figure 37: Combination indices (CI) for the combined treatment of our MPM cell line panel with cisplatin and BI-D1870 as calculated via compusyn software. Most of the used combinations displayed antagonistic effects with CI values > 1. MM05 showed highly synergistic effects with CIs of around 0.5 at high concentrations of BI-D1870.

3.2.2.3. Inhibition of deacetylation of YB-1 sensitizes MPM cells to cisplatin

Finally, we also assessed the effect of combining hyperacetylation of YB-1 with cisplatin treatment. Cisplatin and entinostat were used at concentrations ranging from 0.5 µM to 5 µM. Cell viability was measured after 72 hours (Figure 38). The combined treatment led to marked reductions in cell growth in every cell line in our panel.

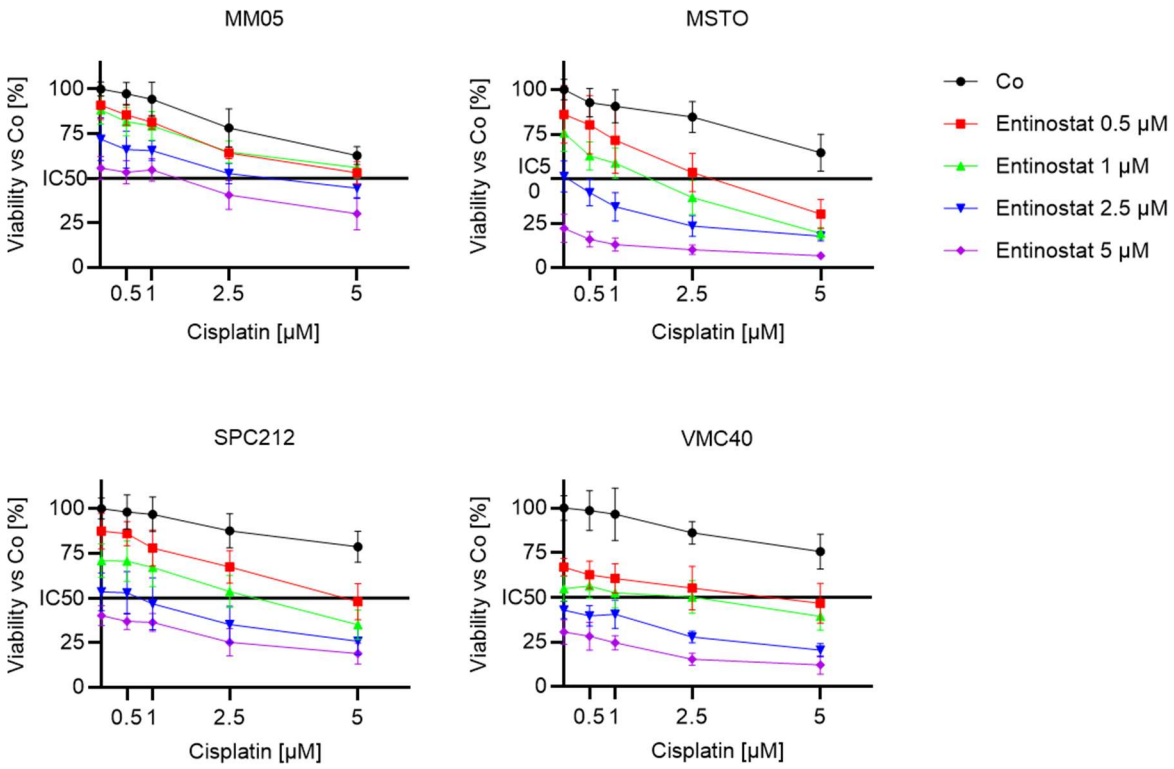

Figure 38: SYBR green-based proliferation assay of our MPM cell line panel 72 hours after combined treatment with cisplatin and entinostat. Cisplatin was combined with entinostat at concentrations ranging from 0.5 µM to 5 µM for both drugs. The combination was compared to cisplatin only treatment (Co). DMSO served as vehicle control.

We calculated the CI values of the combination treatment of entinostat and cisplatin and almost exclusively found synergistic effects (CI < 1) in all MPM cell lines in our panel (Figure 39).

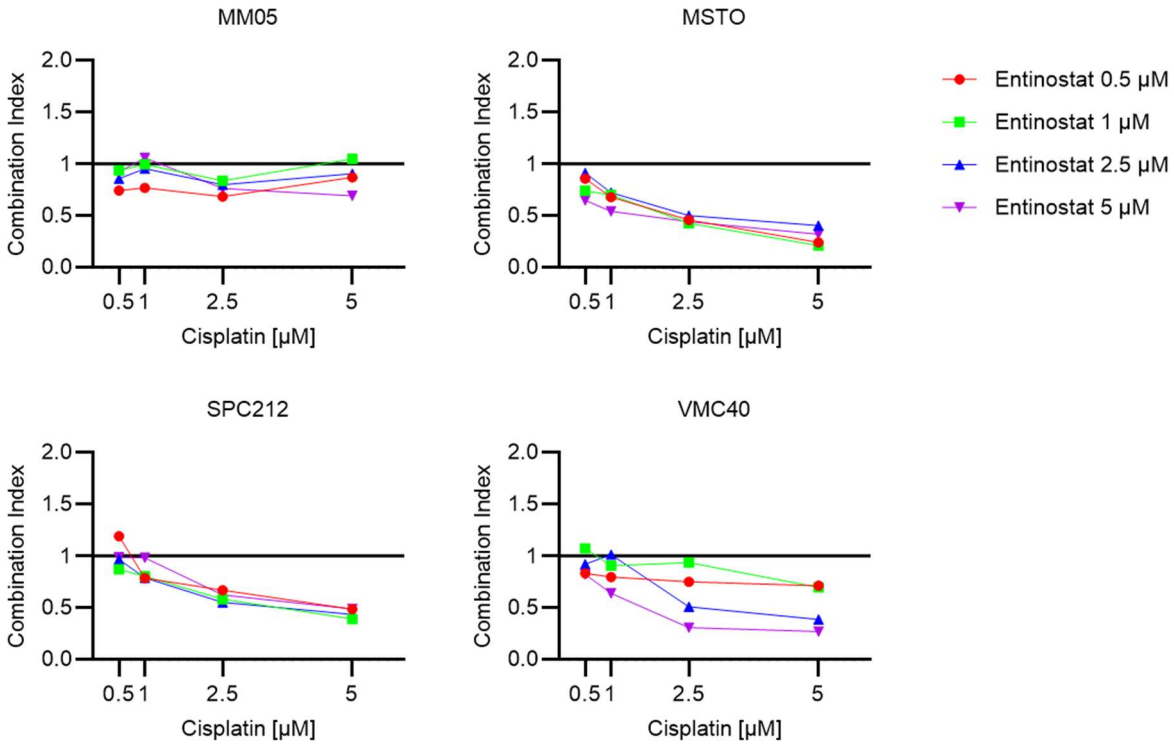

Figure 39: Combination indices (CI) for the combined treatment of our MPM cell line panel with cisplatin and entinostat as calculated via compusyn software. Most of the combinations used resulted in synergistic effects with CIs < 1 in every MPM cell line in our panel.

4. DISCUSSION AND OUTLOOK

4.1. YB-1 overexpression in MPM cells

YB-1 is overexpressed in many cancers such as renal cell carcinoma (Wang et al., 2015), breast cancer (Habibi et al., 2008) and malignant pleural mesothelioma (MPM) (Johnson et al., 2018). Furthermore, YB-1 overexpression is reported to promote proliferation and colony formation of hepatocellular carcinoma cells (Chao et al., 2017). We assessed the effects of YB-1 overexpression in MPM cells. Overall, doxycycline increased YB-1 expression in at least 3 of the 4 cell models we investigated. Our data show that induced YB-1 overexpression did not stimulate cell proliferation in SYBR-green based assays. Compared to normal tissue, MPM cells already overexpress YB-1 and a further increase may not be biologically relevant for cellular growth at these already high levels.

Cytoplasmic YB-1 was reported to promote epithelial-mesenchymal transition (EMT) and invasion in melanoma cells (Kosnopfel et al., 2018) while knockdown of YB-1 led to downregulation of metalloproteinase-1 and reduced invasive potential in triple-negative breast cancer cells (Lim et al., 2019). Here, we observed EMT-like morphology changes and enhanced scattering when YB-1 was overexpressed in clonogenic survival assays. Therefore, we investigated the effects of induced YB-1 overexpression on invasiveness of MPM cells in 3D spheroid sprouting assays. We found that VMC40, which expressed the lowest levels of YB-1 in our panel and showed only a slight increase of YB-1 expression, nevertheless produced significantly longer sprouts compared to controls, while no changes were observed for the other three cell lines in our panel. This suggests that scattering and sprouting are independently triggered by YB-1 in MPM cell lines. It would be interesting to investigate these findings further *in vivo* in a mouse model. Generally, MPM cell lines express relatively high levels of YB-1. Therefore, overexpression achieved only a moderate fold increase in expression. Recently, our group managed to rescue YB-1 expression following knockdown using siRNA that does not target the doxycycline-induced transcript. To investigate a larger amplitude of YB-1 levels, an experiment could be designed by which the effects YB-1 overexpression, its knockdown and re-expression could be compared. Also, it will be important to evaluate whether the observed differences in morphology and scattering are associated with expression changes of EMT markers. Changes of matrix melloproteinase-1 and beta catenin have been linked to YB-1 in triple-negative breast cancer, for instance (Lim et al., 2019).

YB-1 is involved in resistance to platinum-based chemotherapies in bladder cancer (Yamashita et al., 2017), prostate cancer (Shiota et al., 2014) and ovarian cancer (Kang et al., 2013)

among others. When we investigated whether YB-1 overexpression increased resistance to cisplatin, however, we found no differences. Again, the small increase that we detected in cell lines that already overexpressed YB-1 may not be of biological consequence. Phosphorylation of YB-1 at Serine 102 (Ser102) was reported to be required for nuclear shuttling of YB-1 in melanoma cells (Kosnopfel et al., 2018), which potentially could be required for YB-1 to exert its anti-apoptotic effects by interfering with TP53. This rationale could be verified using a transgene cell model overexpressing phosphomimetic Ser102 mutant of YB-1 to see if increased nuclear translocation could enhance chemoresistance.

Stable YB-1 overexpression in non-tumorigenic epithelial Madin-Darby canine kidney cells leads to induction of a partial EMT phenotype and engraftment of viable tumors in SCID mice (Gopal et al., 2015). From previous experiments by our group it was known that SPC212 are not able to form tumors in mice. As mentioned, we observed EMT-like changes after induced YB-1 overexpression. Hence, we explored whether SPC212 stably overexpressing YB-1 could induce tumor growth *in vivo*. The stable overexpression cell model was preferred, in order to avoid feeding the mice daily with doxycycline. Nevertheless, SPC212 pYB-1 cells were not able to engraft. Despite the observed morphologic changes, the increase of YB-1 alone was clearly not sufficient to induce tumorigenicity in this MPM model.

In the near future, our group will investigate the effects of inducible YB-1 overexpression and red fluorescent protein (RFP) *in vivo* in a zebrafish model. RFP will allow tracking of the tumor cells in real time via life cell videomicroscopy in transparent zebrafish larvae.

In essence, we achieved inducible overexpression of YB-1 in MPM cell models, but proliferation was not increased. We found EMT-like changes in all MPM cell lines investigated and significantly enhanced invasion of VMC40 in a collagen matrix in 3D spheroid sprouting assays. Higher YB-1 expression did not enhance resistance to cisplatin in our setting and stable overexpression did not induce tumorigenicity in non-tumorigenic SPC212 in SCID mice. The effects of induced YB-1 overexpression will be further analyzed in a zebrafish model.

4.2. Targeting YB-1 in MPM cells

Knockdown of YB-1 was reported to inhibit proliferation of non-small cell lung cancer (Lasham et al., 2012) and MPM cells (Johnson et al., 2018). We showed that siRNA-mediated knockdown strongly decreased YB-1 expression in our MPM cell line panel. The knockdown effectively inhibited proliferation by more than 50% in every cell line except MM05 where the

maximum achieved reduction in cell viability was 28%. YB-1 is associated with chemoresistance in multiple cancers (Lasham et al., 2013) and was reported to transactivate gene expression *of multi-drug resistance protein 1* (*MDR1)* (Ohga et al., 1998) and *Multidrug resistance-associated protein 1 (MRP1)* (Stein et al., 2001). On the other hand, silencing YB-1 was reported to sensitize various cancers to cisplatin such as neuroblastoma (Wang et al., 2017) and melanoma (Schittek et al., 2007). When we combined YB-1 targeting siRNA and cisplatin we found highly synergistic effects with combination index (CI) values around 0.5 in every cell line in our panel except SPC212. This cell line was the most sensitive to knockdown of YB-1 and the least sensitive to cisplatin. In the combination, siRNA was responsible for most of the reduction of cell viability while cisplatin added little benefit. In future work, these findings could be verified *in vivo* in a mouse model using knockdown of YB-1 prior to injection of tumor cells and cisplatin treatment. This approach, however, could be problematic for cell lines which are rather sensitive to YB-1 silencing. A more elegant method would be the utilization of an inducible knockdown model with small hairpin RNA. With this approach, tumors could be first established before silencing YB-1.

Although several clinical trials using siRNA are ongoing and miRNA mimics which were packed into bacterial shells were successfully employed in the MesomiR phase I clinical trial (van Zandwijk et al., 2017), this approach as targeted therapy remains challenging for translation into the clinics. Upscaling production, reproducibility and consistency are obstacles that have to be overcome (Ahmadzada et al., 2018). Therefore, we explored other avenues for targeting YB-1. To date, there are few pharmacological options to directly inhibit YB-1. For instance, Law and colleagues developed a cell permeable peptide that interferes with Ser102 phosphorylation of YB-1 (Law et al., 2010). We investigated indirect inhibition by modulation of post-translational modifications. Phosphorylation of YB-1 was reported to be critical for completing cytokinesis (Mehta et al., 2020a). YB-1 is phosphorylated at Ser102 by Akt (Sutherland et al., 2005) and p90 RSK (Mendoza et al., 2011). We treated our cells with the p90 RSK specific inhibitor BI-D1870 (Sapkota et al., 2007) and found a decrease in Ser102 phosphorylation of YB-1 at a concentration of 10 µM in SPC212, but not in MM05. This corresponded with the calculated IC_{50} values for BI-D1870 in SPC212 (8.65 µM) and MM05 (19.08 µM). When BI-D1870 was combined with cisplatin, we found additive effects in SPC212 and MSTO and highly synergistic effects in MM05. In contrast, the combination led to antagonistic effects in VMC40. Targeting Ser102 phosphorylation of YB-1 may have its drawbacks, as the resulting cytoplasmic retention of YB-1 was reported to enhance tumorigenicity and metastatic potential in melanoma cells (Kosnopfel et al., 2018). When we

knocked down YB-1 prior to BI-D1870 treatment, the combination led to antagonistic effects in MM05 and MSTO, suggesting that this inhibitor exerted its effects through YB-1 in these cell lines. In SPC212 and VMC40 on the other hand, siRNA-mediated knock down of YB-1 in combination with BI-D1870 led to synergistic effects, suggesting that BI-D1870 additionally inhibited other crucial targets. It was shown that BI-D1870 decreased proliferation and phosphorylation of Glycogen synthase kinase 3 beta (GSK-3B) in A549 lung cancer cells (Abdulrahman et al., 2016) which could be partially responsible for this effect.

We also explored pharmacological modulation of acetylation of YB-1 in our MPM cell line panel. Deacetylation of YB-1 at Lysine 81 was shown to be vital for its translational function in sarcoma cells by controlling the expression of stress-tolerance genes such as *nuclear factor erythroid 2-related factor 2* (*NRF2)* (El-Naggar et al., 2019). We hypothesized that stress tolerance genes could be important for viability and cisplatin resistance in MPM and thus hyperacetylation of YB-1 would impair its functions and be detrimental for MPM cells. Entinostat is an HDAC class I inhibitor and was shown to hinder deacetylation of YB-1 (El-Naggar et al., 2019). Our MPM cell line panel reacted sensitively to entinostat treatment, resulting in IC_{50} values between 0.99 µM and 4.12 µM. When we combined the drug with cisplatin, we almost exclusively found highly synergistic effects across all used concentrations. These findings warrant further verification in mouse models. Entinostat is currently being evaluated as a monotherapy in several clinical phase I and II trials in multiple cancers and has received breakthrough designation status by the FDA for management of advanced breast cancer (Connolly et al., 2017). There are also two ongoing phase III clinical trials for the treatment of advanced breast cancer in combination with exemestane (NCT03538171, NCT02115282). Since entinostat has shown promise in many different cancers, we wondered if its effects are YB-1 dependent in our MPM cell line panel. After silencing YB-1 via siRNA prior to entinostat treatment, we found antagonistic effects in MM05 and SPC212. This suggests that the drug's activity is dependent on YB-1 in these cell lines. On the contrary, knockdown of YB-1 in addition to entinostat treatment showed synergistic effects in MSTO and VMC40, indicating different mechanisms at work. HDAC inhibition leads to histone hyperacetylation, promotes transcription of silenced genes, differentiation and apoptosis and results in decreased cell proliferation (Connolly et al., 2017), all of which are beneficial in cancer therapy.

In summary, we showed that siRNA-mediated knockdown of YB-1 effectively reduced viability in our MPM cell line panel and combination treatment with cisplatin led to synergistic effects.

As there are no specific pharmacological inhibitors, we explored other routes to interfere with the functions of YB-1. The p90 RSK inhibitor BI-D1870 decreased phosphorylation of YB-1 at Ser102 in SPC212 and reduced cell viability in a concentration-dependent manner. Furthermore, combination treatment with cisplatin resulted in synergistic effects. The HDAC class I inhibitor entinostat drastically reduced MPM cell viability and showed highly synergistic effects across almost all used concentrations when combined with cisplatin. The combination effects with YB-1 siRNA suggest that both BI-D1870 and entinostat function in a YB-1 dependent and independent manner, depending on the cell line.

4.3. YB-1 as a promising target in MPM

So far, combination treatment with cisplatin and pemetrexed is the sole frontline therapy for MPM. The 41% of patients who respond to combination therapy (Cinausero et al., 2018) show only a slightly increased overall survival of a few months. New treatment options are urgently needed.

Several different approaches have been reported to increase chemosensitivity of MPM cells. Combination treatment with cisplatin and an mTOR inhibitor led so synergistic effects *in vitro* and *in vivo* (Hoda et al., 2011). Oncolytic adenoviruses were also used in combination with cisplatin and pemetrexed and led to synergistic effects (Kuryk et al., 2016). Oncolytic viruses and chemotherapeutics work in tandem to elicit strong immune responses to newly shed antigens of the cancer cells. Activating the immune system in the fight against cancer is a more recent approach. Immune checkpoint inhibitors aim to reactivate immune cells inhibited by tumors via blockade of signals such as programmed cell death ligand 1 (PD-L1). PD-L1 was shown to be expressed in 40% of MPM tumors and these patients have a much worse median survival (5 vs. 14.5 months) (Mansfield et al., 2014). Tao and colleagues showed that YB-1 promotes expression of PD-L1 in hepatocellular carcinoma cells and that silencing YB-1 reversed chemoresistance as well as the immunosuppressive environment of engrafted tumors *in vivo* (Tao et al., 2019). The connection between YB-1, PD-L1 expression and immune response has not been explored so far in MPM and could be a promising avenue for further research using the overexpression, siRNA and pharmacological approaches elaborated in this thesis.

In conclusion, our data show that we achieved induced YB-1 overexpression in MPM cell lines and overexpression resulted in an EMT-like phenotype. On the other hand, proliferation and

chemoresistance were not stimulated. We showed that knockdown of YB-1 effectively decreased viability of MPM cells and led to their sensitization to cisplatin. The p90 RSK inhibitor BI-D1870 was demonstrated to decrease YB-1 Ser102 phosphorylation in 1 of 2 cell lines and treatment reduced MPM cell viability in a concentration dependent manner. Combination therapy with cisplatin led to synergistic effects in 2 of 4 cell lines. The HDAC inhibitor entinostat, drastically reduced MPM cell viability. Combination treatment with cisplatin led to highly synergistic combination effects in almost all used concentrations. BI-D1870 and entinostat exerted their effects in a YB-1 dependent and independent manner, depending on the cell line. Here, we outlined YB-1 as a promising target and suggest the evaluation of our findings *in vivo*.

5. APPENDIX

5.1. List of abbreviations

ADI-PEG 20 – Pegylated arginine deiminase

ALT – Alternative lengthening of telomeres

ASS1 – Argininosuccinate synthase 1

ATP – Adenosine Triphosphate

BAK – BCL-2 homologous antagonist/killer

BAP1 – BRCA1-associated protein

BAX – BCL-2-like protein 4

BCL-2 – B-cell lymphoma 2

BER – Base excision repair

BSA – Bovine serum albumin

CAM – Cell adhesion molecules

cDNA - complementary deoxyribonucleic acid

CI – Combination indeces

CTL – Cytotoxic T cells

dH_2O – Distilled H_2O

DMF – Dimethyl formamide

DMSO – Dimethyl sulfoxide

DNA – Deoxyribonucleic acid

dNTP – Deoxyribonucleotide triphosphate

Dox – Doxycycline

E2F – E2 promotor binding factors

E-cadherin – Epithelial cadherin

ECM – Extracellular matrix

EDTA – Ethylenediaminetetraacetic acid

EGFR – Epidermal growth factor receptor

EMT – Epithelial-mesenchymal transition

EPP – Extrapleural pneumonectomy

FCS – Fetal calf serum

FGF 2 – Fibroblast growth factor 2

FITC – Fluorescein Isothiocyanate

G3BP1 – Ras GTPase-activating protein-binding protein 1

GSK-3B – Glycogen synthase kinase 3 beta

HDAC – Histone deacetylase

HEPES – 4-(2-hydroxyethyl)-1-piperazineethanesulfonic acid

HIF – Hypoxia-induced factors

HR – Homologous recombination

HRP – Horse radish peroxidase

IC_{50} – half maximal inhibitory concentration

LB II – Lysis buffer II

LMP – Low melting point

LPS – Lipopolysaccharide

Lys81 – Lysine 81

MAPK – Mitogen-activated protein kinase

MDR1 – Multi-drug resistance protein 1

MFI – mean fluorescence intensity

MHC class II – Major histocompatibility complex class II

miRNA – Micro RNA

MMP – Matrix metalloproteinases

MMP1 – Matrix-metalloproteinase-1

MMR – Mismatch repair

Moesin-Ezrin-Radixin-Like Protein – Merlin

MPM – Malignant pleural mesothelioma

MRP1 – Multidrug resistance-associated protein 1

mTOR – mammalian target of rapamycin

n.s. Co – Non-silencing Control

NCD – Non-communicable diseases

NER – Nucleotide excision repair

NF2 – Neurofibromin 2

NHEJ – Non-homologous end joining

NK cells – Natural Killer cells

NLS – Nuclear localization signal

NRF2 – Nuclear factor erythroid 2-related factor 2

OS – Overall survival

P/D – Pleurectomy/decortication

PAA – Polyacrylamide

PBS – Phosphate buffered saline

PD1 – Programmed cell death protein 1

PD-L1 – Programmed death-ligand 1

PFA – Paraformaldehyde

PFS – Progression free survival

P_{hPGK} – Human phosphoglycerate kinase 1 promoter

PI3K – Phosphatidylinositol 3-kinase

PI3KCA – PI3K catalytic subunit alpha

PTEN – Phosphatase and tensin homolog

P_{TRE3GS} – 3rd generation Tet-responsive promoter

PVDF – Polyvinylidene difluoride

qRT-PCR – quantitative real-time polymerase chain reaction

R0 – serum-free RPMI media

R10 – RPMI media supplemented with 10% FCS

RNA – Ribonucleic acid

ROS – Reactive oxygen species

RPMI – Roswell Park Memorial Institute

RSK – Ribosomal s6 kinase

RT – Room temperature

RTK – Receptor tyrosine kinases

RT-PCR – Reverse Transcription polymerase chain reaction

rtTA – Reverse tetracycline-controlled transactivator

SCID – Severe combined immunodeficient

SD – Standard deviation

SDS – Sodium dodecyl sulfate

SDS-Page – Sodium dodecyl sulfate–polyacrylamide gel electrophoresis

Ser102 – Serine 102

siRNA – Small interfering RNA

SV40 – Simian virus 40

TAM – Tumor-associated macrophages

TBE – Tris-borate ethylenediaminetetraacetic acid

TBS – Tris-buffered saline

TBS/T – Tris-buffered saline/tween

Tet – Tetracycline

TF – Transcription factors
TNBC – Triple-negative breast cancer
VEGF – Vascular endothelial growth factor
WHO – World Health Organization
YB-1 – Y box binding protein 1

5.2. List of figures

5.3. List of tables

5.4. Bibliography

ABDULRAHMAN, N., JABALLAH, M., POOMAKKOTH, N., RIAZ, S., ABDELAZIZ, S., ISSA, A. & MRAICHE, F. 2016. Inhibition of p90 ribosomal S6 kinase attenuates cell migration and proliferation of the human lung adenocarcinoma through phospho-GSK-3β and osteopontin. *Mol Cell Biochem,* 418**,** 21-9.

ADAMS, J. M. & CORY, S. 2018. The BCL-2 arbiters of apoptosis and their growing role as cancer targets. *Cell death and differentiation,* 25**,** 27-36.

AGGARWAL, V., TULI, H. S., VAROL, A., THAKRAL, F., YERER, M. B., SAK, K., VAROL, M., JAIN, A., KHAN, M. A. & SETHI, G. 2019. Role of Reactive Oxygen Species in Cancer Progression: Molecular Mechanisms and Recent Advancements. *Biomolecules,* 9**,** 735.

AHMADZADA, T., REID, G. & MCKENZIE, D. R. 2018. Fundamentals of siRNA and miRNA therapeutics and a review of targeted nanoparticle delivery systems in breast cancer. *Biophysical reviews,* 10**,** 69-86.

ANDUJAR, P., PAIRON, J. C., RENIER, A., DESCATHA, A., HYSI, I., ABD-ALSAMAD, I., BILLON-GALLAND, M. A., BLONS, H., CLIN, B., DANEL, C., DEBROSSE, D., GALATEAU-SALLÉ, F., HOUSSET, B., LAURENT-PUIG, P., LE PIMPEC-BARTHES, F., LETOURNEUX, M., MONNET, I., RÉGNARD, J. F., VALIDIRE, P., ZUCMAN-ROSSI, J., JAURAND, M. C. & JEAN, D. 2013. Differential mutation profiles and similar intronic TP53 polymorphisms in asbestos-related lung cancer and pleural mesothelioma. *Mutagenesis,* 28**,** 323-31.

ASTANEHE, A., FINKBEINER, M. R., HOJABRPOUR, P., TO, K., FOTOVATI, A., SHADEO, A., STRATFORD, A. L., LAM, W. L., BERQUIN, I. M., DURONIO, V. & DUNN, S. E. 2009. The transcriptional induction of PIK3CA in tumor cells is dependent on the oncoprotein Y-box binding protein-1. *Oncogene,* 28**,** 2406-18.

ATTANOOS, R. L., CHURG, A., GALATEAU-SALLE, F., GIBBS, A. R. & ROGGLI, V. L. 2018. Malignant Mesothelioma and Its Non-Asbestos Causes. *Arch Pathol Lab Med,* 142**,** 753-760.

BAAS, P., FENNELL, D., KERR, K. M., VAN SCHIL, P. E., HAAS, R. L. & PETERS, S. 2015. Malignant pleural mesothelioma: ESMO Clinical Practice Guidelines for diagnosis, treatment and follow-up†. *Annals of Oncology,* 26**,** v31-v39.

BARGOU, R. C., JÜRCHOTT, K., WAGENER, C., BERGMANN, S., METZNER, S., BOMMERT, K., MAPARA, M. Y., WINZER, K. J., DIETEL, M., DÖRKEN, B. & ROYER, H. D. 1997. Nuclear localization and increased levels of transcription factor YB-1 in primary human breast cancers are associated with intrinsic MDR1 gene expression. *Nat Med,* 3**,** 447-50.

BARIS, Y. I., SAHIN, A. A., OZESMI, M., KERSE, I., OZEN, E., KOLACAN, B., ALTINÖRS, M. & GÖKTEPELI, A. 1978. An outbreak of pleural mesothelioma and chronic fibrosing pleurisy in the village of Karain/Urgüp in Anatolia. *Thorax,* 33**,** 181-192.

BEDDOWES, E., SPICER, J., CHAN, P. Y., KHADEIR, R., CORBACHO, J. G., REPANA, D., STEELE, J. P., SCHMID, P., SZYSZKO, T., COOK, G., DIAZ, M., FENG, X., JOHNSTON, A., THOMSON, J., SHEAFF, M., WU, B.-W., BOMALASKI, J., PACEY, S. & SZLOSAREK, P. W. 2017. Phase 1 Dose-Escalation Study of Pegylated Arginine Deiminase, Cisplatin, and Pemetrexed in Patients With Argininosuccinate Synthetase 1-Deficient Thoracic Cancers. *Journal of clinical oncology : official journal of the American Society of Clinical Oncology,* 35**,** 1778-1785.

BELTRAMI, S., KIM, R. & GORDON, J. 2013. Neurofibromatosis type 2 protein, NF2: an uncoventional cell cycle regulator. *Anticancer Res,* 33**,** 1-11.

BOCCHETTA, M., DI RESTA, I., POWERS, A., FRESCO, R., TOSOLINI, A., TESTA, J. R., PASS, H. I., RIZZO, P. & CARBONE, M. 2000. Human mesothelial cells are unusually susceptible to simian virus 40-mediated transformation and asbestos cocarcinogenicity. *Proceedings of the National Academy of Sciences of the United States of America,* 97**,** 10214-10219.

BOCCHETTA, M., MIELE, L., PASS, H. I. & CARBONE, M. 2003. Notch-1 induction, a novel activity of SV40 required for growth of SV40-transformed human mesothelial cells. *Oncogene,* 22**,** 81-9.

BRABLETZ, T., KALLURI, R., NIETO, M. A. & WEINBERG, R. A. 2018. EMT in cancer. *Nature Reviews Cancer,* 18**,** 128-134.

BRAY, F., FERLAY, J., SOERJOMATARAM, I., SIEGEL, R. L., TORRE, L. A. & JEMAL, A. 2018. Global cancer statistics 2018: GLOBOCAN estimates of incidence and mortality worldwide for 36 cancers in 185 countries. *CA Cancer J Clin,* 68**,** 394-424.

CARBONE, M., YANG, H., PASS, H. I., KRAUSZ, T., TESTA, J. R. & GAUDINO, G. 2013. BAP1 and cancer. *Nat Rev Cancer,* 13**,** 153-9.

CHANG, E. T., LAU, E. C., MOWAT, F. S. & TETA, M. J. 2017. Therapeutic radiation for lymphoma and risk of second primary malignant mesothelioma. *Cancer Causes Control,* 28**,** 971-979.

CHAO, H.-M., HUANG, H.-X., CHANG, P.-H., TSENG, K.-C., MIYAJIMA, A. & CHERN, E. 2017. Y-box binding protein-1 promotes hepatocellular carcinoma-initiating cell progression and tumorigenesis via Wnt/β-catenin pathway. *Oncotarget,* 8**,** 2604-2616.

CHENG, L., LOPEZ-BELTRAN, A., MASSARI, F., MACLENNAN, G. T. & MONTIRONI, R. 2018. Molecular testing for BRAF mutations to inform melanoma treatment decisions: a move toward precision medicine. *Modern pathology : an official journal of the United States and Canadian Academy of Pathology, Inc,* 31**,** 24-38.

CHOU, T.-C. & TALALAY, P. 1983. Analysis of combined drug effects: a new look at a very old problem. *Trends in Pharmacological Sciences,* 4**,** 450-454.

CHOU, T. C. 2006. Theoretical basis, experimental design, and computerized simulation of synergism and antagonism in drug combination studies. *Pharmacol Rev,* 58**,** 621-81.

CINAUSERO, M., RIHAWI, K., SPERANDI, F., MELOTTI, B. & ARDIZZONI, A. 2018. Chemotherapy treatment in malignant pleural mesothelioma: a difficult history. *Journal of thoracic disease,* 10**,** S304-S310.

CONNOLLY, R. M., RUDEK, M. A. & PIEKARZ, R. 2017. Entinostat: a promising treatment option for patients with advanced breast cancer. *Future oncology (London, England),* 13**,** 1137-1148.

DASARI, S. & TCHOUNWOU, P. B. 2014. Cisplatin in cancer therapy: molecular mechanisms of action. *European journal of pharmacology,* 740**,** 364-378.

DIDIER, D. K., SCHIFFENBAUER, J., WOULFE, S. L., ZACHEIS, M. & SCHWARTZ, B. D. 1988. Characterization of the cDNA encoding a protein binding to the major histocompatibility complex class II Y box. *Proc Natl Acad Sci U S A,* 85**,** 7322-6.

DONEHOWER, L. A., SOUSSI, T., KORKUT, A., LIU, Y., SCHULTZ, A., CARDENAS, M., LI, X., BABUR, O., HSU, T.-K., LICHTARGE, O., WEINSTEIN, J. N., AKBANI, R. & WHEELER, D. A. 2019. Integrated Analysis of TP53 Gene and Pathway Alterations in The Cancer Genome Atlas. *Cell Reports,* 28**,** 1370-1384.e5.

EL-NAGGAR, A. M., SOMASEKHARAN, S. P., WANG, Y., CHENG, H., NEGRI, G. L., PAN, M., WANG, X. Q., DELAIDELLI, A., RAFN, B., CRAN, J., ZHANG, F., ZHANG, H., COLBORNE, S., GLEAVE, M., MANDINOVA, A., KEDERSHA, N., HUGHES, C. S., SURDEZ, D., DELATTRE, O., WANG, Y., HUNTSMAN, D. G., MORIN, G. B. & SORENSEN, P. H. 2019. Class I HDAC inhibitors enhance YB-1 acetylation and oxidative stress to block sarcoma metastasis. *EMBO Rep,* 20**,** e48375.

EL-NAGGAR, AMAL M., VEINOTTE, CHANSEY J., CHENG, H., GRUNEWALD, THOMAS G. P., NEGRI, GIAN L., SOMASEKHARAN, SYAM P., CORKERY, DALE P., TIRODE, F., MATHERS, J., KHAN, D., KYLE, ALASTAIR H., BAKER, JENNIFER H., LEPARD, NANCY E., MCKINNEY, S., HAJEE, S., BOSILJCIC, M., LEPRIVIER, G., TOGNON, CRISTINA E., MINCHINTON, ANDREW I., BENNEWITH, KEVIN L., DELATTRE, O., WANG, Y., DELLAIRE, G., BERMAN, JASON N. & SORENSEN, POUL H. 2015. Translational Activation of HIF1α by YB-1 Promotes Sarcoma Metastasis. *Cancer Cell,* 27**,** 682-697.

EVDOKIMOVA, V., TOGNON, C., NG, T., RUZANOV, P., MELNYK, N., FINK, D., SOROKIN, A., OVCHINNIKOV, L. P., DAVICIONI, E., TRICHE, T. J. & SORENSEN, P. H. B. 2009. Translational Activation of Snail1 and Other Developmentally Regulated Transcription Factors by YB-1 Promotes an Epithelial-Mesenchymal Transition. *Cancer Cell,* 15**,** 402-415.

FINKBEINER, M. R., ASTANEHE, A., TO, K., FOTOVATI, A., DAVIES, A. H., ZHAO, Y., JIANG, H., STRATFORD, A. L., SHADEO, A., BOCCACCIO, C., COMOGLIO, P., MERTENS, P. R., EIREW, P., RAOUF, A., EAVES, C. J. & DUNN, S. E. 2009. Profiling YB-1 target genes uncovers a new mechanism for MET receptor regulation in normal and malignant human mammary cells. *Oncogene,* 28**,** 1421-31.

FINN, O. J. 2018. A Believer's Overview of Cancer Immunosurveillance and Immunotherapy. *Journal of immunology (Baltimore, Md. : 1950),* 200**,** 385-391.

FRYE, B. C., HALFTER, S., DJUDJAJ, S., MUEHLENBERG, P., WEBER, S., RAFFETSEDER, U., EN-NIA, A., KNOTT, H., BARON, J. M., DOOLEY, S., BERNHAGEN, J. & MERTENS, P. R. 2009. Y-box protein-1 is actively secreted through a non-classical pathway and acts as an extracellular mitogen. *EMBO reports,* 10**,** 783-789.

GELTNER, C., ERRHALT, P., BAUMGARTNER, B., AMBROSCH, G., MACHAN, B., ECKMAYR, J., KLIKOVITS, T., HODA, M. A., POPPER, H., KLEPETKO, W. & AUSTRIAN MESOTHELIOMA INTEREST, G. 2016. Management of malignant pleural mesothelioma - part 1: epidemiology, diagnosis, and staging : Consensus of the Austrian Mesothelioma Interest Group (AMIG). *Wiener klinische Wochenschrift,* 128**,** 611-617.

GIBBONS JOHNSON, R. M. & DONG, H. 2017. Functional Expression of Programmed Death-Ligand 1 (B7-H1) by Immune Cells and Tumor Cells. *Front Immunol,* 8**,** 961.

GILMORE, E., MCCABE, N., KENNEDY, R. D. & PARKES, E. E. 2019. DNA Repair Deficiency in Breast Cancer: Opportunities for Immunotherapy. *Journal of Oncology,* 2019**,** 4325105.

GOPAL, S. K., GREENING, D. W., MATHIAS, R. A., JI, H., RAI, A., CHEN, M., ZHU, H. J. & SIMPSON, R. J. 2015. YBX1/YB-1 induces partial EMT and tumourigenicity through secretion of angiogenic factors into the extracellular microenvironment. *Oncotarget,* 6**,** 13718-30.

GOUDAR, R. K. 2008. Review of pemetrexed in combination with cisplatin for the treatment of malignant pleural mesothelioma. *Therapeutics and clinical risk management,* 4**,** 205-211.

GRAZIANI, I., ELIASZ, S., DE MARCO, M. A., CHEN, Y., PASS, H. I., DE MAY, R. M., STRACK, P. R., MIELE, L. & BOCCHETTA, M. 2008. Opposite effects of Notch-1 and Notch-2 on mesothelioma cell survival under hypoxia are exerted through the Akt pathway. *Cancer Res,* 68**,** 9678-85.

HA, B., LEE, E. B., CUI, J., KIM, Y. & JANG, H. H. 2015. YB-1 overexpression promotes a TGF-β1-induced epithelial-mesenchymal transition via Akt activation. *Biochem Biophys Res Commun,* 458**,** 347-51.

HABIBI, G., LEUNG, S., LAW, J. H., GELMON, K., MASOUDI, H., TURBIN, D., POLLAK, M., NIELSEN, T. O., HUNTSMAN, D. & DUNN, S. E. 2008. Redefining prognostic factors for breast cancer: YB-1 is a stronger predictor of relapse and disease-specific survival than estrogen receptor or HER-2 across all tumor subtypes. *Breast Cancer Res,* 10**,** R86.

HANAHAN, D. & WEINBERG, R. A. 2000. The hallmarks of cancer. *Cell,* 100**,** 57-70.

HANAHAN, D. & WEINBERG, R. A. 2011. Hallmarks of cancer: the next generation. *Cell,* 144**,** 646-74.

HESTERBERG, T. W. & BARRETT, J. C. 1985. Induction by asbestos fibers of anaphase abnormalities: mechanism for aneuploidy induction and possibly carcinogenesis. *Carcinogenesis,* 6**,** 473-5.

HILLEN, F. & GRIFFIOEN, A. W. 2007. Tumour vascularization: sprouting angiogenesis and beyond. *Cancer metastasis reviews,* 26**,** 489-502.

HODA, M. A., MOHAMED, A., GHANIM, B., FILIPITS, M., HEGEDUS, B., TAMURA, M., BERTA, J., KUBISTA, B., DOME, B., GRUSCH, M., SETINEK, U., MICKSCHE, M., KLEPETKO, W. & BERGER, W. 2011. Temsirolimus inhibits malignant pleural mesothelioma growth in vitro and in vivo: synergism with chemotherapy. *J Thorac Oncol,* 6**,** 852-63.

HOMER, C., KNIGHT, D. A., HANANEIA, L., SHEARD, P., RISK, J., LASHAM, A., ROYDS, J. A. & BRAITHWAITE, A. W. 2005. Y-box factor YB1 controls p53 apoptotic function. *Oncogene,* 24**,** 8314-25.

JOHNSON, T. G., SCHELCH, K., CHENG, Y. Y., WILLIAMS, M., SARUN, K. H., KIRSCHNER, M. B., KAO, S., LINTON, A., KLEBE, S., MCCAUGHAN, B. C., LIN, R. C. Y., PIRKER, C., BERGER, W., LASHAM, A., VAN ZANDWIJK, N. & REID, G. 2018. Dysregulated Expression of the MicroRNA miR-137 and Its Target YBX1 Contribute to the Invasive Characteristics of Malignant Pleural Mesothelioma. *J Thorac Oncol,* 13**,** 258-272.

JOHNSON, T. G., SCHELCH, K., MEHTA, S., BURGESS, A. & REID, G. 2019. Why Be One Protein When You Can Affect Many? The Multiple Roles of YB-1 in Lung Cancer and Mesothelioma. *Front Cell Dev Biol,* 7**,** 221.

KANG, Y., HU, W., IVAN, C., DALTON, H. J., MIYAKE, T., PECOT, C. V., ZAND, B., LIU, T., HUANG, J., JENNINGS, N. B., RUPAIMOOLE, R., TAYLOR, M., PRADEEP, S., WU, S. Y., LU, C., WEN, Y., HUANG, J., LIU, J. & SOOD, A. K. 2013. Role of Focal Adhesion Kinase in Regulating YB–1–Mediated Paclitaxel Resistance in Ovarian Cancer. *JNCI: Journal of the National Cancer Institute,* 105**,** 1485-1495.

KAUFMANN, T., STRASSER, A. & JOST, P. J. 2012. Fas death receptor signalling: roles of Bid and XIAP. *Cell Death Differ,* 19**,** 42-50.

KOSNOPFEL, C., SINNBERG, T., SAUER, B., BUSCH, C., NIESSNER, H., SCHMITT, A., FORCHHAMMER, S., GRIMMEL, C., MERTENS, P. R., HAILFINGER, S., DUNN, S. E., GARBE, C. & SCHITTEK, B. 2018. YB-1 Expression and Phosphorylation Regulate

Tumorigenicity and Invasiveness in Melanoma by Influencing EMT. *Mol Cancer Res,* 16**,** 1149-1160.
KURYK, L., HAAVISTO, E., GAROFALO, M., CAPASSO, C., HIRVINEN, M., PESONEN, S., RANKI, T., VASSILEV, L. & CERULLO, V. 2016. Synergistic anti-tumor efficacy of immunogenic adenovirus ONCOS-102 (Ad5/3-D24-GM-CSF) and standard of care chemotherapy in preclinical mesothelioma model. *International Journal of Cancer,* 139**,** 1883-1893.
LANE, D. P. 1992. p53, guardian of the genome. *Nature,* 358**,** 15-16.
LASHAM, A., LINDRIDGE, E., RUDERT, F., ONRUST, R. & WATSON, J. 2000. Regulation of the human fas promoter by YB-1, Puralpha and AP-1 transcription factors. *Gene,* 252**,** 1-13.
LASHAM, A., PRINT, C. G., WOOLLEY, A. G., DUNN, S. E. & BRAITHWAITE, A. W. 2013. YB-1: oncoprotein, prognostic marker and therapeutic target? *Biochem J,* 449**,** 11-23.
LASHAM, A., SAMUEL, W., CAO, H., PATEL, R., MEHTA, R., STERN, J. L., REID, G., WOOLLEY, A. G., MILLER, L. D., BLACK, M. A., SHELLING, A. N., PRINT, C. G. & BRAITHWAITE, A. W. 2012. YB-1, the E2F pathway, and regulation of tumor cell growth. *J Natl Cancer Inst,* 104**,** 133-46.
LAW, J. H., LI, Y., TO, K., WANG, M., ASTANEHE, A., LAMBIE, K., DHILLON, J., JONES, S. J. M., GLEAVE, M. E., EAVES, C. J. & DUNN, S. E. 2010. Molecular Decoy to the Y-Box Binding Protein-1 Suppresses the Growth of Breast and Prostate Cancer Cells whilst Sparing Normal Cell Viability. *PLOS ONE,* 5**,** e12661.
LIBERTI, M. V. & LOCASALE, J. W. 2016. The Warburg Effect: How Does it Benefit Cancer Cells? *Trends in biochemical sciences,* 41**,** 211-218.
LIM, J. P., NAIR, S., SHYAMASUNDAR, S., CHUA, P. J., MUNIASAMY, U., MATSUMOTO, K., GUNARATNE, J. & BAY, B. H. 2019. Silencing Y-box binding protein-1 inhibits triple-negative breast cancer cell invasiveness via regulation of MMP1 and beta-catenin expression. *Cancer Lett,* 452**,** 119-131.
LINTON, A., VARDY, J., CLARKE, S. & VAN ZANDWIJK, N. 2012. The ticking time-bomb of asbestos: Its insidious role in the development of malignant mesothelioma. *Critical Reviews in Oncology/Hematology,* 84**,** 200-212.
LOCKE, M., GHAZALY, E., FREITAS, M. O., MITSINGA, M., LATTANZIO, L., LO NIGRO, C., NAGANO, A., WANG, J., CHELALA, C., SZLOSAREK, P. & MARTIN, S. A. 2016. Inhibition of the Polyamine Synthesis Pathway Is Synthetically Lethal with Loss of Argininosuccinate Synthase 1. *Cell reports,* 16**,** 1604-1613.
MA, S., SONG, W., XU, Y., SI, X., ZHANG, D., LV, S., YANG, C., MA, L., TANG, Z. & CHEN, X. 2020. Neutralizing tumor-promoting inflammation with polypeptide-dexamethasone conjugate for microenvironment modulation and colorectal cancer therapy. *Biomaterials,* 232**,** 119676.
MANSFIELD, A. S., RODEN, A. C., PEIKERT, T., SHEININ, Y. M., HARRINGTON, S. M., KRCO, C. J., DONG, H. & KWON, E. D. 2014. B7-H1 expression in malignant pleural mesothelioma is associated with sarcomatoid histology and poor prognosis. *Journal of thoracic oncology : official publication of the International Association for the Study of Lung Cancer,* 9**,** 1036-1040.
MAZZONI, E., CORALLINI, A., CRISTAUDO, A., TARONNA, A., TASSI, G., MANFRINI, M., COMAR, M., BOVENZI, M., GUASCHINO, R., VANIGLIA, F., MAGNANI, C., CASALI, F., REZZA, G., BARBANTI-BRODANO, G., MARTINI, F. & TOGNON, M. G. 2012. High prevalence of serum antibodies reacting with simian virus 40 capsid protein mimotopes in patients affected by malignant pleural mesothelioma. *Proceedings of the National Academy of Sciences,* 109**,** 18066.

MCCLATCHEY, A. I. & GIOVANNINI, M. 2005. Membrane organization and tumorigenesis--the NF2 tumor suppressor, Merlin. *Genes Dev,* 19**,** 2265-77.

MEHTA, S., ALGIE, M., AL-JABRI, T., MCKINNEY, C., KANNAN, S., VERMA, C. S., MA, W., ZHANG, J., BARTOLEC, T. K., MASAMSETTI, V. P., PARKER, K., HENDERSON, L., GOULD, M. L., BHATIA, P., HARFOOT, R., CHIRCOP, M., KLEFFMANN, T., COHEN, S. B., WOOLLEY, A. G., CESARE, A. J. & BRAITHWAITE, A. 2020a. Critical role for cold shock protein YB-1 in cytokinesis. *bioRxiv***,** 2020.03.18.997817.

MEHTA, S., MCKINNEY, C., ALGIE, M., VERMA, C. S., KANNAN, S., HARFOOT, R., BARTOLEC, T. K., BHATIA, P., FISHER, A. J., GOULD, M. L., PARKER, K., CESARE, A. J., CUNLIFFE, H. E., COHEN, S. B., KLEFFMANN, T., BRAITHWAITE, A. W. & WOOLLEY, A. G. 2020b. Dephosphorylation of YB-1 is Required for Nuclear Localisation During G(2) Phase of the Cell Cycle. *Cancers (Basel),* 12.

MENDOZA, M. C., ER, E. E. & BLENIS, J. 2011. The Ras-ERK and PI3K-mTOR pathways: cross-talk and compensation. *Trends in Biochemical Sciences,* 36**,** 320-328.

NEUMANN, V., LÖSEKE, S., NOWAK, D., HERTH, F. J. F. & TANNAPFEL, A. 2013. Malignant pleural mesothelioma: incidence, etiology, diagnosis, treatment, and occupational health. *Deutsches Arzteblatt international,* 110**,** 319-326.

NICHOLSON, A. G., SAUTER, J. L., NOWAK, A. K., KINDLER, H. L., GILL, R. R., REMY-JARDIN, M., ARMATO, S. G., 3RD, FERNANDEZ-CUESTA, L., BUENO, R., ALCALA, N., FOLL, M., PASS, H., ATTANOOS, R., BAAS, P., BEASLEY, M. B., BRCIC, L., BUTNOR, K. J., CHIRIEAC, L. R., CHURG, A., COURTIOL, P., DACIC, S., DE PERROT, M., FRAUENFELDER, T., GIBBS, A., HIRSCH, F. R., HIROSHIMA, K., HUSAIN, A., KLEBE, S., LANTUEJOUL, S., MOREIRA, A., OPITZ, I., PEROL, M., RODEN, A., ROGGLI, V., SCHERPEREEL, A., TIRODE, F., TAZELAAR, H., TRAVIS, W. D., TSAO, M. S., VAN SCHIL, P., VIGNAUD, J. M., WEYNAND, B., LANG-LAZDUNSKI, L., CREE, I., RUSCH, V. W., GIRARD, N. & GALATEAU-SALLE, F. 2020. EURACAN/IASLC Proposals for Updating the Histologic Classification of Pleural Mesothelioma: Towards a More Multidisciplinary Approach. *J Thorac Oncol,* 15**,** 29-49.

NICOLINI, F., BOCCHINI, M., BRONTE, G., DELMONTE, A., GUIDOBONI, M., CRINÒ, L. & MAZZA, M. 2020. Malignant Pleural Mesothelioma: State-of-the-Art on Current Therapies and Promises for the Future. *Frontiers in Oncology,* 9.

NORMAND, G., HEMMATI, P. G., VERDOODT, B., VON HAEFEN, C., WENDT, J., GÜNER, D., MAY, E., DÖRKEN, B. & DANIEL, P. T. 2005. p14ARF induces G2 cell cycle arrest in p53- and p21-deficient cells by down-regulating p34cdc2 kinase activity. *J Biol Chem,* 280**,** 7118-30.

NUYTS, V., NAWROT, T., NEMERY, B. & NACKAERTS, K. 2018. Hotspots of malignant pleural mesothelioma in Western Europe. *Translational lung cancer research,* 7**,** 516-519.

OHGA, T., UCHIUMI, T., MAKINO, Y., KOIKE, K., WADA, M., KUWANO, M. & KOHNO, K. 1998. Direct involvement of the Y-box binding protein YB-1 in genotoxic stress-induced activation of the human multidrug resistance 1 gene. *J Biol Chem,* 273**,** 5997-6000.

OKAMOTO, K. & SEIMIYA, H. 2019. Revisiting Telomere Shortening in Cancer. *Cells,* 8**,** 107.

OKAMOTO, T., IZUMI, H., IMAMURA, T., TAKANO, H., ISE, T., UCHIUMI, T., KUWANO, M. & KOHNO, K. 2000. Direct interaction of p53 with the Y-box binding protein, YB-1: a mechanism for regulation of human gene expression. *Oncogene,* 19**,** 6194-6202.

POMERANTZ, J., SCHREIBER-AGUS, N., LIÉGEOIS, N. J., SILVERMAN, A., ALLAND, L., CHIN, L., POTES, J., CHEN, K., ORLOW, I., LEE, H.-W., CORDON-CARDO, C. & DEPINHO, R. A. 1998. The Ink4a Tumor Suppressor Gene Product, p19Arf, Interacts with MDM2 and Neutralizes MDM2's Inhibition of p53. *Cell,* 92**,** 713-723.

RAJABI, M. & MOUSA, S. A. 2017. The Role of Angiogenesis in Cancer Treatment. *Biomedicines,* 5**,** 34.

REID, G., PEL, M. E., KIRSCHNER, M. B., CHENG, Y. Y., MUGRIDGE, N., WEISS, J., WILLIAMS, M., WRIGHT, C., EDELMAN, J. J. B., VALLELY, M. P., MCCAUGHAN, B. C., KLEBE, S., BRAHMBHATT, H., MACDIARMID, J. A. & VAN ZANDWIJK, N. 2013. Restoring expression of miR-16: a novel approach to therapy for malignant pleural mesothelioma. *Annals of Oncology,* 24**,** 3128-3135.

ROLLINS, K. D. & LINDLEY, C. 2005. Pemetrexed: a multitargeted antifolate. *Clin Ther,* 27**,** 1343-82.

RUDD, R. M. 2010. Malignant mesothelioma. *British Medical Bulletin,* 93**,** 105-123.

SAPKOTA, G. P., CUMMINGS, L., NEWELL, F. S., ARMSTRONG, C., BAIN, J., FRODIN, M., GRAUERT, M., HOFFMANN, M., SCHNAPP, G., STEEGMAIER, M., COHEN, P. & ALESSI, D. R. 2007. BI-D1870 is a specific inhibitor of the p90 RSK (ribosomal S6 kinase) isoforms in vitro and in vivo. *Biochem J,* 401**,** 29-38.

SCHERPEREEL, A., WALLYN, F., ALBELDA, S. M. & MUNCK, C. 2018. Novel therapies for malignant pleural mesothelioma. *The Lancet Oncology,* 19**,** e161-e172.

SCHITTEK, B., PSENNER, K., SAUER, B., MEIER, F., IFTNER, T. & GARBE, C. 2007. The increased expression of Y box-binding protein 1 in melanoma stimulates proliferation and tumor invasion, antagonizes apoptosis and enhances chemoresistance. *International Journal of Cancer,* 120**,** 2110-2118.

SEKIDO, Y. 2013. Molecular pathogenesis of malignant mesothelioma. *Carcinogenesis,* 34**,** 1413-1419.

SEMENZA, G. L. 2014. Oxygen Sensing, Hypoxia-Inducible Factors, and Disease Pathophysiology. *Annual Review of Pathology: Mechanisms of Disease,* 9**,** 47-71.

SHAH, S. C., KAYAMBA, V., PEEK, R. M., JR. & HEIMBURGER, D. 2019. Cancer Control in Low- and Middle-Income Countries: Is It Time to Consider Screening? *J Glob Oncol,* 5**,** 1-8.

SHIOTA, M., ITSUMI, M., YOKOMIZO, A., TAKEUCHI, A., IMADA, K., KASHIWAGI, E., INOKUCHI, J., TATSUGAMI, K., UCHIUMI, T. & NAITO, S. 2014. Targeting ribosomal S6 kinases/Y-box binding protein-1 signaling improves cellular sensitivity to taxane in prostate cancer. *The Prostate,* 74**,** 829-838.

SHIOTA, M., YOKOMIZO, A., ITSUMI, M., UCHIUMI, T., TADA, Y., SONG, Y., KASHIWAGI, E., MASUBUCHI, D. & NAITO, S. 2011. Twist1 and Y-box-binding protein-1 promote malignant potential in bladder cancer cells. *BJU International,* 108**,** E142-E149.

SHIOTA, M., YOKOMIZO, A., TADA, Y., UCHIUMI, T., INOKUCHI, J., TATSUGAMI, K., KUROIWA, K., YAMAMOTO, K., SEKI, N. & NAITO, S. 2010. P300/CBP-associated factor regulates Y-box binding protein-1 expression and promotes cancer cell growth, cancer invasion and drug resistance. *Cancer Science,* 101**,** 1797-1806.

SIROHI, B., CHALKIDOU, K., PRAMESH, C. S., ANDERSON, B. O., LOEHER, P., EL DEWACHI, O., SHAMIEH, O., SHRIKHANDE, S. V., VENKATARAMANAN, R., PARHAM, G., MWANAHAMUNTU, M., EDEN, T., TSUNODA, A., PURUSHOTHAM, A., STANWAY, S., RATH, G. K. & SULLIVAN, R. 2018. Developing institutions for cancer care in low-income and middle-income countries: from cancer units to comprehensive cancer centres. *Lancet Oncol,* 19**,** e395-e406.

SOMASEKHARAN, S. P., EL-NAGGAR, A., LEPRIVIER, G., CHENG, H., HAJEE, S., GRUNEWALD, T. G. P., ZHANG, F., NG, T., DELATTRE, O., EVDOKIMOVA, V., WANG, Y., GLEAVE, M. & SORENSEN, P. H. 2015. YB-1 regulates stress granule formation and tumor progression by translationally activating G3BP1. *The Journal of cell biology,* 208**,** 913-929.

STEIN, U., JÜRCHOTT, K., WALTHER, W., BERGMANN, S., SCHLAG, P. M. & ROYER, H. D. 2001. Hyperthermia-induced nuclear translocation of transcription factor YB-1 leads to enhanced expression of multidrug resistance-related ABC transporters. *J Biol Chem,* 276**,** 28562-9.

SUGARBAKER, D. J., RICHARDS, W. G. & BUENO, R. 2014. Extrapleural Pneumonectomy in the Treatment of Epithelioid Malignant Pleural Mesothelioma: Novel Prognostic Implications of Combined N1 and N2 Nodal Involvement Based on Experience in 529 Patients. *Annals of Surgery,* 260.

SUTHERLAND, B. W., KUCAB, J., WU, J., LEE, C., CHEANG, M. C. U., YORIDA, E., TURBIN, D., DEDHAR, S., NELSON, C., POLLAK, M., LEIGHTON GRIMES, H., MILLER, K., BADVE, S., HUNTSMAN, D., BLAKE-GILKS, C., CHEN, M., PALLEN, C. J. & DUNN, S. E. 2005. Akt phosphorylates the Y-box binding protein 1 at Ser102 located in the cold shock domain and affects the anchorage-independent growth of breast cancer cells. *Oncogene,* 24**,** 4281-4292.

SZLOSAREK, P. W., KLABATSA, A., PALLASKA, A., SHEAFF, M., SMITH, P., CROOK, T., GRIMSHAW, M. J., STEELE, J. P., RUDD, R. M., BALKWILL, F. R. & FENNELL, D. A. 2006. In vivo loss of expression of argininosuccinate synthetase in malignant pleural mesothelioma is a biomarker for susceptibility to arginine depletion. *Clin Cancer Res,* 12**,** 7126-31.

TAKAHASHI, K. & LANDRIGAN, P. J. 2016. The Global Health Dimensions of Asbestos and Asbestos-Related Diseases. *Annals of Global Health,* 82**,** 209-213.

TAO, Z., RUAN, H., SUN, L., KUANG, D., SONG, Y., WANG, Q., WANG, T., HAO, Y. & CHEN, K. 2019. Targeting the YB-1/PD-L1 Axis to Enhance Chemotherapy and Antitumor Immunity. *Cancer Immunol Res,* 7**,** 1135-1147.

THOMPSON, J. K., WESTBOM, C. M. & SHUKLA, A. 2014. Malignant mesothelioma: development to therapy. *Journal of cellular biochemistry,* 115**,** 1-7.

TO, K., FOTOVATI, A., REIPAS, K. M., LAW, J. H., HU, K., WANG, J., ASTANEHE, A., DAVIES, A. H., LEE, L., STRATFORD, A. L., RAOUF, A., JOHNSON, P., BERQUIN, I. M., ROYER, H.-D., EAVES, C. J. & DUNN, S. E. 2010. Y-Box Binding Protein-1 Induces the Expression of CD44 and CD49f Leading to Enhanced Self-Renewal, Mammosphere Growth, and Drug Resistance. *Cancer Research,* 70**,** 2840.

TUBBS, A. & NUSSENZWEIG, A. 2017. Endogenous DNA Damage as a Source of Genomic Instability in Cancer. *Cell,* 168**,** 644-656.

VAN HOEVE, J. C., ELFERINK, M. A., KLAASE, J. M., KOUWENHOVEN, E. A., SCHIPHORST, P. P. & SIESLING, S. 2015. Long-term effects of a regional care pathway for patients with rectal cancer. *Int J Colorectal Dis,* 30**,** 787-95.

VAN ZANDWIJK, N., CLARKE, C., HENDERSON, D., MUSK, A. W., FONG, K., NOWAK, A., LOERAGAN, R., MCCAUGHAN, B., BOYER, M., FEIGEN, M., CURROW, D., SCHOFEILD, P., PAVLAKIS, B. I. N., MCLEAN, J., MARSHALL, H., LEONG, S., KEENA, V. & PENMAN, A. 2013. Guidelines for the diagnosis and treatment of malignant pleural mesothelioma. *Journal of Thoracic Disease,* 5**,** E254-E307.

VAN ZANDWIJK, N., PAVLAKIS, N., KAO, S. C., LINTON, A., BOYER, M. J., CLARKE, S., HUYNH, Y., CHRZANOWSKA, A., FULHAM, M. J., BAILEY, D. L., COOPER, W. A., KRITHARIDES, L., RIDLEY, L., PATTISON, S. T., MACDIARMID, J., BRAHMBHATT, H. & REID, G. 2017. Safety and activity of microRNA-loaded minicells in patients with recurrent malignant pleural mesothelioma: a first-in-man, phase 1, open-label, dose-escalation study. *The Lancet Oncology,* 18**,** 1386-1396.

VERMA, V., AHERN, C. A., BERLIND, C. G., LINDSAY, W. D., SHABASON, J., SHARMA, S., CULLIGAN, M. J., GROVER, S., FRIEDBERG, J. S. & SIMONE, C. B. 2018. Survival

by Histologic Subtype of Malignant Pleural Mesothelioma and the Impact of Surgical Resection on Overall Survival. *Clinical Lung Cancer,* 19**,** e901-e912.
WANG, H., SUN, R., CHI, Z., LI, S. & HAO, L. 2017. Silencing of Y-box binding protein-1 by RNA interference inhibits proliferation, invasion, and metastasis, and enhances sensitivity to cisplatin through NF-κB signaling pathway in human neuroblastoma SH-SY5Y cells. *Molecular and Cellular Biochemistry,* 433**,** 1-12.
WANG, Y., CHEN, Y., GENG, H., QI, C., LIU, Y. & YUE, D. 2015. Overexpression of YB1 and EZH2 are associated with cancer metastasis and poor prognosis in renal cell carcinomas. *Tumour Biol,* 36**,** 7159-66.
WARBURG, O. H. 1930. *The metabolism of tumours: investigations from the Kaiser Wilhelm Institute for Biology, Berlin-Dahlem*, Constable & Company Limited.
WEDLER, H. W. 1943. Lung cancer in asbestosis patients. *Arch Klinischen Medizin***,** 191:189—209.
WEINBERG, R. A. 2014. Coming full circle-from endless complexity to simplicity and back again. *Cell,* 157**,** 267-71.
WHO 2020. WHO report on cancer: setting priorities, investing wisely and providing care for all.
WITKIEWICZ, A. K., KNUDSEN, K. E., DICKER, A. P. & KNUDSEN, E. S. 2011. The meaning of p16(ink4a) expression in tumors: functional significance, clinical associations and future developments. *Cell cycle (Georgetown, Tex.),* 10**,** 2497-2503.
WOLFFE, A. P., TAFURI, S., RANJAN, M. & FAMILARI, M. 1992. The Y-box factors: a family of nucleic acid binding proteins conserved from Escherichia coli to man. *New Biol,* 4**,** 290-8.
XU, J., KADARIYA, Y., CHEUNG, M., PEI, J., TALARCHEK, J., SEMENTINO, E., TAN, Y., MENGES, C. W., CAI, K. Q., LITWIN, S., PENG, H., KARAR, J., RAUSCHER, F. J. & TESTA, J. R. 2014. Germline mutation of Bap1 accelerates development of asbestos-induced malignant mesothelioma. *Cancer research,* 74**,** 4388-4397.
YAHATA, H., KOBAYASHI, H., KAMURA, T., AMADA, S., HIRAKAWA, T., KOHNO, K., KUWANO, M. & NAKANO, H. 2002. Increased nuclear localization of transcription factor YB-1 in acquired cisplatin-resistant ovarian cancer. *J Cancer Res Clin Oncol,* 128**,** 621-6.
YAMASHITA, T., HIGASHI, M., MOMOSE, S., MOROZUMI, M. & TAMARU, J.-I. 2017. Nuclear expression of Y box binding-1 is important for resistance to chemotherapy including gemcitabine in TP53-mutated bladder cancer. *International Journal of Oncology,* 51**,** 579-586.
YU, H., PAK, H., HAMMOND-MARTEL, I., GHRAM, M., RODRIGUE, A., DAOU, S., BARBOUR, H., CORBEIL, L., HÉBERT, J., DROBETSKY, E., MASSON, J. Y., DI NOIA, J. M. & AFFAR, E. B. 2014. Tumor suppressor and deubiquitinase BAP1 promotes DNA double-strand break repair. *Proceedings of the National Academy of Sciences,* 111**,** 285.
ZALCMAN, G., MAZIERES, J., MARGERY, J., GREILLIER, L., AUDIGIER-VALETTE, C., MORO-SIBILOT, D., MOLINIER, O., CORRE, R., MONNET, I., GOUNANT, V., RIVIÈRE, F., JANICOT, H., GERVAIS, R., LOCHER, C., MILLERON, B., TRAN, Q., LEBITASY, M. P., MORIN, F., CREVEUIL, C., PARIENTI, J. J. & SCHERPEREEL, A. 2016. Bevacizumab for newly diagnosed pleural mesothelioma in the Mesothelioma Avastin Cisplatin Pemetrexed Study (MAPS): a randomised, controlled, open-label, phase 3 trial. *Lancet,* 387**,** 1405-1414.
ZHAO, S., WANG, Y., GUO, T., YU, W., LI, J., TANG, Z., YU, Z., ZHAO, L., ZHANG, Y., WANG, Z., WANG, P., LI, Y., LI, F., SUN, Z., XUAN, Y., TANG, R., DENG, W.-G.,

GUO, W. & GU, C. 2016. YBX1 regulates tumor growth via CDC25a pathway in human lung adenocarcinoma. *Oncotarget; Vol 7, No 50*.